Persistent features and anomalies in the surface deformation of Campi Flegrei based on DinSAR data from the last 30 years

Antonella Amoruso[1], Luca Crescentini[1]
1 Department of Physics, University of Salerno, Fisciano, Italy

Monitoring the evolution of the deformation field of Campi Flegrei from the 1990s onwards is possible thanks to the use of SAR images from different missions. In particular, the ERS/ENVISAT and Sentinel-1 missions of ESA cover the periods 1993–2010 and 2015 to the present day, respectively. The time gap between these two periods has recently been filled using Radarsat-2 images.

Therefore, we were able to carry out a comprehensive analysis of Phlegraean deformation over the last 30 years by combining the ERS/ENVISAT deformation time series provided by IREA/CNR, the Radarsat-2 series from Amoruso et al. (2025), and the Sentinel-1 series from Giudicepietro et al. (2024). The LOS directions for RADARSAT-2 and Sentinel-1 are very similar across Campi Flegrei, with incidence angles of around 35°. This would enable the LOS displacement time series to be connected. Conversely, the LOS directions for ERS/ENVISAT are quite different, with incidence angles of around 22.5°. We have therefore computed the quasi-vertical and eastward displacements in order to connect the three time series. Examples of long-term deformation are given in Fig.1. Weekly cGPS time series from De Martino et al. (2023) are also plotted for comparison.

We will present the preliminary results obtained using linear regression models. These models have been used to verify whether the deformation field has remained unchanged within the margin of error between 1993 and the present day. They have also been used to highlight possible local deformation anomalies, such as those evidenced in Amoruso et al. (2014) and Giudicepietro et al. (2024).

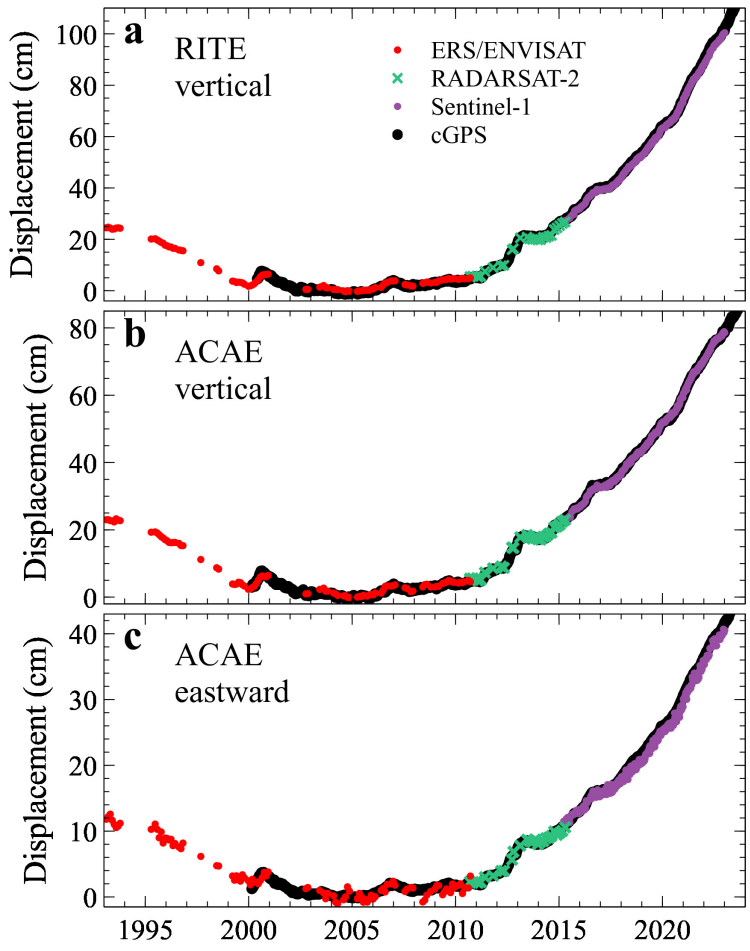

Fig.1 – Examples of long-term deformation, obtained by connecting the displacement time seriesfrom ERS/ENVISAT, RADARSAT-2, and Sentinel-1 imagery. Black dots, weekly cGPS data (De Martino et al., 2023). Red dots, ERS/ENVISAT. Green crosses, RADARSAT-2. Violet dots, Sentinel-1. (a) Vertical displacement at the cGPS RITE station. (b) Vertical displacement at the cGPS ACAE station. (c) Eastward displacement at the cGPS ACAE station. RITE (Rione Terra) is close to the area of maximum vertical displacement. ACAE (Accademia Aeronautica) is close to the area of maximum eastward displacement.

Anomalies in the Solfatara-Pisciarelli-Accademia Aeronautica area during the subsidence from 1993 to the early 2000s (Amoruso et al. 2014) and in the Accademia Aeronautica area after approximately 2019 (Giudicepietro et al. 2024) have been confirmed, with further information on their geometric characteristics being provided.

Even more interestingly, the initial results of the analyses seem to indicate the coexistence of two stationary deformation fields throughout the entire investigated period. The field with the larger amplitude has dimensions similar to those of the caldera and a temporal history comparable to the vertical displacement in the area near the RITE cGPS station (Fig. 1a). The other field is less conspicuous, but potentially has even more significant implications. It is more extensive and shifted eastwards relative to the centre of the caldera. It is characterised by an approximately constant uplift velocity since at least the beginning of the available DInSAR time series. This second stationary field has a shape similar to that obtained from ERS/ENVISAT data using variational Bayesian independent component analysis for the period 1993–2010 (Amoruso et al., 2024). We

will also discuss the degree of complexity of the sources necessary to account for the shapes of the two stationary deformation fields within the measurement errors.

References

Amoruso, A., Crescentini, L., and Sabbetta, I.; 2014: Paired deformation sources of the Campi Flegrei caldera (Italy) required by recent (1980–2010) deformation history. Journal of Geophysical Research: Solid Earth, Vol. 119, pp. 858–879, http://doi.org/10.1002/2013JB010392

Amoruso, A., Gualandi, A., and Crescentini, L.; 2024: On the Initial Phase of the Ongoing Unrest at Campi Flegrei and Its Relation with Subsidence at Vesuvio (Italy). Remote Sensing, Vol. 16, 1717, https://doi.org/10.3390/rs16101717.

Amoruso, A., Salicone, G., and Crescentini, L.; 2025: Campi Flegrei and Vesuvio, Italy: Ground Deformation Between ERS/ENVISAT and Sentinel-1 Missions from RADARSAT-2 Imagery. Remote Sensing, Vol. 17, 3268, https://doi.org/10.3390/rs17193268

De Martino, P., Dolce, M., Brandi, G., and Scarpato, G.; 2023: Campi Flegrei cGPS Weekly Positions Time Series. https://zenodo.org/records/10082466

Giudicepietro, F., et al.; 2024: First evidence of a geodetic anomaly in the Campi Flegrei caldera (Italy) ground deformation pattern revealed by DInSAR and GNSS measurements during the 2021–2023 escalating unrest phase. International Journal of Applied Earth Observation and Geoinformation, Vol. 132, 104060, http://doi.org/10.1016/j.jag.2024.104060

Corresponding author: lcrescen@unisa.it

On the use of the ACE Climate Model Emulator to investigate the climatic impact of volcanic activity

Authors: Lorenzo Basile (1, 2, *), Eleonora Amato (1), Vito Zago (1), Ciro Del Negro (1)

(1) *Istituto Nazionale di Geofisica e Vulcanologia (INGV), Sezione Osservatorio Etneo, Catania, Italy*

(2) *Department of Mathematical and Computer Sciences, Physical Sciences and Earth Sciences, University of Messina, Italy*

(*) Corresponding author: lorenzo.basile@ingv.it (L. Basile)

Volcanic activity can affect the climate system across multiple timescales, from rapid atmospheric fluctuations to longer-term responses driven by stratospheric aerosol forcing associated to major explosive eruptions. Rapid evaluation of the atmospheric response to such events calls for approaches that combine physical understanding with computationally efficient predictive tools. Predicting and quantifying these impacts using numerical Earth system models remains computationally expensive, limiting the systematic exploration of uncertainty and sensitivity across different eruption scenarios.

Machine-learning-based climate emulators have emerged as a promising complement to traditional numerical models, enabling fast predictions of atmospheric evolution. State-of-the-art emulators, such as the AI2 Climate Emulator (ACE) [1], are trained on outputs from climate model simulations or on reanalysis datasets such as ERA5 [2], which provide realistic representations of the atmospheric state. However, their application to volcanic forcing remains underrepresented due to the rarity of major eruptions in the historical record, the limited availability of consistent volcanic forcing datasets, and the lack of standardized representations of stratospheric sulfur dioxide (SO_2) and aerosol-related perturbations suitable for emulator training.

Here, we investigate how to design volcanic forcing and initial conditions datasets suitable for emulator-based frameworks such as ACE. We explore different strategies for representing sulfur dioxide (SO_2) forcing, assess available observational and model-based datasets, and discuss training

and fine-tuning approaches aimed reproducing the dynamic atmospheric response to volcanic perturbations. The proposed methodological framework is intended to support efficient sensitivity analysis and ensemble experiments of volcanic eruption scenarios using machine-learning-based atmospheric emulators.

References:

1. Watt-Meyer, O., Henn, B., McGibbon, J. *et al.* ACE2: accurately learning subseasonal to decadal atmospheric variability and forced responses. *npj Clim Atmos Sci* **8**, 205 (2025). https://doi.org/10.1038/s41612-025-01090-0
2. Hersbach, H., Bell, B., Berrisford, P., Biavati, G., Horányi, A., Muñoz Sabater, J., Nicolas, J., Peubey, C., Radu, R., Rozum, I., Schepers, D., Simmons, A., Soci, C., Dee, D., Thépaut, JN. (2023): ERA5 hourly data on single levels from 1940 to present. Copernicus Climate Change Service (C3S) Climate Data Store (CDS), DOI: 10.24381/cds.adbb2d47

Analytical modelling of thermo-poro-elastic spherical sources in a half-space, with application to Vulcano Island (Italy)

Samuel Battolini[1], Massimo Nespoli[1], Maria Elina Belardinelli[1]

[1] *Department of Physics and Astronomy, Alma Mater Studiorum, Università di Bologna, Bologna, Italy*

Fluids play a key role in controlling deformation, stress redistribution and seismicity in volcanic and geothermal systems. Classical formulations, such as the Mogi source (Mogi 1958) have long been used to describe surface displacements caused by magmatic intrusions, nevertheless they are limited in representing the coupled effects of fluids pressurizing and heating a porous medium, which are central to hydrothermal systems. Moreover, these models predict an isotropic stress state within the deformation source and thus cannot explain seismicity occurring inside it.

Other approaches adopt thermo-poro-elasticity (TPE) theory to incorporate the influence of temperature and pore pressure of hydrothermal fluids (e.g., Rinaldi et al., 2010). Recently, TPE inclusion models have undergone significant development (e.g., Belardinelli et al., 2019). A TPE inclusion represents a limited porous and permeable region where temperature (T) and pore pressure (p) variations occur, due to the arrival of a plume of fluids exsolved from a deep magma chamber. Such parameters define the potency of the TPE source $\epsilon_0 = \frac{1}{3H}p + \frac{1}{3}\alpha T$, where H is the Biot's constant and α is the coefficient of thermal expansion in drained conditions. The inclusion is enclosed in a poroelastic matrix assumed to be in isothermal and drained conditions. Disk shaped TPE models have successfully reproduced the deformation and seismicity patterns observed during the unrest episodes at Campi Flegrei Caldera (Mantiloni et al., 2020).

This work aims to enhance the physical realism of the previous analytical models that consider spherical and spherical shell geometric TPE inclusions. In particular, we extended the solutions of Belardinelli et al., (2019) in order to account for the presence of the free surface, which strongly influences the mechanical response of the medium and is essential for comparison with surface observations. Closed-form analytical solutions are derived for displacement, strain, and stress throughout the domain, including the interior of the source.

The model adopts a fully analytical framework. Owing to the axisymmetric nature of the problem, cylindrical coordinates are employed (Fig. 1). Two complementary techniques are combined to satisfy the free-surface boundary conditions: the image source method, which eliminates the shear stress component, and the Galerkin formulation, which allows the normal stress to vanish at the free surface (Bonafede 1990). The approach is first developed for a spherical inclusion (Fig. 1a), which may represent a reservoir where hot and pressurized fluids accumulate. In addition to this configuration, a spherical Mogi source embedded within a spherical TPE shell is also considered (Fig. 1b). The latter could represent a mechanically distinct region, such as a damaged or fractured rock volume, surrounding the magma chamber, capable of responding to thermo-poro-elastic coupling.

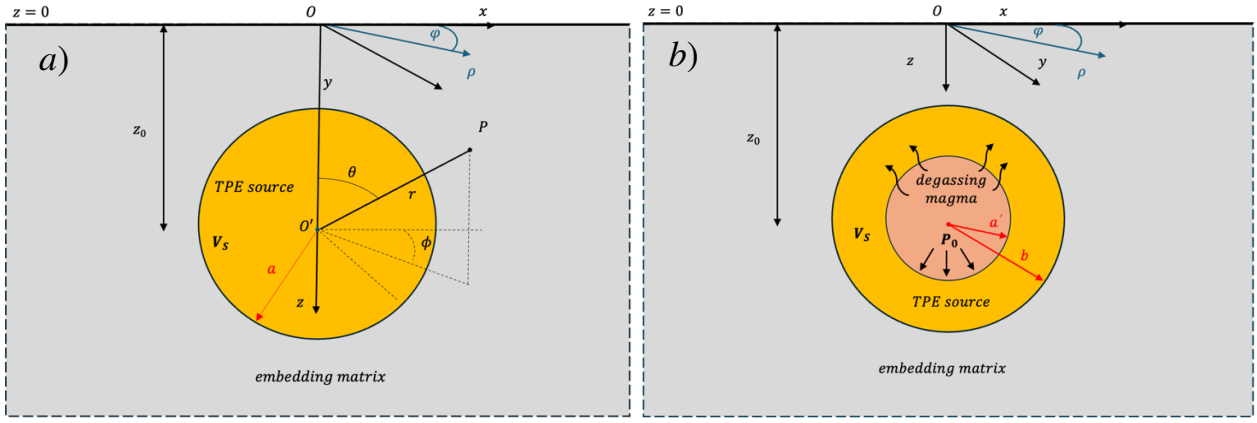

Fig. 1 – Spherical (a) TPE region (yellow) of radius a and spherical shell TPE region (b) of inner radius a' and outer radius b, surrounded by an embedding matrix (gray) in drained isothermal conditions. The reference system, in cartesian (black) coordinates (x, y, z) and cylindrical (blue) coordinates (ρ, φ, z), is also represented. The origin of the reference system lies on the free surface $(z = 0)$ and the z−axis is taken positive in the downward direction. The center of the median plane of the TPE shell is located at $(0; 0; z_0)$. The reference system used by Belardinelli et al., (2019) expressed in spherical coordinates (r, θ, ϕ) and with the origin located in the center of the sphere, is also reported in (a). V_s is the volume of the TPE source and P_0 the overpressure of the magmatic source embedded within the spherical shell.

The obtained results reveal that the presence of the free surface profoundly modifies the deformation and stress fields relative to the unbounded configuration. If the source is very deep, and thus far from the free surface, the solutions obtained in the half-space coincide with those of the full-space model; otherwise, significant differences arise in all mechanical fields. This underscores the importance of including the effects of the free surface when comparing with real data.

The analysis also shows that thinner shells exhibit larger internal shear stress, while the external field weakens. This suggests that thin shells are more prone to internal failure, potentially explaining seismicity within the source region itself, a behavior that classical models of pressurized magma filled cavities with isotropic stress inside cannot reproduce.

For the spherical inclusion, the solutions are exact and satisfy all boundary conditions. For the spherical shell the procedure described in section 2 ensures only an approximate solution, as the normal traction continuity on the inner spherical surface is not perfectly reproduced. For this reason, leading order corrections to the surface displacement are evaluated following the iterative approach proposed by McTigue (1987) for magmatic sources.

The 2021 unrest at Vulcano Island further illustrates the capability of the present model to jointly explain deformation and seismicity. By adopting a suitable set of source parameters derived from the inversion of geodetic data (Tab. 1), the models successfully reproduce the observed surface displacements. Shear stress concentration in the range of [10^4; 10^7] Pa result both within and in the vicinity of the source, offering a physically consistent explanation for the clustered very shallow seismic events recorded near the crater of Vulcano Island.

	z_0^* (m)	ϵ_0	radius (m)
TPE sphere	722	6.1×10^{-4}	$a = \frac{z_0}{3}$

TPE shell	722	7.2×10^{-4}	$a' = \frac{z_0}{6}; b = \frac{z_0}{3}$

Tab. 1 – Parameters of the spherical and spherical shell TPE inclusions under isothermal conditions. Here, z_0 denotes the depth of the source center, ϵ_0 the potency, a the radius of the spherical inclusion, a' and b the inner and outer radii of the spherical shell, respectively. The spherical shell model is considered under the assumption that the pressure inside the magma chamber remains constant during degassing. The value of z_0 (marked with *) is taken from Stissi et al. (2023), while ϵ_0 and a are chosen such that the resulting source volume change, $\Delta V_S = 107{,}499$ m³, is consistent with the value reported in Stissi et al. (2023). The parameters of the spherical TPE shell are finally chosen in order to reproduce the same surface displacement as the spherical inclusion.

References

Belardinelli, M.E., Bonafede, M. and Nespoli, M.; 2019: Stress heterogeneities and failure mechanisms induced by temperature and pore-pressure increase in volcanic regions. Earth and Planetary Science Letters Vol. 525, 115765, https://doi.org/10.1016/j.epsl.2019.115765

Bonafede, M.; 1990: Axi-symmetric deformation of a thermo-poro-elastic half-space: inflation of a magma chamber. Geophysical Journal International, Vol. 103, n. 2, pp. 289-299, https://doi.org/10.1111/j.1365-246X.1990.tb01772.x

Mantiloni, L., Nespoli M., Belardinelli, M.E. and Bonafede, M.; 2020: Deformation and stress in hydrothermal regions: the case of a disk-shaped inclusion in a half-space. Journal of Volcanology and Geothermal Research, Vol. 403, 107011, https://doi.org/10.1016/j.jvolgeores.2020.107011

McTigue, D.F.; 1987: Elastic stress and deformation near a finite spherical magma body: Resolution of the point source paradox. Journal of Geophysical Research: Solid Earth, Vol. 92, n. B12, pp. 12931-12940. DOI: https://doi.org/10.1029/JB092iB12p12931

Mogi, K.; 1958: Relation between the eruptions of various volcanoes and deformations of the ground surfaces around them. Tokyo Earthquake Research Institute, Vol. 36, n. 99, e134.

Rinaldi, A., Todesco, M. and Bonafede. M.; 2010: Hydrothermal instability and ground displacement at the campi flegrei caldera. Physics of the Earth and Planetary Interiors, Vol. 178, n. 3, pp. 155–161, https://doi.org/10.1016/j.pepi.2009.09.005

Stissi, S.C., Currenti, G., Cannavò, F. and Napoli. R.; 2023: Evidence of poro-elastic inflation at the onset of the 2021 Vulcano Island (Italy) unrest. Frontiers in Earth Science, Vol. 11, 1179095, https://doi.org/10.3389/feart.2023.1179095

Corresponding author: samuel.battolini2@unibo.it

Merging field data and numerical modelling for a better understanding of dyke-induced faults

*F.L. Bonali[1,2], A. Luppino[1], S. Brando[1], F. Pasquaré Mariotto[3], S. Bolognino Galli[1], E. De Beni[4], A. Tibaldi[1,2]**

[1] *Department of Earth and Environmental Sciences, University of Milan-Bicocca, Milan, Italy*
[2] *CRUST – Interuniversity Centre for 3D Seismotectonics with Territorial Applications, Chieti, Italy*
[3] *Department of Human and Innovation Sciences, Insubria University, Como, Italy*
[4] *Istituto Nazionale di Geofisica e Vulcanologia, Osservatorio Etneo, Sezione di Catania, Catania, Italy*

*Corresponding author: fabio.bonali@unimib.it

Background

Shallow dike emplacement plays a fundamental role in controlling brittle deformation at the Earth's surface in volcanic and rift environments, commonly producing normal faults and graben structures. Comparable deformation patterns may also result from regional tectonic extension, and in many volcano-tectonic settings these processes act concurrently. Discriminating between tectonic and intrusion-induced deformation therefore remains a major challenge, with important implications for magma transport pathways, fault reactivation, and volcanic hazard assessment. This contribution presents an integrated synthesis of six complementary scientific studies that combine detailed field observations with numerical modelling to investigate the mechanisms governing dike-induced graben formation at shallow crustal levels. Field-based structural analyses form the backbone of this work were systematically applied across all case studies using historical aerial photographs, archival imagery, UAV-based photogrammetry, remote sensing data, and detailed field surveys (e.g Fig. 1). This multi-source dataset enabled a quantitative reconstruction of fracture swarms, graben geometry, fault kinematics, vertical displacements, and the temporal evolution of surface deformation associated with shallow dike emplacement.

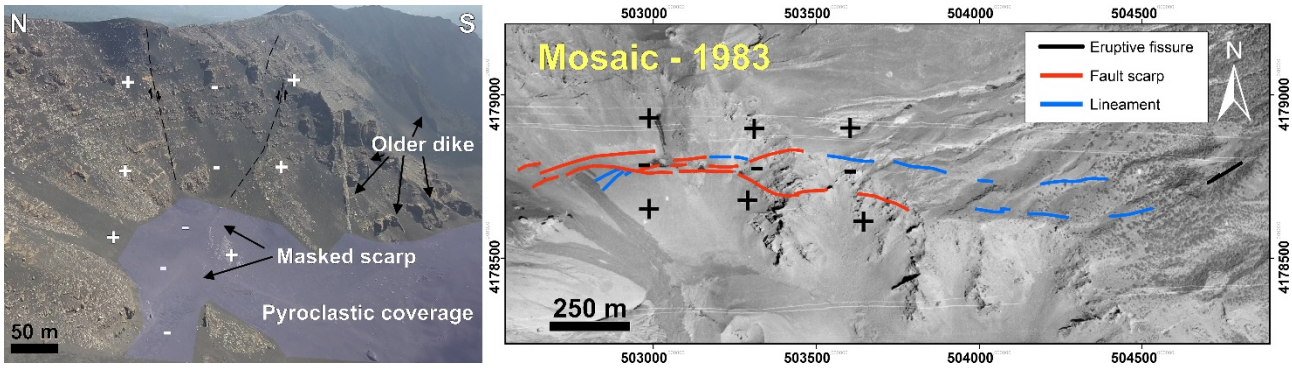

Fig. 1 - Composite figure of the dyke-induced graben formed during the 1971 Mt. Etna eruption. *(Left)* Oblique UAV-derived view showing the graben in cross section, with the downthrown block (negative symbols) and bounding normal faults indicated. *(Right)* 1983 aerial photograph mosaic with mapped eruptive fissures (black), fault scarps (red), and lineaments (blue), highlighting the overall graben geometry. Modified after Bonali et al. (2024).

Results

Field observations and elastic FEM modelling of the 1928 fissure eruption at Mt. Etna demonstrate that shallow dike intrusion alone is sufficient to generate graben structures and surface faulting, even in the absence of significant regional extension. This study highlights the dominant role of magma overpressure and dike geometry in controlling the style and magnitude of surface deformation (Tibaldi et al., 2022).

High-resolution 3D structural analyses of the 1971 eruption at Mt. Etna further show that intrusion-induced deformation can be strongly asymmetric when dike emplacement occurs beneath sloping topography (Fig. 1). Numerical models constrained by field data quantitatively demonstrate that local topographic modifies the local stress field, promoting preferential fault nucleation and asymmetric graben geometries (Bonali et al., 2024).

The interaction between propagating dikes and inherited fracture networks is addressed by two complementary studies focusing on the 1947 lateral eruption along the NE Rift of Mt. Etna. By integrating field observations, analogue experiments, and numerical modelling, these studies demonstrate that pre-existing fractures exert a first-order control on dike trajectory, segmentation, and arrest, as well as on the localisation of surface faulting. Fracture spacing and connectivity are shown to determine whether dike propagation is enhanced or inhibited, providing a mechanical explanation for the observed spatial variability of eruptive fissures and deformation patterns (Luppino et al., 2025; Tibaldi et al., 2025).

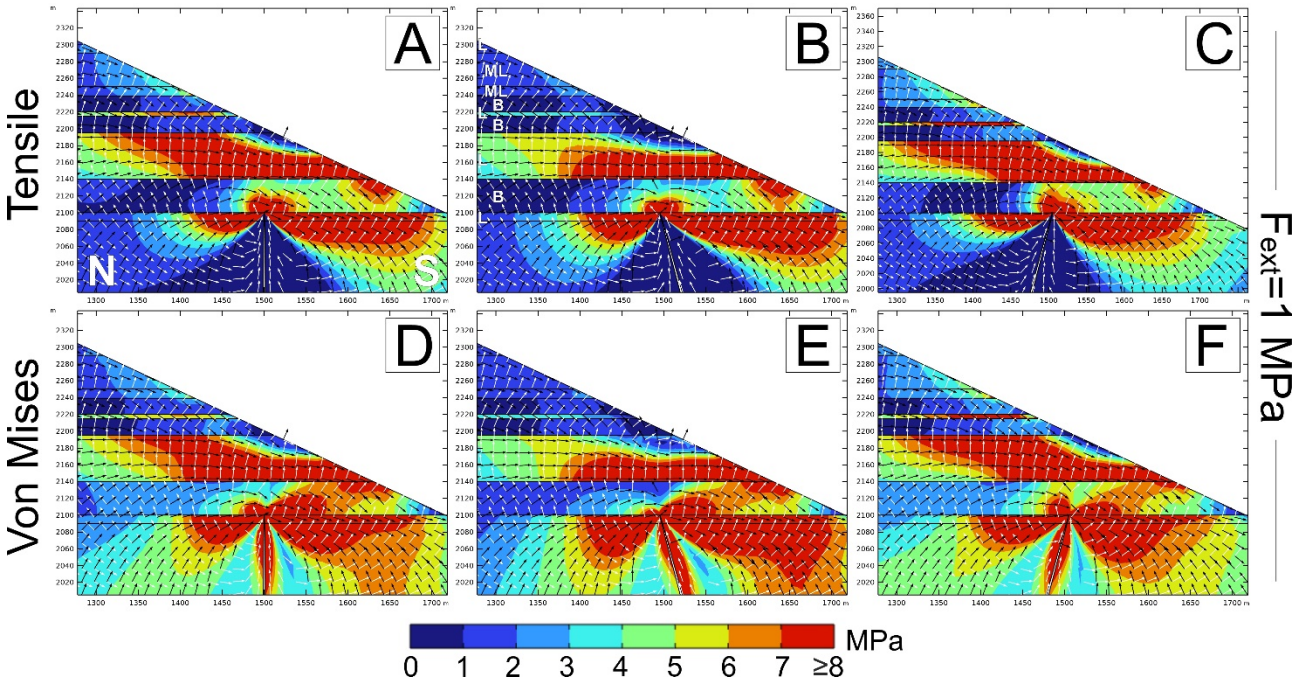

Fig. 2 - Numerical models for the 1971 case study. The dyke is modelled with different attitudes under a regional extensional stress field of 1 MPa. (A–C) Tensile stress distributions and (D–F) von Mises shear stress distributions are shown using the colour scale (MPa). Principal stress trajectories are indicated by white arrows (σ_1) and black arrows (σ_3). Axes are expressed in metres; the vertical axis represents elevation above sea level (a.s.l.).

An additional case study from the Northern Volcanic Zone of Iceland documents the development of an asymmetric graben above a shallow dike intruding a subglacial volcanic cone (Fig. 3). Structural data indicate that a pre-existing rift fault guided dike ascent to the surface, consequently

promoting the development of antithetic faulting and enhancing graben asymmetry (Bonali et al., under review).

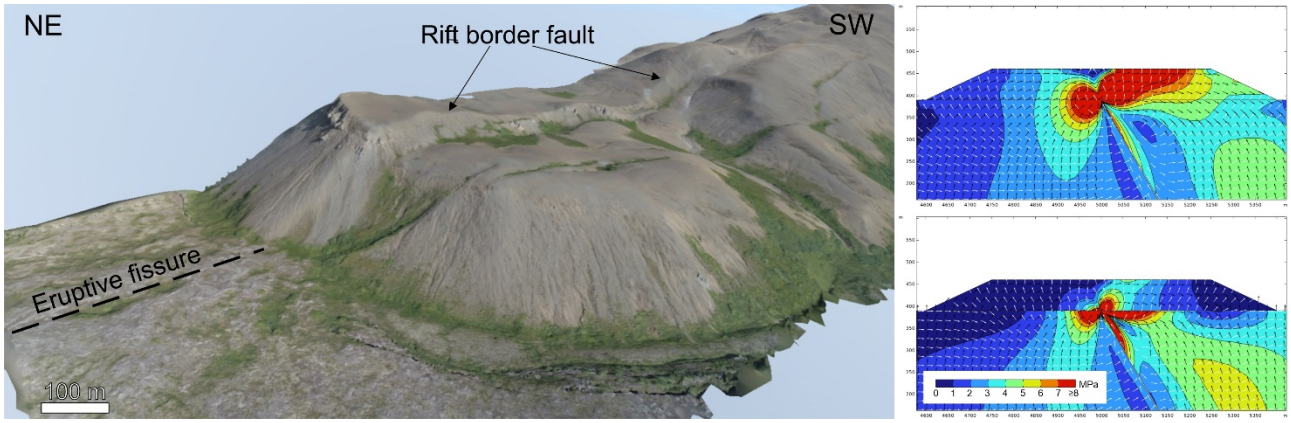

Fig. 3 - Oblique 3D view of the Vestari Skógarmannafjöll ridge and associated numerical modelling results. Left panel: panoramic view of the summit graben affecting the volcanic cone, derived from a photogrammetry-based 3D model. Right panels: numerical model results showing von Mises shear stress distribution for a dyke emplaced at the base of the cone, modelled under homogeneous conditions and with a mechanical contrast between the cone and the substratum.

Future perspectives

Future work will focus on the development of elasto-plastic numerical models specifically designed to investigate the generation of fault zones during shallow dyke emplacement. Unlike elastic approaches, elasto-plastic modelling allows faults to emerge as zones of shear-strain localisation, providing a more realistic framework for simulating fault nucleation and evolution.

Ongoing modelling is aimed at exploring fault generation under flat topographic conditions, in order to isolate the intrinsic mechanical effects of magma-induced stress perturbations. Particular attention will be devoted to the role of mechanical (rheological) contrast, by comparing homogeneous host-rock configurations with layered systems, and to the influence of dyke-tip depth, systematically varied from shallow to deeper emplacement levels.

This approach will enable the investigation of how fault localisation and graben geometry evolve under elasto-plastic conditions and whether new quantitative relationships between dyke-tip depth and graben width emerge.

References

Bonali, F. L., Corti, N., Pasquaré Mariotto, F., De Beni, E., Bressan, S., Cantarero, M., Russo, E., Neri, M., & Tibaldi, A. (2024). 3D study of dyke-induced asymmetric graben: The 1971 Mt. Etna (Italy) case by structural data and numerical modelling. Journal of Structural Geology, 187, 105231. https://doi.org/10.1016/j.jsg.2024.105231

Bonali, F. L., Brando, S., Pasquaré Mariotto, F., Luppino, A., & Tibaldi, A. *Magmatically driven antithetic faulting: structural and numerical insights*. **Journal of Structural Geology**, under review.

Luppino, A., Bonali, F. L., Gudmundsson, A., & Tibaldi, A. (2025). Effects of pre-existing fractures on dike propagation: new insights from field data and numerical modelling. *Journal of Structural Geology*, 105563.

https://doi.org/10.1016/j.jsg.2025.105563

Tibaldi, A., Bonali, F. L., Corti, N., Russo, E., Drymoni, K., De Beni, E., Branca, S., Neri, M., Cantarero, M., & Pasquarè Mariotto, F. (2022). Surface deformation during the 1928 fissure eruption of Mt. Etna (Italy): Insights from field data and FEM numerical modelling. Tectonophysics, 837, 229468. https://doi.org/10.1016/j.tecto.2022.229468

Tibaldi, A., Luppino, A., De Beni, E., Corti, N., Cantarero, M., Mariotto, F. P., & Bonali, F. L. (2025). Effects of lateral dyke propagation and pre-existing fractures on shallow deformation: Data from the Etna 1947 eruption and analogue models. Journal of Volcanology and Geothermal Research, 108349.

https://doi.org/10.1016/j.jvolgeores.2025.108349

Geofluid-Controlled Fault Dynamics and Long-Term Human Occupation on Mount Etna's Southeastern Flank

C. Bottari[1], S. Giammanco[1], F. Sortino[2], M. Palano[3,1], G. Groppelli[4], S. Alparone[1], A. Luppino[5], F. Forni[6], G. Tringali[7]

[1] Istituto Nazionale di Geofisica e Vulcanologia, Sezione Osservatorio Etneo, Catania
[2] Istituto Nazionale di Geofisica e Vulcanologia, Sezione Palermo
[3] Dipartimento di Scienze della Terra e del Mare, Università degli Studi di Palermo
[4] Consiglio Nazionale delle Ricerche, Istituto di Geologia Ambientale e Geoingegneria, Milano
[5] Dipartimento di Scienze dell'Ambiente e della Terra, Università degli Studi di Milano-Bicocca
[6] Dipartimento di Scienze della Terra "Ardito Desio", Università degli Studi di Milano
[7] Dipartimento di Scienza e Alta Tecnologia, Università degli Studi dell'Insubria, Como.

1. Introduction

Geofluids play a fundamental role in modulating stress, fault mechanics and deformation processes in active volcanic and tectonic environments. Variations in fluid pressure and permeability can promote aseismic slip, trigger seismicity and control hydrothermal circulation in geothermal fields (Sibson, 1992; Chiodini et al., 1996). In volcanic settings, these processes are further influenced by magma intrusion and gravitational instability, producing complex feedbacks between deformation, fluid migration and surface degassing (Bonaccorso & Calvari, 2013; Walter et al., 2005).

Mount Etna represents a natural laboratory to investigate these interactions, particularly along its southeastern flank, where slow slip events (SSEs), fault creep and shallow seismicity coexist with diffuse gas emissions and thermal springs (Fig.1; Azzaro et al., 2000; Liotta et al., 2017). This study integrates geodetic, seismic and geochemical observations to investigate how geofluids modulate fault behaviour and hydrothermal circulation, and how these same processes have sustained long-term human exploitation of geothermal resources at Santa Venera al Pozzo (SVP).

From a mechanical perspective, the interaction between geofluids and active faults is increasingly recognized as a key factor controlling the transition between seismic and aseismic deformation. Transient increases in pore pressure can reduce effective normal stress, promote fault creep and facilitate slow slip events, thereby modulating both earthquake occurrence and surface deformation patterns (Sibson, 1992). In volcanic environments, these processes are further complicated by magma intrusion and flank instability, which can repeatedly reorganize stress fields and permeability structures. In this context, integrating geophysical and geochemical observations with long-term indicators offers a unique opportunity to investigate the persistence of fluid-controlled fault behaviour across different temporal scales.

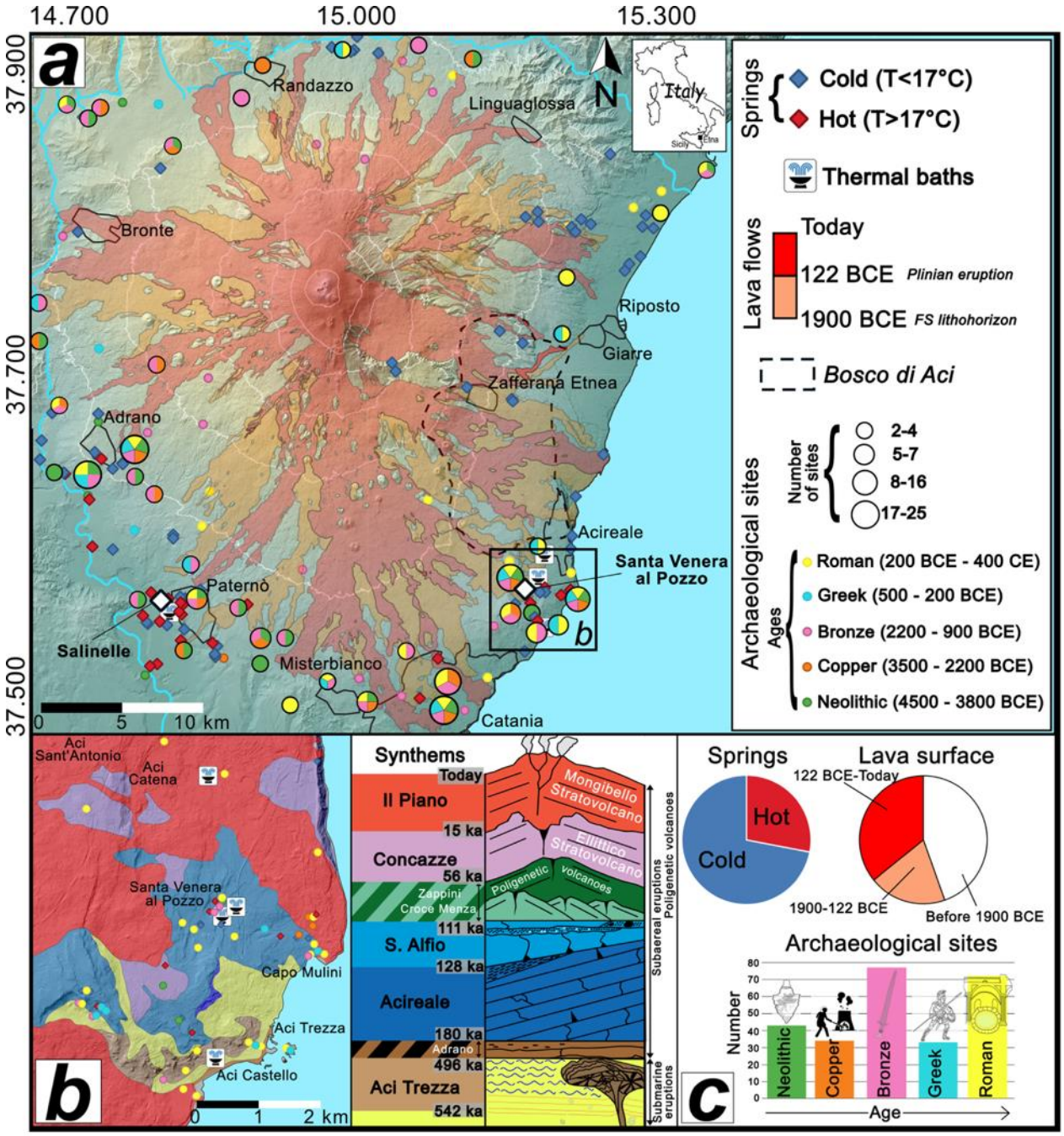

Fig.1 -Map of Mount Etna showing the location of key archaeological sites and geothermal features.
(a) Historical and pre-historical lava flows on Mount Etna with major archaeological sites and thermal springs. Santa Venera al Pozzo (SVP) and the Salinelle of Paternò are highlighted, together with cold springs and historical thermal baths. Archaeological sites are scaled according to the number of preserved structures and color-coded by cultural period (Biscari, 1781; Brancato and Tortorici, 2021; Branca et al., 2021). Lava flows from Branca et al., (2011) and Proietti et al., (2024).
(b) Close-up of the SVP area showing archaeological features and hydrothermal manifestations (Brusca et al., 2001), superimposed on local geological synthems (De Beni et al., 2011): Aci Trezza (pillow lavas from submarine eruptions on a sedimentary basement), Acireale (massive lava flows from fissural subaerial eruptions), S. Alfio (lavas and pyroclastics from subaerial eruptions), Concazze and Il Piano (lavas and pyroclastics from polygenetic volcanoes). Synthems indicated with colored patterns outside the study area are not discussed.
(c) Pie charts showing the proportions of hot and cold springs, and a histogram illustrating the distribution of lava-flow surfaces by age (Brusca et al., 2001).

2. Geological and Seismotectonic Framework

The southeastern flank of Mount Etna is one of the most tectonically active sectors of the volcano and is affected by a dense network of Quaternary normal faults belonging to the Timpe Fault System (TFS), which accommodates a significant portion of the seaward sliding of the volcanic edifice (Fig.2; Azzaro et al., 2012; Tibaldi et al., 2016). These structures are characterized by steep fault scarps, aligned eruptive fissures and diffuse ground deformation, reflecting the interaction between regional tectonic stress, magmatic intrusion and gravitational instability (Branca & Abate, 2017).

The TFS is composed of several N–S striking fault segments (e.g. Fiandaca, Aci Platani and Aci Catena faults) that locally show surface faulting, aseismic creep and repeated shallow seismic ruptures (Azzaro et al., 2000; Azzaro & D'Amico, 2019). Instrumental seismicity is dominated by shallow earthquakes (generally < 5 km depth, M ≤ 5), often organized in swarms, which are interpreted as the surface expression of stress redistribution processes affecting the unstable eastern flank.

Geodetic observations indicate that these faults are kinematically linked to the long-term eastward motion of the flank, while transient deformation episodes, including slow slip events (SSEs), locally modify stress conditions and fault permeability (Palano et al., 2024). The spatial coincidence between active fault traces, thermal springs and soil gas anomalies demonstrates that these structures act as long-lived, permeable pathways for geofluid ascent (Giammanco et al., 1997; Liotta et al., 2017).

Santa Venera al Pozzo is located at the intersection of major TFS segments, where repeated fault reactivation has favoured the development of a localized hydrothermal system, making the area particularly sensitive to fluid–fault interactions.

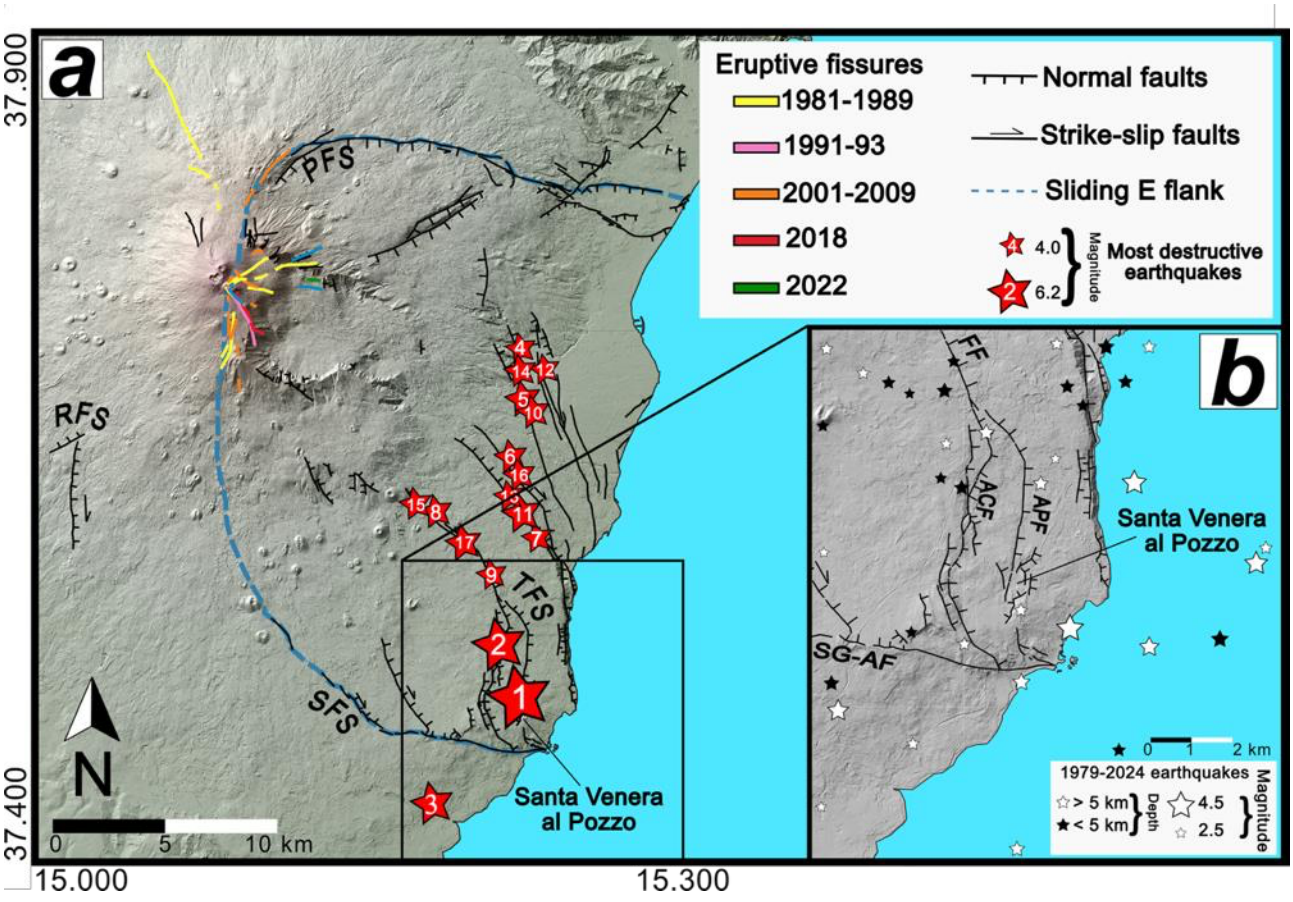

Fig.2 - Tectonic structures and seismicity of Mount Etna's southeastern flank.
(a) Main fault systems and eruptive fissures. Fault abbreviations: PFS = Pernicana Fault System; RFS = Ragalna Fault System; SFS = South Fault System; TFS = Timpe Fault System; FF = Fiandaca Fault; SG–AF = San Gregorio–Acitrezza Fault; APF = Aci Platani Fault; ACF = Aci Catena Fault. Epicenters of major historical earthquakes are shown as stars and numbered according to their reference in Table 1 (Guidoboni et al., 2014; Guidoboni et al., 2019; Azzaro and D'Amico, 2019).
(b) Instrumental seismicity from 1981 to 2024, color-coded by depth. Faults data from Azzaro et al. (2012) and Branca et al. (2011); eruptive fissures from Bevilacqua et al. (2022) and Proietti et al. (2024).

3. Data and Methods

This study is based on the integration of geodetic, seismic and geochemical datasets acquired on Mount Etna's southeastern flank over different temporal scales, with particular focus on the role of geofluids in fault dynamics and hydrothermal circulation.
Geodetic data consist of continuous GNSS time series recorded between 2006 and 2024 by the INGV permanent network. Stations located on the summit area and on the lower southeastern flank were selected to capture both long-term eastward sliding of the volcanic edifice and transient deformation episodes. These data allow the identification of slow slip events (SSEs) and aseismic fault motion affecting shallow fault segments (Palano et al., 2024).
Seismic data were obtained from INGV instrumental catalogues and include local earthquakes with magnitudes generally lower than 5 and hypocentral depths mostly shallower than 5 km (Azzaro et al., 2000; Alparone et al., 2020; Barberi et al., 2020). Seismicity is mainly organized in swarms and spatially clustered along the Timpe Fault System, providing constraints on active fault segments and stress redistribution processes (Azzaro et al., 2012; Azzaro et al., 2013; Bonforte et al., 2013).
Geochemical data include long-term monitoring of thermal waters and gas emissions at Santa Venera al Pozzo (SVP). Gas measurements focus on CO_2, CH_4 and H_2S concentrations, acquired through discrete sampling and continuous micro-gas chromatograph monitoring. These datasets document both the long-term stability of the hydrothermal system and short-lived geochemical anomalies associated with tectonic stress variations, including pre-seismic signals observed before the 26 December 2018 Fiandaca earthquake (Liotta et al., 2017; Sortino et al., 2022).
Additional constraints are provided by soil CO_2 flux surveys carried out in the SVP area, which highlight the spatial correspondence between degassing anomalies and active fault traces, confirming the structural control on geofluid migration (Giammanco et al., 1997).
Archaeological data from Santa Venera al Pozzo are used as a long-term indicator of persistent hydrothermal activity and geothermal resource availability. The continuous exploitation of thermal springs from the Hellenistic period to the Middle Ages provides independent evidence that fault-controlled fluid pathways have remained active over millennial timescales (Branciforti, 2006; Bottari et al., 2020).

4. Results

Given this seismotectonic setting, deformation and fluid migration on the southeastern flank of Mount Etna are strongly controlled by transient stress changes affecting shallow fault segments. GNSS time series reveal persistent eastward motion of the southeastern flank, superimposed by millimetric SSEs lasting days to weeks (Palano et al., 2024). These aseismic deformation episodes are interpreted as fluid-assisted slip along shallow fault segments, where elevated pore pressure reduces effective normal stress (Sibson, 1992).

Geochemical data show a hydrothermal system dominated by crustal CO_2 and CH_4, with transient anomalies temporally associated with tectonic stress changes. In particular, increases in methane and hydrogen sulfide concentrations were observed prior to the 26 December 2018 Fiandaca earthquake, indicating permeability enhancement and upward migration of deep geofluids in response to stress accumulation (Sortino et al., 2022).
Archaeological evidence documents continuous exploitation of the SVP thermal springs from the Hellenistic period to the Middle Ages, despite recurrent seismic and volcanic activity (Branciforti, 2006; Bottari et al., 2020). The spatial coincidence between ancient hydraulic structures, modern degassing anomalies and active faults suggests long-term persistence of fault-controlled geofluid pathways.

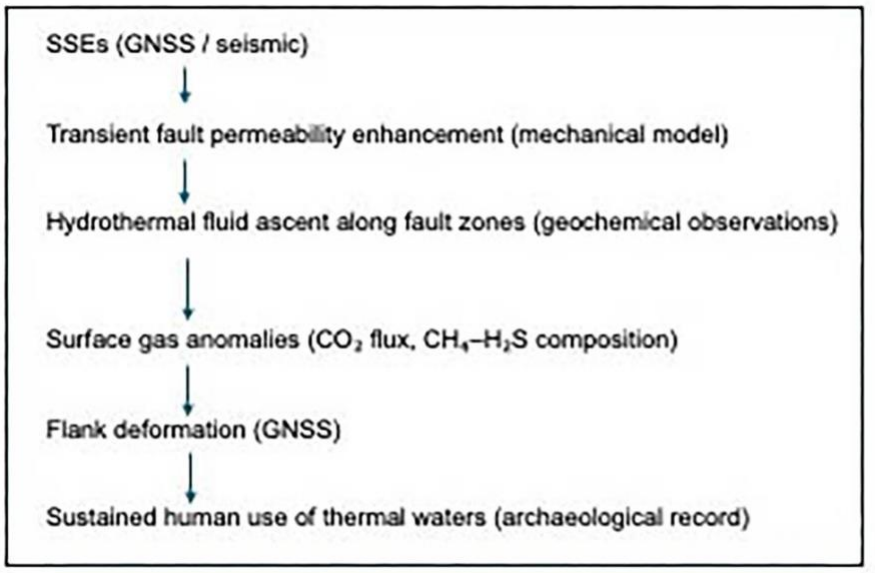

Fig.3 - Conceptual model linking shallow SSE-driven stress redistribution, transient permeability enhancement, fault-guided ascent of hydrothermal fluids, episodic gas anomalies, flank deformation and long-term human use of thermal resources on the southeastern flank of Mt. Etna.

5. Discussion and Conclusions

The integrated dataset supports a model in which geofluids play an active role in modulating fault mechanics on Mount Etna's southeastern flank (Fig. 3). Shallow SSEs and fault creep are interpreted as fluid-assisted deformation processes, where transient increases in permeability promote hydrothermal circulation and surface degassing, in agreement with classical models of pore-pressure–controlled fault behaviour (Sibson, 1992; Giammanco et al., 1997; Palano et al., 2024). The long-term archaeological record indicates that these geofluid pathways have remained active over millennial timescales, sustaining geothermal resources despite ongoing deformation. This study highlights the central role of geofluids in coupling earthquakes, volcanic deformation and geothermal systems, and demonstrates how integrating geophysical and geochemical observations with long-term indicators can improve our understanding of fault dynamics in active volcanic regions.

References

Alparone S., Barberi G., Giampiccolo E., Maiolino V., Mostaccio A., Musumeci C.; 2020: Seismological constraints on the 2018 Mt. Etna (Italy) flank eruption and implications for the flank dynamics of the volcano. *Terra Nova*, 32, 334–344.

Azzaro R., Barbano M.S., D'Amico S., Mostaccio A.; 2000: Tectonic and volcanic deformation at Mt. Etna: Constraints from geodetic and seismic data. *Journal of Geodynamics*, 29, 187–210.

Azzaro R., D'Amico S.; 2019: Catalogo Macrosismico dei Terremoti Etnei (CMTE). INGV.

Azzaro R., Bonforte A., Branca S., Guglielmino F.; 2013: Geometry and kinematics of the fault systems controlling the unstable flank of Etna volcano (Sicily). *Journal of Volcanology and Geothermal Research*, 160, 210–222.

Azzaro R., Branca S., Gwinner K., Coltelli M.; 2012: The volcano-tectonic map of Etna volcano, 1:100,000 scale. *Italian Journal of Geosciences*, 131, 153–170.

Barberi G., Di Grazia G., Ferrari F., Giampiccolo E., Maiolino V., Mostaccio A., et al.; 2020: Mt. Etna Revised Seismic Catalog 2020 (EtnaRSC2020). INGV.

Bevilacqua A., Azzaro R., Branca S., D'Amico S., Flandoli F., Neri A.; 2022: Quantifying the statistical relationships between flank eruptions and major earthquakes at Mt. Etna volcano (Italy). *Journal of Geophysical Research: Solid Earth*, 127.

Biscari I.P.; 1781: *Viaggio per tutte le antichità della Sicilia*. Stamperia Simoniana, Napoli.

Bonaccorso A., Calvari S.; 2013: Major effusive eruptions and recent lava fountains: Balance between expected and erupted magma volumes at Etna volcano. *Geophysical Research Letters*, 40, 6069–6073.

Bonforte A., Guglielmino F., Puglisi G.; 2013: Interaction between magma intrusion and flank dynamics at Mt. Etna in 2008 from integrated GPS and DInSAR data. *Geochemistry, Geophysics, Geosystems*, 14, 2818–2835.

Bottari C., Giammanco S., Cavallaro D., Sortino F., Scudero S., Amari S., Bonfanti P., Daolio M., Groppelli G.; 2020: Multidisciplinary detection of hidden faults and historical earthquake damage in archaeological sites: The mid-third century CE Mt. Etna earthquake. *Tectonophysics*, 790, 228544.

Branca S., Abate T.; 2017: Geological evolution of Mount Etna volcano. In: Branca S., Coltelli M., Groppelli G., Lentini F. (eds.), *The Geology of Mount Etna*. Geological Society, London, Memoirs, 47, 1–39.

Branca S., Coltelli M., Groppelli G., Lentini F.; 2011: Geological map of Etna volcano, 1:50,000 scale. *Italian Journal of Geosciences*, 130, 265–291.

Branca S., Privitera F., Palio O., Turco M.; 2021: Prehistoric human presence on Mount Etna (Sicily) in relation to geological evolution. *Annals of Geophysics*, 64(5), VO542.

Brancato R., Tortorici E.; 2021: *Carta Archeologica del territorio delle Aci*. Edizioni Quasar, Roma.

Branciforti M.G.; 2006: *L'area archeologica di Santa Venera al Pozzo – Acium*. Antiquarium, Palermo.

Brusca L., Aiuppa A., D'Alessandro W., Parello F., Allard P., Agnès M.; 2001: Geochemical mapping of magmatic gas–water–rock interactions in the aquifer of Mount Etna volcano. *Journal of Volcanology and Geothermal Research*, 108, 199–218.

Chiodini G., Frondini F., Raco B.; 1996: Diffuse emission of CO_2 from the Fossa crater, Vulcano Island (Italy). *Bulletin of Volcanology*, 58, 41–50.

De Beni E., Branca S., Coltelli M., Groppelli G.; 2011: $^{40}Ar/^{39}Ar$ isotopic dating of the Etna volcanic succession. *Italian Journal of Geosciences*, 130(3), 292–305.

Giammanco S., Parello F., D'Alessandro W.; 1997: Soil CO_2 degassing along tectonic structures of Mount Etna (Sicily). *Applied Geochemistry*, 12, 429–436.

Guidoboni E., Ciuccarelli C., Mariotti D., Comastri A., Bianchi M.G.; 2014: *L'Etna nella Storia*. Bononia University Press, Bologna.

Guidoboni E., Ferrari G., Tarabusi G., Sgattoni G., Comastri A., Mariotti D., Ciuccarelli C., Bianchi M.G., Valensise G.; 2019: CFTI5Med: Catalogue of strong earthquakes in Italy. *Scientific Data*, 6, 188.

Liotta M., D'Alessandro W., Arienzo I., Longo M.; 2017: Tracing the circulation of groundwater in volcanic systems using the $^{87}Sr/^{86}Sr$ ratio: Application to Mt. Etna. *Journal of Volcanology and Geothermal Research*, 331, 102–107.

Palano M., Pezzo G., Chiarabba C.; 2024: Magma budget, plutonic growth and lateral spreading at Mt. Etna. *Communications Earth & Environment*, 5, 95.

Proietti C., De Beni E., Cantarero M.; 2024: One hundred lava flows of Mt. Etna, Italy: July 2019–December 2023 update. *Journal of Maps*, 20, 1–13.

Sibson R.H.; 1992: Implications of fault-valve behaviour for rupture nucleation and recurrence. *Tectonophysics*, 211, 283–293.

Sortino F., Giammanco S., Bonfanti P., Bottari C.; 2022: Stress-induced changes in hydrothermal gas discharges along active faults near Mt. Etna volcano (Sicily, Italy). *Tectonophysics*, 836, 229388.

Tibaldi A., Bonali F.L., Corazzato C., Apuani T.; 2016: Tectonics of Mount Etna volcano. *Journal of Volcanology and Geothermal Research*, 327, 581–597.

Walter T.R., Troll V.R., Cailleau B., Belousov A., Schmincke H.-U., Amelung F.; 2005: Magma-induced stress and fluid migration. *Geophysical Research Letters*, 32, L05307.

Corresponding author: carla.bottari@ingv.it

Interpretation of corrected sea floor HVSR data on a gas emitting structure in the Sea of Marmara

A. Brindisi[1,2], S. D'Amico[3,4], L. Beranzoli[3], D. Embriaco[3], A. Giuntini[3], D. Albarello[1,5]

[1]Dipartimento di Scienze Fisiche, della Terra e dell'Ambiente, Università degli Studi di Siena, Siena, Italia
[2]Museo Nazionale dell'Antartide "Felice Ippolito", Università degli Studi di Siena, Siena, Italia
[3]Istituto Nazionale di Geofisica e Vulcanologia, Sezione Roma2, Roma, Italia
[4]Università di Catania, Dipartimento di Scienze Biologiche, Geologiche e Ambientali, Sezione di Scienze della Terra, Catania, Italia
[5]Consiglio Nazionale delle Ricerche, Istituto di Geologia Ambientale e Geoingegneria, Rome, Italia

In the last years multiple studies have proposed measurements of ambient vibrations as an efficient seismic methodology to investigate the location and characteristics of hydrocarbon reservoirs (e.g., Lambert et al., 2007; Saenger et al., 2009). Inland gas reservoirs associated with mud volcano fields in Italy (Antunes et al., 2022; Brindisi et al., 2025; Grassi et al., 2022; Panzera et al., 2016) show specific Horizontal to Vertical Spectral Ratio (HVSR) of ambient vibrations signatures, and this method (for an extensive methodological review see Molnar et al., 2022) has been widely applied worldwide as a fast and effective tool for inland subsurface seismic characterization in many different contexts (e.g., Mele et al., 2021; Comina et al., 2023; Keskinsezer et al., 2023). In this framework, the aim of this study is to extend the application of HVSR analysis offshore, where Ocean Bottom Seismometer (OBS) data are available, to constrain the local seismostratigraphical configuration of the offshore subsoil and characterize potential gas reservoirs.

The study focuses on an offshore gas-emitting structure corresponding to the submerged westernmost edge of the North Anatolian Fault (NAF) in the İzmit Gulf area (Eastern Mediterranean) (Fig. 1), where methane seepage from the seabed is present (Embriaco et al., 2014). To apply the inversion procedures commonly considered for the interpretation of HVSR inland (Brindisi et al., 2025) to sea-bottom observations, the effect of the water column must be accurately removed.

A new correction procedure derived from the approach proposed by Albarello (2025) is introduced to account for resonance effects of the water column and to recover an HVSR curve comparable to that obtained inland. This method is based on the body-wave model by Herak (2008) and enables the use of the well-established inversion procedure implemented by Bignardi et al. (2016).

It has been suggested that strong water flows can significantly affect the HVSR pattern at very low frequencies (< 0.2 Hz) due, for example, to sensor tilting. At higher frequencies, however, these water-flow-related effects mainly produce minor changes in peak amplitudes without affecting peak frequencies. Accordingly, we assume that the relevant part of the HVSR pattern remains only weakly influenced by oceanic disturbances and still provides valuable information on the subsoil structure in terms of V_s and V_p profiles, similarly to inland conditions.

The inversion results reveal three main seismic impedance contrasts at approximately 10, 100 and 500 m below the seafloor (Fig. 2), in good agreement with geological unconformities detected by seismic reflection data (Kurt and Yücesoy, 2009; Mitchum et al., 1977; Okyar et al., 2008). Moreover, interpretation of body-wave-derived velocity profiles and of V_p/V_s ratios (Tinivella, 2002) suggests the presence of unconsolidated material down to about 500 m below sea level, with an estimated porosity on the order of 10%. The good fit between the body-wave velocity profiles and those inferred by Biot–Gassmann Theory by Lee (BGTL) modelling (Lee, 2004) further indicates that gas plays a significant role in this area, with a preliminary estimate of gas saturation of approximately 50% of pore space between 100 and 500 m depth.

These findings demonstrate that HVSR analysis from OBS measurements provides a promising methodology for offshore subsurface characterization in gas-bearing environments. Furthermore, the combination of HVSR inversion and BGTL modelling shows potential for estimating gas concentration within marine reservoir systems, thereby confirming the effectiveness and practical applicability of this integrated approach.

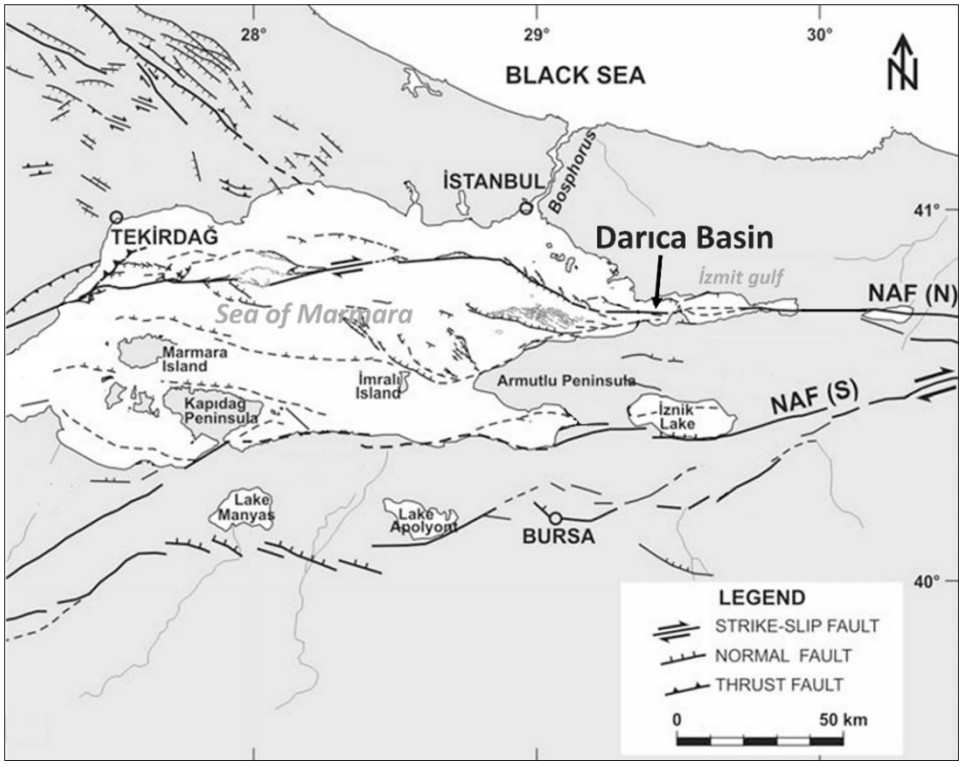

Fig. 1 – Tectonic map of the Marmara region modified from Okyar et al., 2008.

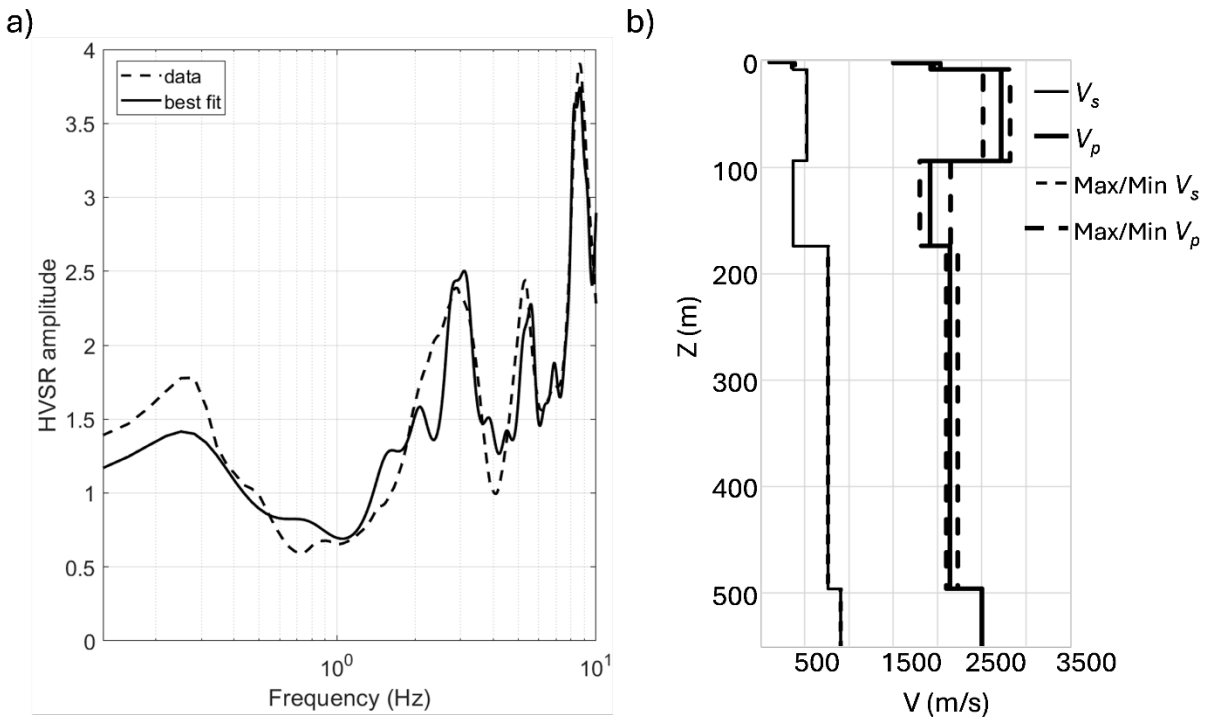

Fig. 2 – Inversion of the HVSR experimental curves after the removal of the water column effects. a) Comparison between the best fitting HVSR curve obtained by the inversion procedure (solid line) and the data, represented by the mean HVSR curve (dashed line), corresponding to periods of low flow intensity. b) The solid black line represents the V_s profile considered to obtain the best fitting curve in (a), the dashed black lines represent the profile of the maximum and minimum V_s value at each depth. The solid bold black line represents the V_p profile considered to obtain the best fitting curve in (a), the dashed bold black lines represent the profile of the maximum and minimum V_p value at each depth.

References

Albarello D.; 2025: Reducing Horizontal to Vertical Spectral Ratios of ambient vibrations measured at the sea bottom to inland equivalent values. Mar. Geophys. Res., 46, 29, https://doi.org/10.1007/s11001-025-09591-6

Antunes, V., Planès, T., Obermann, A., Panzera, F., D'Amico, S., Mazzini A., Lupi, M.; 2022: Insights into the dynamics of the Nirano Mud Volcano through seismic characterization of drumbeat signals and V/H analysis. J. Volcanol. Geoth. Res., 431, 107619. https://doi.org/10.1016/j.jvolgeores.2022.107619

Bignardi, S., Mantovani, A., Zeid, N.A.; 2016: OpenHVSR: imaging the subsurface 2D/3D elastic properties through multiple HVSR modeling and inversion. Comput. Geosci. 93, 103–113. https://doi.org/10.1016/j.cageo.2016.05.009

Brindisi, A., Paolucci, E., Carfagna, N., Albarello, D.; 2025: Passive seismic measurements to characterize gas reservoirs in a mud volcano field in Northern Italy. Mar. Pet. Geol., 173, p.107275. https://doi.org/10.1016/j.marpetgeo.2024.107275

Comina, C., Di Chiara, G., Foti, S.; 2023: On the direct estimation of bedrock depth and time-weighted average VS from surface waves dispersion and HVSR curves. J. Appl. Geophys., 215, 105086, https://doi.org/10.1016/j.jappgeo.2023.105086

Embriaco, D., Marinaro, G., Frugoni, F., Monna, S., Etiope, G., Gasperini, L., Polonia, A., Del Bianco, F., Çağatay, M.N., Ulgen, U.B., Favali, P.; 2014: Monitoring of gas and seismic energy release by multiparametric benthic observatory along the North Anatolian Fault in the Sea of Marmara (NW Turkey). Geophys. J. Int., 196(2), pp.850-866. https://doi.org/10.1093/gji/ggt436

Grassi, S., De Guidi, G., Patti, G., Brighenti, F., Carnemolla, F., Imposa, S.; 2022: 3D subsoil reconstruction of a mud volcano in central Sicily by means of geophysical surveys. Acta Geophys., 70(3), 1083-1102. https://doi.org/10.1007/s11600-022-00774-y

Herak, M.; 2008: ModelHVSR-A Matlab tool to model horizontal-to-vertical spectral ratio of ambient noise. Comput. Geosci. 34, 1514–1526. https://doi.org/10.1016/j. cageo.2007.07.009

Keskinsezer, A., Karaaslan, H., Silahtar, A., Beyhan, G.; 2023: The soil characterization of the region between the Maltepe-Beykoz Fault and the Marmara Sea in İstanbul (Türkiye) with the integrated HVSR (Nakamura technique) and MASW method. J. Appl. Geophys.,219, 105245. https://doi.org/ 10.1016/j.jappgeo.2023.105245

Kurt, H., Yücesoy, E.; 2009: Submarine structures in the Gulf of İzmit, based on multichannel seismic reflection and multibeam bathymetry. Mar. Geophys. Res., 30(2), pp.73-84. https:// doi.org/10.1007/s11001-009-9068-y

Lambert, M, Schmalholz, S.M, Podladchikov, Y.Y., Saenger, E.H.; 2007: Low frequency anomalies in spectral ratios of single station microtremor measurements: observations across an oil and gas field in Austria. In: 77th Annual international meeting, SEG, extended abstracts, 1352–1356. https://doi.org/10.1190/1.2792751

Lee, M.W.; 2004: Elastic velocities of partially gas-saturated unconsolidated sediments. Mar. Pet. Geol. 21 (6), 641–650. https://doi.org/10.1016/j.marpetgeo.2003.12.004

Mele, M., Bersezio, R., Bini, A., Bruno, M., Giudici, M., Tantardini, D.; 2021: Subsurface profiling of buried valleys in central alps (northern Italy) using HVSR single-station passive seismic. J. Appl. Geophys., 193, 104407, https://doi.org/10.1016/j.jappgeo.2021.104407

Mitchum, R.M., Vail, P.R., Sangree, J.B.; 1977: Seismic stratigraphy and global changes of sea level, Part 6: stratigraphic interpretation of seismic reflection patterns in depositional sequences. In: Payton CE (ed) Seismic stratigraphy-applications to hydrocarbon exploration. AAPG Mem., 26, Tulsa, Oklahoma, pp. 117–133. https://doi.org/10.1306/M26490C8

Molnar, S., Sirohey, A., Assaf, J., Bard, P.Y., Castellaro, S., Cornou, C., Cox, B., Guillier, B., Hassani, B., Kawase, H., Matsushima, S.; 2022: A review of the microtremor horizontal-to-vertical spectral ratio (MHVSR) method. J. Seismol., 26(4), pp.653-685. https://doi.org/10.1007/s10950-021-10062-9

Okyar, M., Pinar, A., Tezcan, D., Kamaci, Z.; 2008: Late quaternary seismic stratigraphy and active faults of the Gulf of Izmit (NE Marmara Sea). Mar. Geophys. Res., 29, pp. 89-107. https://doi.org/10.1007/s11001-008-9049-6

Panzera, F., Sicali, S., Lombardo, G., Imposa, S., Gresta, S., D'Amico, S.; 2016: A microtremor survey to define the subsoil structure in a mud volcanoes area: the case study of Salinelle (Mt. Etna, Italy). Environ. Earth Sci., 75, 1-13. https://doi.org/10.1007/s12665-016-5974-x

Saenger, E.H., Schmalholz, S.M., Lambert, M.A., Nguyen, T.T., Torres, A., Metzger, S., Habiger, R.M., Müller, T., Rentsch, S., Méndez-Hernández, E.; 2009: A passive seismic survey over a gas field: Analysis of low-frequency anomalies. Geophysics, 74(2), O29-O40. https://doi.org/10.1190/1.3078402

Tinivella, U.; 2002: The seismic response to over-pressure versus gas hydrate and free gas concentration. J. Seism. Explor. 11 (3), 283–305.

Corresponding author: albachiara.brindi@student.unisi.it

Fault–Fluid Interactions and Vents Distribution Offshore Campi Flegrei: Insights from Ultra-High-Resolution 3D Seismic Interpretation

C. Cirelli[1], M. Corradino[1], D. Iacopini[2], P. Burrato[3], H. Duarte[4], L. Ferranti[2], V. Maselli[5], C. Monaco[6], O. Monrigal[7], M. Sacchi[8], F. Pepe[1]

[1] Dipartimento di Scienze della Terra e del Mare, Palermo University, Italy
[2] Dipartimento di Scienze della Terra, dell'Ambiente e delle Risorse, Federico II Napoli University, Italy
[3] Istituto Nazionale di Geofisica e Vulcanologia, Roma, Italy
[4] GeoSurvey Lda, Aveiro, Portugal
[5] Dipartimento di Scienze Chimiche e Geologiche, Modena and Reggio Emilia University, Italy
[6] Dipartimento di Scienze Biologiche, Geologiche e Ambientali, Catania University, Italy
[7] Geo Marine Survey System B.V., Rotterdam, The Netherlands
[8] Istituto per l'Ambiente Marino Costiero, Consiglio Nazionale delle Ricerche, Napoli, Italy

The offshore sector of Campi Flegrei (Gulf of Pozzuoli, southern Italy), within the Neapolitan Yellow Tuff (NYT) caldera system, is characterised by active volcano-tectonic deformation, caldera-floor uplift (resurgence), and intense hydrothermal activity. The area has been extensively investigated to delineate the structural architecture and geological evolution of the system (e.g., Sacchi et al., 2014; Corradino et al., 2021; Natale et al., 2022), but despite previous works, the metre-scale geometry of the apical fault network associated with the resurgent dome, and its role in controlling shallow fluid migration, remain poorly constrained. Conventional 2D seismic data generally lack the vertical and lateral resolution and areal coverage required to image such small-scale structures. As a result, the identification of hydrothermal vents and the relationship between fault architecture, fluid migration, and local stress redistribution - potentially linked to seismicity - remain poorly understood in the marine sector of the resurgent dome.

This study exploits ultra-high-resolution (UHR) 3D seismic reflection data acquired in the Gulf of Pozzuoli (Fig. 1), enabling metre-scale imaging of tectonic structures, seismo-stratigraphic units, sedimentary architectures, and fluid-related features. Fluid migration is inferred from seismic responses such as amplitude anomalies, and bright spots that crosscut major seismo-stratigraphic boundaries, suggesting active ascent pathways. To enhance both structural and fluid-related signals, a suite of seismic attributes was applied to the 3D volume. Discontinuity and structural attributes (e.g., semblance, variance, dip, and azimuth) support detailed fault delineation, while amplitude- and frequency-related attributes (e.g., RMS amplitude, chaos, spectral measures, and frequency decomposition) highlight potential fluid-charged sediments and migration pathways. Vents are identified as vertically persistent disturbance zones characterised by amplitude blanking,

bright spots and polarity reversals that are coherent across multiple attribute domains and traceable toward shallow reflectors.

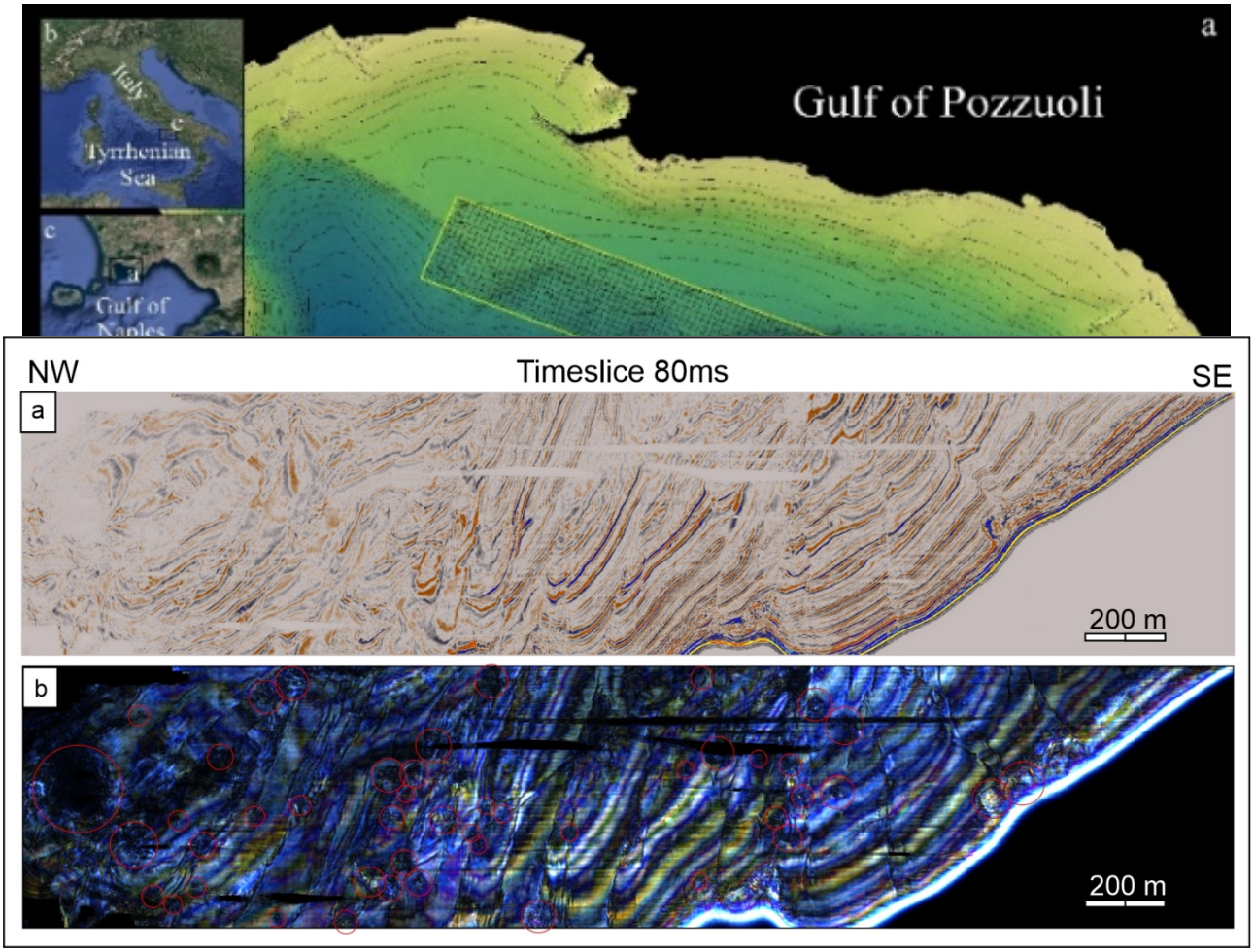

Fig. 1 – **a)** Bathymetric map of Gulf of Pozzuoli and location of the UHR3D seismic volume (yellow box). **b)** Localization of the study area in Italy with **c)** zoom of Gulf of Naples.

The 3D seismic interpretation (Fig. 2) resolves the metre-scale fault architecture of the resurgent dome summit area, including fault strikes, dips, spatial extent, segmentation, and network geometry. More than 60 predominantly normal faults are identified, organised into distinct strike domains that define an overall radial pattern converging toward the centre of resurgence. Dominant fault orientations are NE–SW, NNE–SSW and NNW–SSE, with a subordinate ENE–WSW set.

Fig. 2 – Bathymetric map of Gulf of Pozzuoli with fault segments (red lines) organized with radial geometry.

Integrated interpretation and attribute analysis allowed the identification and mapping of approximately 50 vent-related features within the shallow substrate. These vents display variable geometries, with horizontal dimensions ranging from 20 to 50 m and vertical extents reaching up to approximately 60 m. They initiate at different seismo-stratigraphic levels and commonly terminate in paleo-pockmark-like features, indicating episodic discharge and stratigraphically

controlled sealing. Spatial comparison with the reconstructed fault network shows that vent distribution is only partially fault-controlled: while some vents align with mapped fault planes and associated discontinuities, others are laterally offset from major fault traces (Fig. 3).

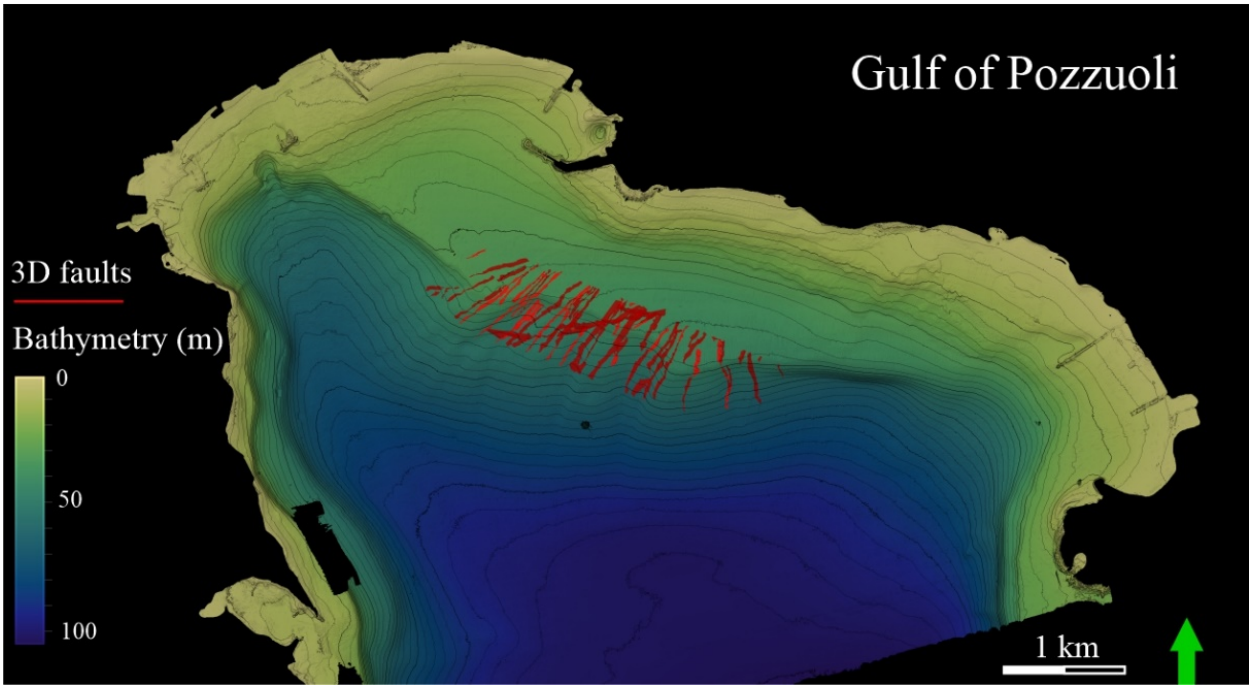

Fig. 3 – Time-slice visualization at 80 ms depth for vents mapping of the marine sector of the resurgent dome within the Flegrean Fields. a) Time-slice displayed in amplitude, after noise reduction. Blue/yellow scale gradational colour adopted to highlights zones of reduced amplitude signal. b) Blend view of time-slice 80 ms after spectral analysis and frequency decomposition. RGB scale: R = 988.24 Magnitude, G = 763.64 Magnitude, B = 525.00 Magnitude. Red circles represent the fluid vents mapped at 80 ms depth.

Overall, the integration of UHR3D imaging and attribute-driven interpretation provides a robust and reproducible framework to resolve fault–fluid interactions in the offshore Campi Flegrei system. The radially organised fault network locally focuses fluid ascent, yet the distribution of vent-related features demonstrates that migration pathways are not exclusively confined to fault planes. This points to spatially heterogeneous permeability and temporally episodic hydrothermal discharge within the shallow subsurface, with important implications for understanding hydrothermal circulation and its coupling with volcano-tectonic deformation during unrest.

References

Corradino, M. et al.; 2021: Resurgent uplift at large calderas and relationship to caldera-forming faults and the magma reservoir: New insights from the Neapolitan Yellow Tuff caldera (Italy). Journal of Volcanology and Geothermal Research, Vol. 411, 107183, https://doi.org/10.1016/j.jvolgeores.2021.107183

Natale, J. et al.; 2022: Fault systems in the offshore sector of the Campi Flegrei caldera (southern Italy): Implications for nested caldera structure, resurgent dome, and volcano-tectonic evolution Journal of Structural Geology, Vol. 163, 104723, https://doi.org/10.1016/j.jsg.2022.104723

Sacchi, M. et al. 2014: The Neapolitan Yellow Tuff caldera offshore the Campi Flegrei: Stratal architecture and kinematic reconstruction during the last 15 ky. Marine Geology, Vol. 354, pp. 15-33, https://doi.org/10.1016/j.margeo.2014.04.012

Corresponding author: claudia.cirelli@unipa.it

3D Audio-Magnetotelluric Imaging of the Aeolian Islands for Geothermal Resource Assessment

C. De Paola, M.G. Di Giuseppe, R. Isaia, A. Troiano, P. Boni, A. Fedele, G. Gonzalez, F. Pagliara, M. Sposato.

INGV - Sezione di Napoli - Osservatorio Vesuviano - Naples - Italy

Introduction

The Aeolian archipelago (Southern Italy) hosts several volcanic islands characterized by active hydrothermal manifestations and represents a strategic area for evaluating geothermal resources in insular settings. Within the IRGIE project, the primary objective is to build a comprehensive inventory of geothermal resources across the Aeolian Islands, providing a scientific basis for evaluating their potential contribution to local energy supply and possible energy autonomy.

The assessment of geothermal resources in volcanic areas requires robust constraints on subsurface structure, fluid circulation, and permeability distribution. In this context, geophysical methods play a key role by providing indirect but quantitative information on the physical properties of the subsurface and on the structural controls governing hydrothermal systems.

This study presents the results of a large-scale geophysical investigation carried out on the islands of Lipari, Salina, Vulcano, and Panarea, providing a geophysically constrained geothermal assessment at the archipelago scale.

The focus is on the application of the *Audio-Magnetotelluric (AMT)* method, which allows three-dimensional imaging of subsurface electrical resistivity and provides key constraints on hydrothermal alteration, fluid circulation, and the structural framework relevant to geothermal exploration.

Geological and Volcanological Setting

The Aeolian Islands form a volcanic arc in the southern Tyrrhenian Sea related to the subduction of the African plate beneath the Eurasian plate. Their geological evolution is controlled by the interaction between regional tectonic structures, primarily NW-SE striking fault systems and NE-SW extensional trends, shallow magmatism, and widespread hydrothermal circulation (Ventura et al., 1999; De Astis et al., 2003).
The four islands investigated in this study exhibit distinct geological features (Forni et al., 2013) that influence their geothermal potential.

Vulcano, as the southernmost island, is an active system characterized by high-enthalpy geothermal potential. It is very recent history is dominated by the activity of the *La Fossa* cone, where vigorous fumarolic degassing presently occurs. The subsurface is a complex overlapping of varying magmatic products (lavas, pyroclastics), intersected by volcano-tectonic structures, facilitating the rise of magmatic gases and also the circulation of meteoric water, which favors the development of a wide shallow hydrothermal system.
Panarea, although smaller, is part of a vast, largely submerged volcanic complex. It hosts an active hydrothermal system, most clearly expressed by the intense underwater degassing near the islets to the east. The structural setting here is dominated by NE-SW faults that act as preferential pathways for hot fluids rising from depth.
Lipari, the largest island of the archipelago, shows a complex history of recurrent volcanic activity, with the most recent eruptions (rhyolitic pumice and obsidian flows) occurring in medieval times. While surface thermal manifestations are less vigorous than at Vulcano, the presence of distinct thermal springs and fumaroles suggests a residual thermal anomaly and a potentially exploitable medium-enthalpy resource.
Salina, in contrast to its neighbors, is considered the most "volcanically mature" of the group, with no eruptions in the Holocene. It consists of twin stratovolcanoes (*Monte Fossa delle Felci* and *Monte dei Porri*). The geothermal interest here lies in investigating whether deep hydrothermal circulation persists despite the lack of recent eruptive activity, potentially offering low-enthalpy resources for direct uses.

Methodology

The audio-magnetotelluric method is a passive electromagnetic technique that reconstructs the spatial distribution of electrical resistivity by measuring natural variations of the electric and magnetic fields over a frequency range suitable for imaging the shallow to intermediate crust (Simpson & Bahr, 2005).
In volcanic environments, AMT surveys are particularly effective for characterizing surface geothermal systems, both in terms of geometric definition and physical properties, as electrical resistivity is highly sensitive to fluid content, temperature, and hydrothermal alteration (Muñoz, 2014). In addition, AMT provides key constraints on major structural discontinuities controlling fluid circulation at depth (Spichak & Manzella, 2009).
Measurements were carried out using a Geode-EM3D system (Geometrics), equipped with electric dipoles and low-frequency magnetometers, covering a frequency band from 0.1 to 10^5 Hz. A total of 153 soundings were acquired across the islands of Vulcano, Panarea, Lipari, and Salina (Fig. 1) representing one of the densest geophysical datasets collected in the Aeolian archipelago.

Fig. 1 – Location of the AMT survey carried out on the islands of Lipari, Salina, Vulcano, and Panarea (Aeolian archipelago in Southern Italy).

Survey locations were designed to cover both areas characterized by active hydrothermal manifestations and peripheral sectors of the islands. Data processing included robust techniques to mitigate anthropic electromagnetic noise, followed by three-dimensional inversion using the ModEM code (Egbert and Kelbert, 2012) incorporating both bathymetry and topography. All inversions achieved stable convergence with RMS misfits consistently below 5.

Results

The 3D AMT resistivity models reveal a marked variability in subsurface electrical structure across the investigated islands, reflecting differences in geothermal system development, fluid circulation, and structural control. The results do not indicate a uniform geothermal structure across the archipelago, but instead highlight island-specific resistivity patterns.

At Vulcano, the resistivity structure is characterized by a prominent resistive body located beneath the La Fossa crater, extending from shallow levels down to depths exceeding 2–2.5 km b.s.l. This anomaly is interpreted as a conduit-like structure permeated by deep, hot magmatic fluids and represents the main pathway for fluid ascent. Surrounding this resistive core, a shallow conductive domain is imaged within the upper few hundred meters, consistent with a hydrothermal system affected by intense alteration and saline fluids. Sharp resistivity contrasts delineate caldera-related structures and major volcano-tectonic lineaments, particularly along a N–S direction, which exert a strong control on fluid circulation and surface degassing (Fig. 2). The spatial correspondence

between resistivity contrasts and degassing areas confirms the key role of structural control in the Vulcano geothermal system.

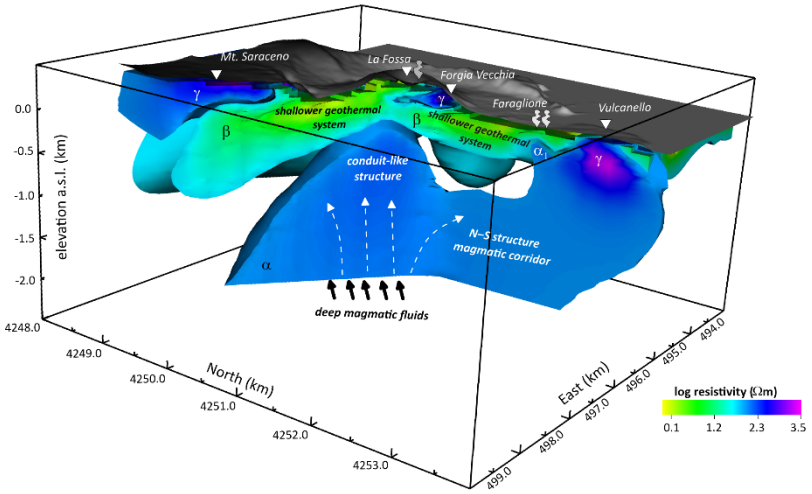

Fig. 2 – 3D electrical resistivity volume of Vulcano Island (Aeolian archipelago in Southern Italy).

In contrast, the AMT models at Lipari (Fig. 3) do not show evidence of a continuous deep conduit or a well-developed geothermal reservoir comparable to that observed at Vulcano. The resistivity structure is instead characterized by strong lateral heterogeneity and compartmentalization, with localized conductive anomalies associated with altered volcanic units and structurally controlled zones of residual hydrothermal circulation. These features suggest a waning geothermal system, with potential mainly confined to shallow to intermediate depths and compatible with low- to medium-enthalpy applications rather than high-temperature exploitation.

At Panarea, the AMT resistivity models mainly resolve the shallow subsurface beneath the emerged portion of the island. Shallow conductive zones are imaged in spatial association with the main fault systems affecting the island and are consistent with the occurrence of active hydrothermal circulation, in agreement with surface and submarine degassing observations reported in the area. However, due to the limited areal extent of the emerged island and the largely offshore development of the volcanic system, the current on-land AMT dataset provides only limited constraints on deeper structures. As a result, no detailed interpretation of the geometry or extent of the deeper geothermal system can be derived from the available resistivity models.

At Salina, AMT data acquisition has been completed, but three-dimensional inversion is still ongoing. Consequently, only preliminary qualitative considerations can be made at this stage. The available data indicate a predominantly resistive response associated with the main volcanic edifices; however, in the absence of a fully converged resistivity model, no robust interpretation of subsurface structure or hydrothermal circulation is currently possible. The Salina dataset is therefore intended to complement the archipelago-scale geothermal inventory once inversion results become available, enabling future integration within a consistent interpretative framework.

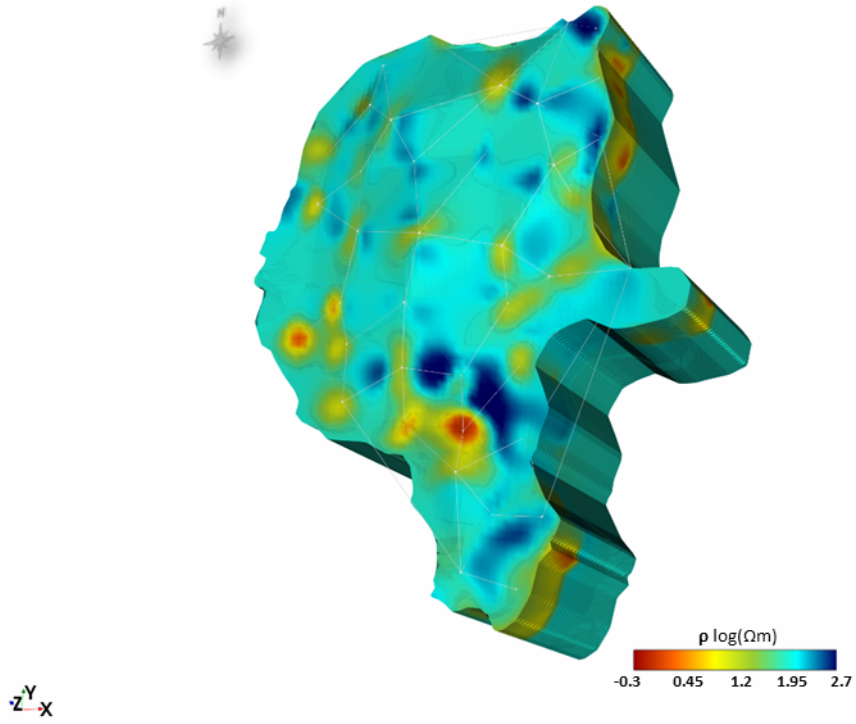

Fig. 3 – 3D electrical resistivity volume of Lipari Island (Aeolian archipelago in Southern Italy).

Conclusions

At Vulcano, the AMT models robustly image a conduit-like resistive structure connected to a shallow conductive hydrothermal system, confirming the key role of volcano-tectonic discontinuities in controlling fluid ascent and geothermal activity. Lipari shows a more heterogeneous and compartmentalized resistivity structure, consistent with residual hydrothermal circulation and suggesting a lower geothermal potential compared to other active systems. At Panarea, the current on-land dataset constrains only the shallow portion of the system, while deeper structures likely remain offshore and unresolved. At Salina, data acquisition is complete, but inversion is still ongoing, and no definitive conclusions can yet be drawn.

Overall, this study demonstrates the effectiveness of AMT resistivity imaging in discriminating between different geothermal settings and in identifying structural controls on fluid circulation in complex volcanic island environments. These results firmly contribute to the construction of an inventory of geothermal resources at the archipelago scale and provide a robust basis for future integration with geological, geochemical, and geophysical datasets, supporting informed evaluations and modelling of sustainable geothermal exploitation scenarios in the Aeolian Islands.

References

De Astis, G., Ventura, G., Vilardo, G. (2003). *Geodynamic significance of the Aeolian volcanism (Southern Tyrrhenian Sea, Italy) in light of structural, seismological, and geochemical data*. Tectonics 22.

Egbert, G. D., Kelbert, A. (2012). *Computational recipes for electromagnetic inverse problems*. Geophysical Journal International, 189(1), 251-267.

Forni, F. Lucchi, F., Peccerillo, A., Tranne, C. A., Rossi, P. L., Frezzotti, M. L. (2013). *Chapter 10 Stratigraphy and geological evolution of the Lipari volcanic complex (central Aeolian archipelago).* Geological Society, London, Memoirs 2013, v.37; p213-279. https://doi.org/10.1144/M37.10

Muñoz, G. (2014). *Exploring for geothermal resources with electromagnetic methods*. Surv. Geophys. 35, 101–122.

Simpson, F., Bahr, K. (2005). Practical Magnetotellurics. https://doi.org/10.1017/CBO9780511614095

Spichak, V., Manzella, A. (2009). *Electromagnetic sounding of geothermal zones*. J. Appl. Geophys. 68, 459–478.

Ventura, G., Vilardo, G., Milano, G., Pino, N. A. (1999). *Relationships among crustal structure, volcanism and strike-slip tectonics in the Lipari-Vulcano Volcanic Complex (Aeolian Islands, Southern Tyrrhenian Sea, Italy)*. Phys. Earth Planet. Inter. 116, 31–52.

Corresponding author: claudio.depaola@ingv.it

Hydrologically induced geophysical processes in the Cansiglio Plateau, southern Alps

Roberto Devoti[1], Alessandra Borghi[2], Adriano Cavaliere[2], Leonardo Martelli[2], Letizia Elia[2], Francesco Pintori[2], Enrico Serpelloni[2], Paolo Fabris3, David Zuliani[3], Carla Braitenberg[4], Barbara Grillo[4], Alberto Pastorutti[4]

[1] Istituto Nazionale di Geofisica e Vulcanologia, Osservatorio Nazionale Terremoti, Via di Vigna Murata, Roma

[2] Istituto Nazionale di Geofisica e Vulcanologia, Sezione di Bologna, Viale C. Berti Pichat, Bologna

[3] Istituto Nazionale di Oceanografia e di Geofisica Sperimentale, Borgo Grotta Gigante Trieste

[4] Università di Trieste, Dipartimento di matematica, informatica e geoscienze, Trieste

The Cansiglio Plateau is a carbonate karst system situated in the southern sector of the Alps, between the Veneto and Friuli Venezia Giulia regions. This tectonically active massif is shaped by the combined effects of thrust-related deformation and hydrologically driven mechanical processes. Its structural configuration is primarily governed by basal thrusting along the southern Alpine front, which imposes a compressional stress regime on the overlying carbonate succession. This stress field promotes the development of dense fracture networks and fault systems within the plateau. The resulting structures, typically high-angle faults and joints, provide preferential pathways for karstification and groundwater circulation.

The GNSS time series computed by INGV, accessible at this portal, constitute an extensive database that documents crustal deformations across the Eurasia–Africa plate boundary. Within this framework, the present study examines a distinctive deformation pattern that was first identified and monitored about a decade ago in the Cansiglio Plateau. This pattern exhibits a robust correlation with precipitation events and broader climatic cycles. Furthermore, unpublished GNSS time series from stations located at the foothills of the Cansiglio Massif further refine the characterization of this phenomenon. Figure 1 illustrates the directions of rainfall-induced deformation inferred from the last five years of GNSS observations. Despite the relatively modest precipitation recorded during this interval, GNSS stations exhibit systematic displacements of several centimetres, oriented orthogonally to the primary basal thrust system.

The interaction between shallow seismicity and hydrologically induced processes has been the subject of considerable research interest, both at regional and global scales, including several studies focused on the northeastern Alps. In this context, we analyse the seismic catalogue compiled by OGS to evaluate whether climatic forcing exerts a measurable influence on background seismicity in the study area. Our analysis is aimed at identifying temporal correlations between seismicity rates and climatic variations of hydrological variables, such as precipitation and

water storage content, with particular emphasis on shallow earthquakes, which are more likely to respond to surface and near-surface loading effects and pore-pressure perturbations.

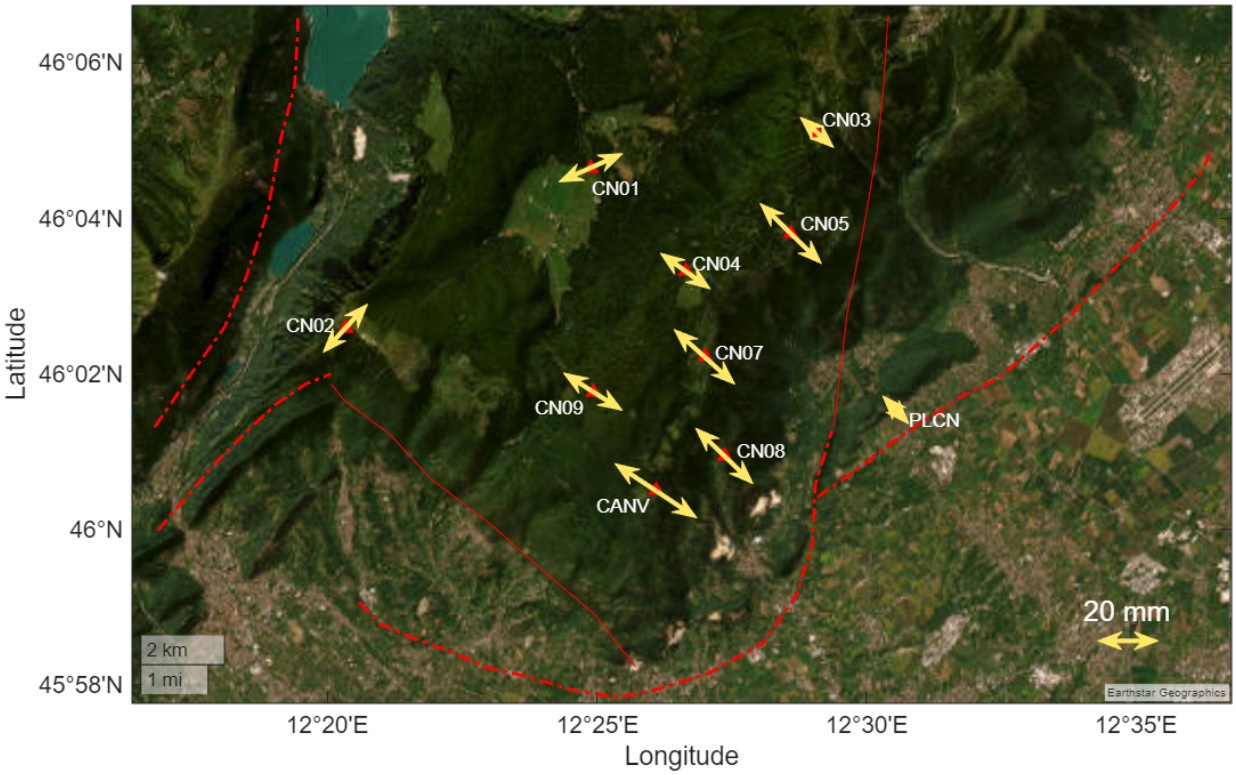

Fig. 1 - Map of the Cansiglio Plateau showing the directions and amplitudes of hydrologic deformation measured at GNSS stations (yellow double arrows). Continuous red lines indicate the main tectonic lineaments in the region, dash–dotted lines represent thrust faults (taken from ITHACA database, ITaly HAzard from CApable faulting).

Corresponding author: roberto.devoti@ingv.it

Ambient Noise Tomography of Campi Flegrei caldera (Naples, Italy): High Frequency Phase-Velocity Anomalies beneath the Solfatara–Pisciarelli Hydrothermal System

C. Di Dato[1,2], A. Tramelli[2], L. De Siena[1,2]

[1] Dipartimento di Fisica e Astronomia "Augusto Righi", Alma Mater Studiorum, Università di Bologna, Bologna, Italy

[2]Istituto Nazionale di Geofisica e Vulcanologia (INGV), Sezione Osservatorio Vesuviano, Napoli, Italy

The Campi Flegrei caldera (Napoli, Italy) is one of the most active volcanic systems worldwide, continuously monitored by the Istituto Nazionale di Geofisica e Vulcanologia, Sezione Osservatorio Vesuviano (INGV-OV). Intense hydrothermal activity, recurrent seismicity and significant episodes of ground uplift (bradyseism) peaking at the caldera centre over the last decades have been related to the dynamics of a complex magmatic–hydrothermal system. Previous studies indicate active fluid migration through the Solfatara-Pisciarelli hydrothermal system (Calò & Tramelli, 2018; Petrosino & De Siena, 2021; Calò & Tramelli, 2025), as well as strong small-scale heterogeneities and gas accumulation and release (Gammaldi et al., 2018) in this area. In this work, we produced a time dependent Rayleigh-wave tomography model of the Campi Flegrei caldera using the Python Package SeisLib (Magrini et al., 2022). We applied the method to three years of ambient noise data (from January 2022 to December 2024). This period corresponds to the most significant seismic unrest of the last 40 years, with a total of 37 seismic events with duration magnitude $M_d \geq 3.0$ and a maximum magnitude of $M_d=4.4$ on May 20, 2024. We used records of 18 seismic stations of the INGV-OV network, 17 from the IV network and 1 (CFB3) from the Medusa network (Fig. 1). We processed the continuous seismic records using a standard ambient-noise processing workflow, including the removal of transient seismic swarms and band-pass filtering. Data were then resampled and crosscorrelated for all available station pairs, knowing that cross-correlation of seismic ambient noise can be related to the surface-wave Green's function between two points of observation (Campillo et al., 2014; Boschi & Weemstra, 2015; Magrini et al., 2022). From these, we extracted Rayleigh-wave dispersion curves to produce phase-velocity maps at 0.25 Hz, 0.50 Hz, 0.75 Hz, 1.0 Hz, 1.25 Hz and 1.50 Hz. Here, we focused on the three highest frequencies (1.0 Hz, 1.25 Hz and 1.50 Hz) (Fig. 2), which provide the best resolution in the shallowest portion of the caldera (Fig. 3). Inversions for Rayleigh-wave phase velocities reveal high-velocity anomalies in the Solfatara–Pisciarelli area, with values ~100 m/s above average velocities, and sensitivity extending to a few hundred meters of depth. These velocities are consistent with the presence, below the Solfatara-Pisciarelli region, of a shallow hydrothermal system comprising an aquifer and shallow faults

(Akande et al., 2019).

The spatial distribution of the anomalies is also qualitatively consistent with geophysical models indicating the presence of a clay cap atop a highly resistive plume, constrained by faults, that feeds the fumaroles on the surface (Siniscalchi et al., 2019). High-frequency Rayleigh-wave phase velocities, obtained from the inversion, are also consistent with the presence of an elongated shallow zone of high rigidity. This transfer structure, formed by lateral stress accumulation in the crust, crosses the resistive plume that stores steam and gas beneath the Solfatara-Pisciarelli system (Petrosino & De Siena, 2021). The results are also consistent with the findings of Tan et al. (2025), supporting the interpretation that shallow faults in the Solfatara–Pisciarelli area act as preferential conduits for ascending gases and hydrothermal fluids.

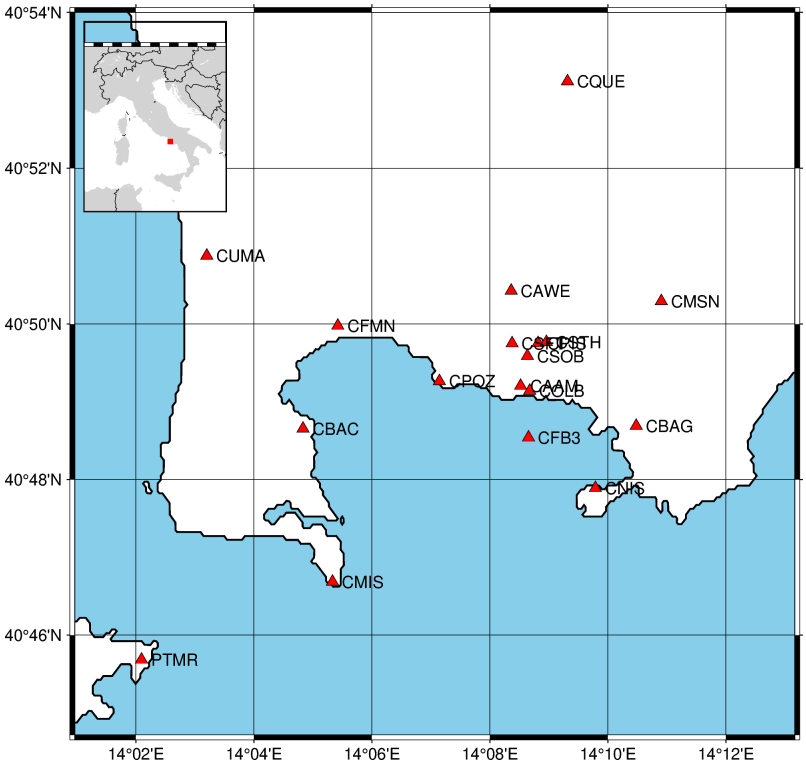

Fig. 1 – Campi Flegrei seismic network managed by INGV – OV.

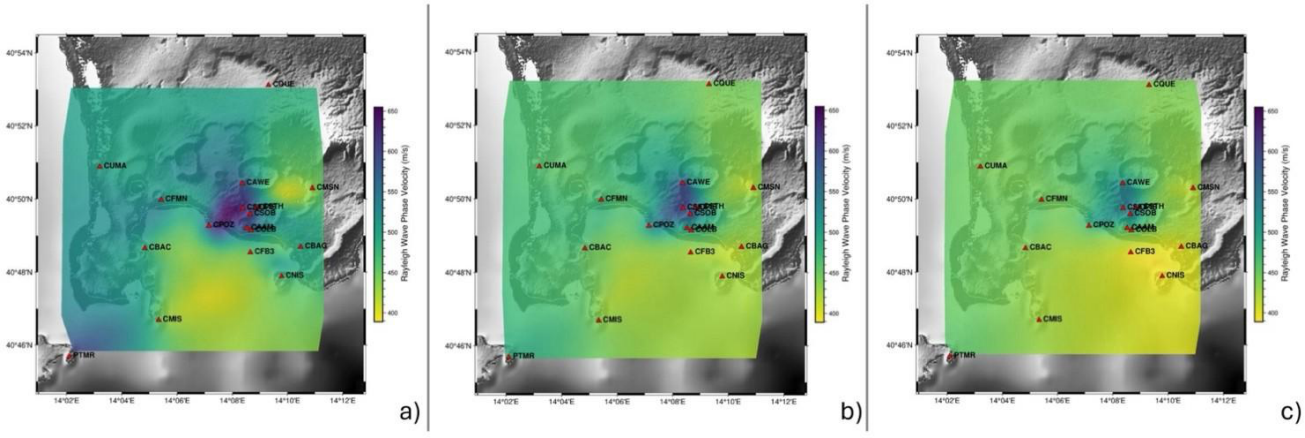

Fig. 2 – Rayleigh-wave phase velocity maps for: a) 1.0 Hz, b) 1.25 Hz, c) 1.50 Hz.

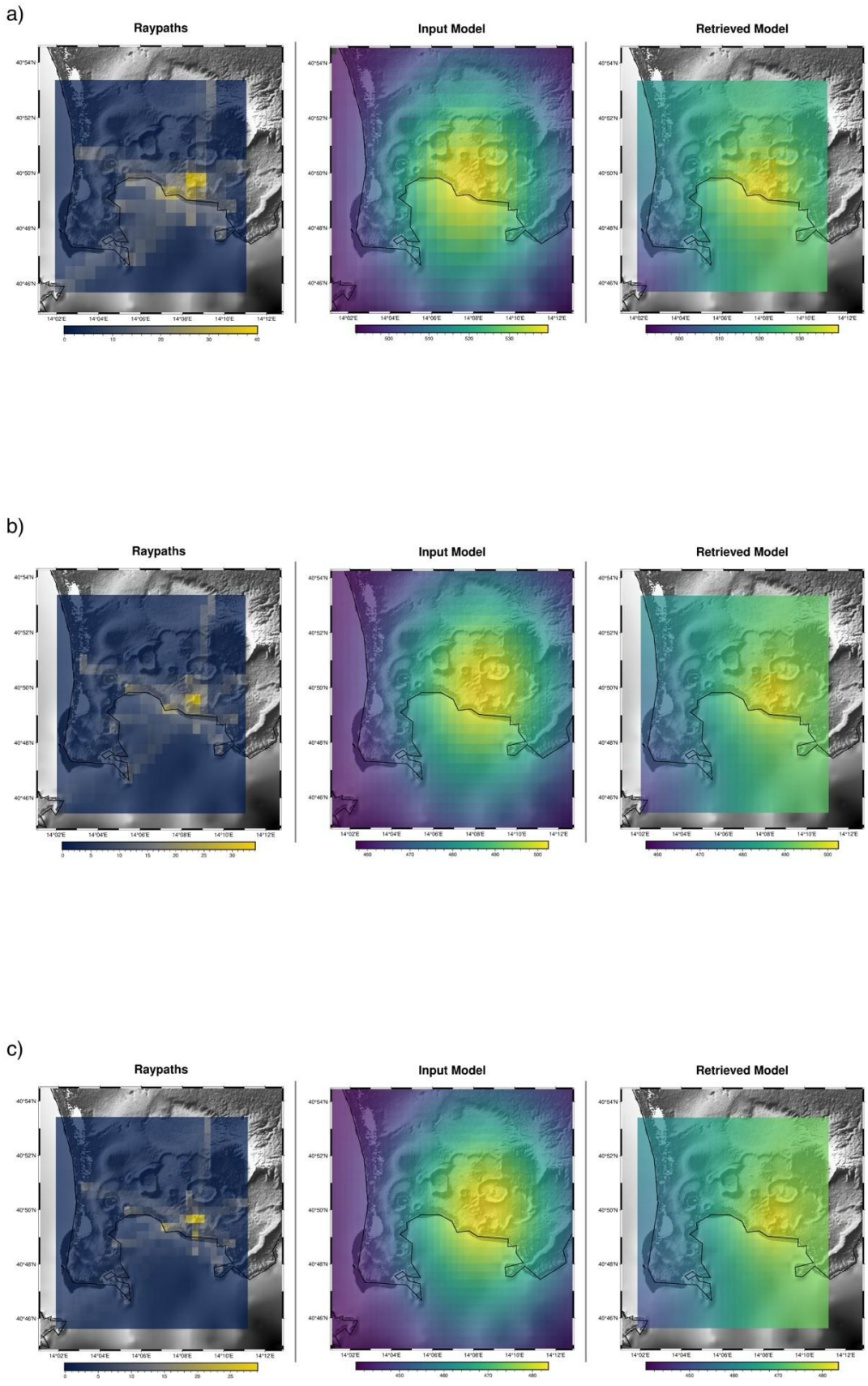

Fig. 3 – Raypath and spike test (input and retrieved models) for: a) 1.0 Hz, b) 1.25 Hz, c) 1.50 Hz.

References

Akande, W. G., De Siena, L., & Gan, Q.; 2019: Three-dimensional kernel-based coda attenuation imaging of caldera structures controlling the 1982-84 Campi Flegrei unrest. J. Volcanol. Geotherm. Res., 381, 273-283.

Boschi, L., & Weemstra, C.;2015: Stationary-phase integrals in the cross correlation of ambient noise. Rev. Geophys., 53(2), 411-451.

Calò, M., & Tramelli, A.; 2018: Anatomy of the Campi Flegrei caldera using enhanced seismic tomography models. Sci. Rep., 8(1), 16254.

Calò, M., & Tramelli, A.; 2025: Evidences of the structures controlling the unrest in Campi Flegrei, Italy; Joint interpretation of ambient noise and local earthquake tomography. J. Volcanol. Geotherm. Res., 457, 108236.

Campillo, M., Roux, P., Romanowicz, B., & Dziewonski, A.; 2014: Seismic imaging and monitoring with ambient noise correlations. Treatise on geophysics, 1, 256-271.

Gammaldi, S., Amoroso, O., D'Auria, L., & Zollo, A.; 2018: High resolution, multi-2D seismic imaging of Solfatara crater (Campi Flegrei Caldera, southern Italy) from active seismic data. J. Volcanol. Geotherm. Res., 357, 177-185.

Magrini, F., Lauro, S., Kästle, E., & Boschi, L.; 2022: Surface-wave tomography using SeisLib: a Python package for multiscale seismic imaging. Geophys. J. Int., 231(2), 1011-1030.

Petrosino, S., & De Siena, L.; 2021; Fluid migrations and volcanic earthquakes from depolarized ambient noise. Nat. Comm., 12(1), 6656.

Siniscalchi, A., Tripaldi, S., Romano, G., Chiodini, G., Improta, L., Petrillo, Z., D'Auria, L., Caliro, S., & Avino, R.; 2019: Reservoir structure and hydraulic properties of the Campi Flegrei geothermal system inferred by audiomagnetotelluric, geochemical, and seismicity study. J. Geophys. Res., 124(6), 5336-5356.

Tan, X., Tramelli, A., Gammaldi, S., Beroza, G. C., Ellsworth, W. L., & Marzocchi, W.; 2025: A clearer view of the current phase of unrest at Campi Flegrei caldera. Science, 390(6768), 70-75.

Corresponding author: ciro.didato4@unibo.it, anna.tramelli@ingv.it, luca.desiena2@unibo.it

High-Frequency Monitoring of Volcanic Plumes over Europe Using the Sentinel-4 Mission aboard MTG-S

G. S. Di Bella[1,2], C. Corradino[2], S. Cariello[2], A. B. Malaguti[2], A. La Spina[2], F. Torrisi[2], C. Del Negro[2]

1 Department of Electrical electronic and computer engineering, University of Catania, Catania, Italy
2 Istituto Nazionale di Geofisica e Vulcanologia, Sezione di Catania, Osservatorio Etneo, Catania, Italy

Monitoring volcanic emissions is essential for assessing the effects of gases and aerosols on air quality and for understanding the chemical and physical processes driving their atmospheric evolution (Bethke et al., 2017). Volcanic plumes can rapidly disperse over large regions (Robock et al., 2000), altering atmospheric composition and influencing climate. High-frequency, high-quality observations are therefore required to describe plume formation, transport, and dispersion with sufficient temporal continuity (Carn et al., 2016). Since volcanic gases represent key geofluids released during eruptive and non-eruptive activity, their continuous monitoring is fundamental for understanding the dynamics of volcanic systems and their impacts.

The Sentinel-4 mission, part of the Meteosat Third Generation (MTG) program developed by ESA and EUMETSAT, introduces a major advancement in geostationary atmospheric monitoring (ESA, 2020; Holmlund et al., 2021; EUMETSAT, 2023). Mounted on the MTG-S platform, Sentinel-4 is a UV–VIS–NIR spectrometer providing continuous observations of Europe and surrounding regions with a spatial resolution of 8 × 8 km² and an hourly revisit time. This capability enables near-real-time detection of rapid changes in atmospheric composition, a key requirement for volcanic-emission monitoring.

Sentinel-4 measures key volcanic-relevant gases, including SO_2, NO_2, O_3, HCHO, CHOCHO, and aerosols. Its observations support the generation of operational products such as column densities, aerosol optical depth, transport parameters, and high-frequency time series. The mission will allow timely detection of new plumes, continuous tracking of their dispersion, and improved assimilation into forecasting systems.

Comparison with the TROPOMI sensor aboard Sentinel-5P highlights the complementarity between the two missions: TROPOMI provides global coverage at about 7 × 7 km² resolution but with a daily revisit time (Theys et al., 2019; Corradino et al., 2024), whereas Sentinel-4 offers higher temporal continuity over a more limited domain. TROPOMI is therefore optimal for global mapping of volcanic emissions (Veefkind et al., 2012), while Sentinel-4 enables detailed, minute-by-minute monitoring of eruptions affecting Europe.

Sentinel-4 also operates within a coordinated constellation of geostationary atmospheric missions, including the TEMPO (Tropospheric Emissions: Monitoring of Pollution) sensor for North America

(Zoogman et al., 2017) and the GEMS (Geostationary Environment Monitoring Spectrometer) mission for East Asia (Kim et al., 2020; Cho et al., 2024). Together, these instruments provide near-continuous coverage of volcanic emissions across the Western Hemisphere.

Here, we provide a comprehensive assessment of the expected potential of Sentinel-4 for volcanic-emission monitoring, based on proxy observations and benchmarks derived from TROPOMI. Preliminary simulations and early test workflows suggest that Sentinel-4 will enable the production of high-frequency SO_2 and aerosol datasets tailored for volcanic applications. The mission's geostationary sampling is expected to provide unprecedented temporal continuity in detecting SO_2 and aerosol plumes, complementing the spectral performance of Sentinel-5P and supporting future improvements in plume tracking, dispersion analysis, and short-term forecasting through data-assimilation frameworks used by the volcanological and atmospheric-modelling community.

References

Bethke, I., Outten, S., Otterå, O. H., Hawkins, E., Wagner, S. and Sigl, M., Thorne, P.; 2017: Potential volcanic impacts on future climate variability. Nature Climate Change, Vol. 7, n. 11, pp. 799-805, https://doi.org/10.1038/nclimate3394

Carn, S.A., Clarisse, L. and Prata, A.J.; 2016: Multi-decadal satellite measurements of global volcanic degassing. Journal of Volcanology and Geothermal Research, Vol. 311, pp. 99-134, https://doi.org/10.1016/j.jvolgeores.2016.01.002

Cho, Y., Kim, J., Go, S., Kim, M., Lee, S., Kim, M., Chong, H., Lee, W.-J., Lee, D.-W., Torres, O., and Park, S.S.: First atmospheric aerosol-monitoring results from the Geostationary Environment Monitoring Spectrometer (GEMS) over Asia, Atmos. Meas. Tech., 17, 4369–4390, https://doi.org/10.5194/amt-17-4369-2024, 2024.

Corradino, C., Jouve, P., La Spina, A. and Del Negro, C.; 2024: Monitoring Earth's atmosphere with Sentinel-5 TROPOMI and Artificial Intelligence: Quantifying volcanic SO2emissions. Remote Sensing of Environment, Vol. 315, 114463, https://doi.org/10.1016/j.rse.2024.114463

ESA; 2020: Sentinel-4 Mission Overview. European Space Agency. https://sentinels.copernicus.eu/missions/sentinel-4/overview

EUMETSAT; 2023: MTG-S Sentinel-4 Mission Requirements Document (MRD)

Holmlund, K., et al.; 2021: Meteosat Third Generation (MTG): Continuationand Innovation of Observations from Geostationary Orbit. Bulletin of the American Meteorological Society, Vol. 102, E990-E1015, https://doi.org/10.1175/BAMS-D-19-0304.1

Kim, J., et al.; 2020: New Era of Air Quality Monitoring from Space: Geostationary Environment Monitoring Spectrometer (GEMS). Bull. Amer. Meteor. Soc., 101, E1–E22, https://doi.org/10.1175/BAMS-D-18-0013.1

Robock, A.; 2000: Volcanic eruptions and climate. Reviews of Geophysics, Vol. 38, pp. 191-219, https://doi.org/10.1029/1998RG000054

Theys, N., et al.; 2019: Global Monitoring of Volcanic SO2Degassing with Unprecedented Resolution from TROPOMI Onboard Sentinel-5 Precursor. Scientific Reports, Vol. 9, 2643, https://doi.org/10.1038/s41598-019-39279-y

Veefkind, J. P., et al.; 2012: TROPOMI on the ESA Sentinel-5 Precursor: A GMES mission for global observations of the atmospheric composition for climate, air quality and ozone layer applications. Remote sensing of environment, Vol. 120, pp. 70-83, https://doi.org/10.1016/j.rse.2011.09.027

Zoogman, P., et al.; 2017: Tropospheric Emissions: Monitoring of Pollution (TEMPO). Journal of Quantitative Spectroscopy and Radiative Transfer, Vol. 186, pp. 17-39, 10.1016/j.jqsrt.2016.05.008

Corresponding author: Giovanni Salvatore Di Bella. giovanni.dibella@phd.unict.it

Earthquake-related fluids behaviour at Salse di Nirano mud volcano field (Italy)

E. Ferrari[1], A.L. Rizzo[2,1], G. Capelli Ghioldi[3], A. Sciarra[4], G. Tamburello[3], F. Viveiros[5], S. Lovati[1], M. Massa[1]

[1] Istituto Nazionale di Geofisica e Vulcanologia (INGV), Milano, Italy
[2] Dipartimento di Scienze della Terra e dell'Ambiente, Università Milano-Bicocca, Milano, Italy
[3] Istituto Nazionale di Geofisica e Vulcanologia (INGV), Bologna, Italy
[4] Istituto Nazionale di Geofisica e Vulcanologia (INGV), Roma 1, Italy
[5] Instituto de Vulcanologia e Avaliação de Riscos, Universidade dos Açores, Portugal.

Salse di Nirano (Fiorano Modenese, Italy) host one of the largest mud volcano fields of Europe. They are positioned upon an anticline structure of the NE-verging fold-and-thrust Northern Apennine belt and emit fluids mainly consisting of clay mud, saline water and hydrocarbons (liquid and gas). Like most of the world's mud volcanoes, their gas emissions are primarily composed of methane (> 98%), with minor contributions from carbon dioxide, nitrogen, and other hydrocarbons (Etiope et al., 2007; Mazzini and Etiope, 2017). Two main fault and fracture systems (one NW-SE oriented and the other SW-NE/ENE-WSW oriented) allow fluids migration to the surface (e.g., Bonini, 2008). From a geomorphological point of view, Salse di Nirano are placed within a caldera-like depression presumably formed by progressive collapse due to degassing (e.g. Bonini, 2008) or as the final stage of mud diapir evolution (Castaldini et al., 2005).

As many world's mud volcanoes, Salse di Nirano activity is closely linked to tectonic processes (Coppi, 1875; Martinelli and Ferrari, 1991; Bonini, 2009). With the aim of studying the interplay between geofluids and seismicity, a multiparametric monitoring system was set up in 2023. Two distinct mud pools were selected for the continuous monitoring of mud level/density, temperature and electrical conductivity. In addition, a permanent station measuring CO_2 flux diffused by the soil was installed at the edge of the mud volcanoes field, where higher gas fluxes were detected (Ferrari et al., 2024). Recently, the station has been upgraded with a methane sensor. A meteorological station and a velocimeter were installed to monitor the atmospheric parameters and the seismic activity of the area, respectively.

Overall, the multiparametric monitoring system continuously recorded about two years of data. Periodic oscillations were identified, with some anomalous variations of mud level, temperature, electrical conductivity and soil gas flux that have been compared with environmental data (meteorological and soil-related) and seismicity. Notably, synchronous changes in mud pools electrical conductivity and soil CO_2 fluxes were detected in relation to two distinct seismic swarms occurred in February and August 2024. In addition, differences in the behaviour of the two mud pools were also observed throughout all the time-series and presumably point to extremely local conditions influencing the common feeding system. All these observations highlight the efficiency

of the presented continuous multiparametric monitoring system in inferring new insights on mud volcano crustal fluids dynamics.

Acknowledgments

We would like to thank the Municipality of Fiorano Modenese (MO) and the Salse di Nirano Nature Reserve, in particular Dr. Marzia Conventi and Luciano Callegari, for authorizing and supporting our work in the Nirano mud volcano area.

References

Bonini, M.; 2008: Elliptical mud volcano caldera as stress indicator in an active compressional setting (Nirano, Pede-Apennine margin, northern Italy). Geology Vol. 36, pp. 131-134, https://doi.org/10.1130/G24158A.1.

Bonini M (2009) Mud volcano eruptions and earthquakes in the Northern Apennines and Sicily, Italy. Tectonophysics 474:723-735. doi:10.1016/j.tecto.2009.05.018.

Castaldini, D., Valdati, J., Ilies, D.C., Chiriac, C., Bertogna, I.; 2005: Geo-Tourist Map Of The Natural Reserve Of Salse Di Nirano (Modena Apennines, Northern Italy). Italian Journal of Quaternary Sciences Vol. 18, n. 1, pp. 245-255.

Coppi, F.; 1875: Brevi note sulle Salse Modenesi. Bollettino del R. Comitato Geologico Vol.7-8, pp. 1-7.

Etiope, G., Martinelli, G., Caracausi, A., Italiano, F.; 2007: Methane seeps and mud volcanoes in Italy: Gas origin, fractionation and emission to the atmosphere. Geophysical Research Letters Vol. 34, pp. 1-5, https://doi.org/10.1029/2007GL030341.

Martinelli, G., Ferrari, G.; 1991: Earthquake forerunners in a selected area of Northern Italy: recent developments in automatic geochemical monitoring. Tectonophysics Vol. 193, n. 4, pp. 397-410, https://doi.org/10.1016/0040-1951(91)90348-V.

Mazzini, A., Etiope, G.; 2017: Mud volcanism: An updated review. Earth-Science Reviews Vol. 168, pp. 81-112, http://dx.doi.org/10.1016/j.earscirev.2017.03.001.

Ferrari, E., Massa, M., Lovati, S., Di Michele, F., Rizzo, A.L.; 2024: Multiparametric stations for real-time monitoring and long-term assessment of natural hazards. Frontiers in Earth Science Vol. 12, n. 1412900, pp. 1-26, https://doi.org/10.3389/feart.2024.1412900.

Corresponding author: elisa.ferrari@ingv.it

Ambient Noise Tomography to the Etna Magma System during the 2020-2021 period

S. Floridia[1], S.C.G. Vinciguerra[1], L. De Siena[2], G.M. Adinolfi[1]

[1] *Department of Earth Sciences, University of Turin, Turin, Italy*
[2] *Department of Physics and Astronomy "Augusto Righi", University of Bologna, Bologna, Italy*

Introduction

Mount Etna is a ~3400 m high stratovolcano in an interplate setting, as it lies on the hanging wall of the Sicilian Thrust Belt (Doglioni et al., 1999). Although it is among the most extensively studied volcanoes worldwide, the interplay between magmatic and tectonic processes responsible for its volcanism remain poorly constrained (e.g. Barreca et al., 2020; Duvernay et al., 2021; Gvirtzman and Nur, 1999).

Imaging petrophysical parameters such as temperature, melt content, and porosity is of paramount importance to better constrain the Etna's plumbing system; however, the only means to indirectly infer these parameters is via geophysical investigations. For instance, low-seismic velocity zones are typically associated with reduced rigidity caused either by elevated temperatures, like melt content, or by pervasive fracturing.

Seismic velocity tomography, which is based on earthquake travel times to image the deep subsurface (e.g. Lo Bue et al., 2024), provides key spatial constraints on geodynamic models.

In recent years, thanks to increasingly sensitive seismometers and the establishment of seismic interferometry (Boschi and Weemstra, 2015; Tromp et al, 2010), techniques for tomography based on the use of ambient noise to image the subsurface have developed (Agius et al., 2022).

Under the diffuse-wavefield assumption, cross-correlation between two receivers retrieves the interstation empirical Green's function, whose Fourier transform yields the surface-waves dispersion reflecting the structure along the path.

However, the quantitative validation of seismic velocities needs lithological constraint, in terms of petrophysical parameters. The link between velocity and lithological properties is encoded in empirical (Heap et al., 2020) and theoretical (Aki and Richards, 2002) constitutive relations. Once the stable mineral phases are identified through the Gibbs free-energy minimization algorithms (Riel et al., 2022), these constitutive relations allow the seismic-wave velocities to be computed. This provides the basis for a forward quantitative mapping of petrophysical parameters. Developing a new inversion scheme will deliver a physical validation of the observed velocities to the corresponding physical properties, proving constraints into the mantle–crust coupling.

Here we employed Ambient Noise Tomography implemented via SeisLib, a Python library for

performing Ambient Noise Tomography (Magrini et al., 2022). This approach allowed us to retrieve Rayleigh surface-wave velocity models across the East Sicilian crust at multiple frequencies, each sampling different depth ranges.

Data & Method

We analysed two years from 2020 to 2021 of continuous vertical-component waveforms from 12 seismic stations from the INGV-OE network. Their spatial configuration minimizes the effect of volcanic tremor while maximizing the number of interstation paths beneath Mt. Etna (Fig. 1).

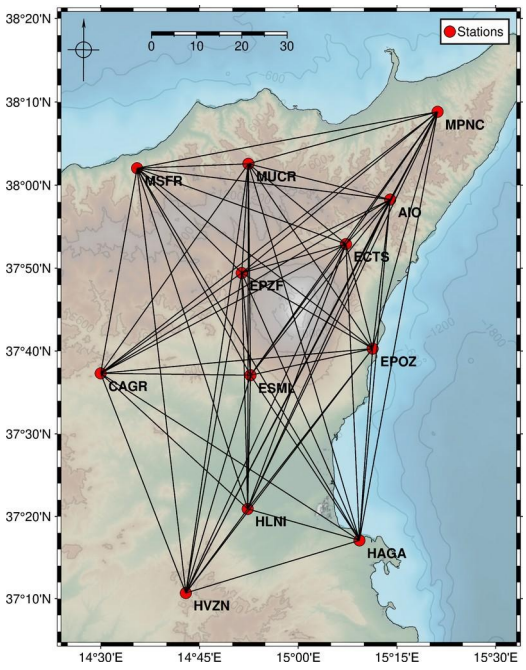

Fig. 1 – Map showing the selected stations (Ns = 12). Black lines indicate the interstation paths connecting the stations. A total of 66 paths ($\propto$ to $Ns^2/2$) were considered in this study.

The selected period is seasonally balanced and does not involve major eruptive activity. The frequency range (0.10-0.40Hz) for the Rayleigh-wave velocity models was chosen to isolate ambient noise generated by the ever-present sea–lithosphere interaction (Yang and Ritzwoller, 2008).

Cross-spectrum were computed using Welch's method (Seats et al., 2012) to enhance the diffuse-wavefield approximation and to reduce the effects of transient signals. Thanks to pre-existing area-specific Rayleigh-wave reference dispersion curves and an appropriate physical velocity range (e.g. 1.5 - 4.5 km/s), the path-specific dispersion curves were selected, reducing instabilities.

Frequency–dependent Rayleigh-wave velocities were then inverted through a regularized least-squares scheme on grids adapted to data coverage. The importance of regularisation is selected via L-curve. An appropriate algorithm (Johnson and Gulrajani, 2000) provided the corner damping parameter, ensuring a good balance between fit and roughness. Synthetic spike tests were performed to assess the resolving power of the inversion.

Discussion and future works

Across the investigated depth range (2–24 km), results reveal a low-velocity anomaly beneath Mt. Etna western flank, whose significance varies with depth (Fig. 2). At shallow levels (≲5 km), it may correspond to the low-rigidity piled sediments constituting the Caltanissetta Basin. At 8–10 km depth, since the increasing temperature gradient, this anomaly may be due as a ductile or molten region trending northeastward. The area remains largely aseismic down to ~18 km, below which clustered seismicity likely may reflect magma migration.

Shallow low-velocity anomalies (~2–3 km) could be related to shallow aquifers or hydrothermal fluids within the Catania Plain. This view is supported by the occurrence of the Salinelle di Paternò mud volcanoes. The moderately high-velocity anomaly beneath Mt. Etna likely well fits a rigid intrusive body beneath the volcanic edifice (Lo Bue et al., 2024). At intermediate depths (~5–10 km), a low-velocity anomaly may indicate a fractured volume beneath the Nebrodi Mountains. This interpretation is supported by overlapping seismicity as well as the ongoing crustal compression. The southeastern sector is characterized by high velocities, indicating a mechanically rigid and thermally cold crust associated with the extinct Hyblean volcanism.

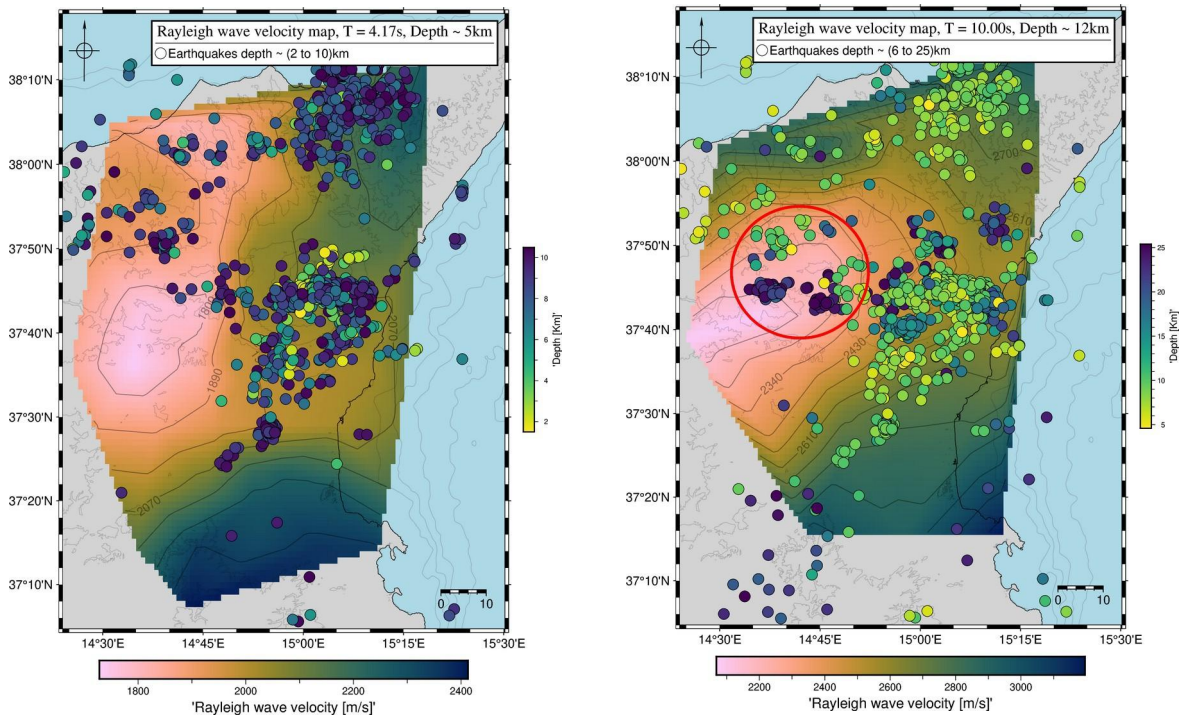

Fig. 2 – Left: Rayleigh-wave phase velocity model at T = 4.17 s, sensitive to depths of ~2–10km. Shallow low-velocity anomalies may be associated with shallow aquifers or hydrothermal fluids in the southern sector and fractured domains in the northwestern sector of Mt. Etna. To the west, the low-rigidity Caltanissetta Basin is also evident. Right: Model at T = 10.00s, sensitive to ~5–20km, showing deeper low-velocity zones that likely correspond to ductile or molten regions beneath Mt. Etna, with, into the red circle, overlying clustered seismicity indicative of magma storage and migration. High-velocity areas indicate rigid, cold crust.

Future work will consider improved data processing tailored to smaller regions with high local seismicity, with performance evaluated through dedicated validation techniques. It will subsequently incorporate Rayleigh radial components and Love waves. A joint Rayleigh–Love inversion will be performed, yielding a high-resolution Vs model with unprecedented depth and lateral coverage. Coupling these results with constitutive-relation frameworks and computational

thermodynamics will enable the development of a new petrophysical inversion scheme. This approach will produce spatially resolved petrophysical parameters, improving our understanding of competing geological mechanisms through a more direct investigation of Etna's inner crust.

References

Agius, M. R., Magrini, F., Diaferia, G., et al.; 2022: Shear-velocity structure and dynamics beneath the Sicily Channel and surrounding regions of the Central Mediterranean inferred from seismic surface waves. Geoch. Geophys. Geosys., 23, e2022GC010394.

Aki, K., and Richards, P. G. ; 2002: Quantitative Seismology. 2nd. Sausalito, CA: University Science Books.

Barreca, G., Branca, S., Corsaro, R. A., et al.; 2020: Slab detachment, mantle flow, and crustal collision in eastern Sicily (southern Italy): Implications on Mount Etna volcanism. Tectonics 39, e2020TC006188.

Boschi, L. and Weemstra, C.; 2015: Stationary-phase integrals in the cross correlation of ambient noise. Rev. Geophys. 53, 411–451.

Doglioni, C., Merlini, S., and Cantarella, G.; 1999: Foredeep geometries at the front of the Apennines in the Ionian Sea Mediterranean). Earth Planet. Sci. Lett., 168, 243–254.

Duvernay, T., Davies, D. R., Mathews, C. R., Gibson, A. H., and Kramer, S. C.; 2021: Linking intraplate volcanism to lithospheric structure and asthenospheric flow. Geoch. Geophys. Geosys., 22, e2021GC009953.

Gvirtzman, Z., and Nur, A.; 1999: The formation of Mount Etna as the consequence of slab rollback. Nature 401, 782–785.

Heap, M. J., Villeneuve, M., Albino, F., et al.; 2020: Toward more realistic values of elastic moduli for volcano modelling. J. Volcanol. Geotherm. Res. 390, 106684.

Johnston, P. R., and Gulrajani, R. M.; 2000: Selecting the corner in the L-curve approach to Tikhonov regularization. IEEE Transactions on Biomedical Engineering 47, 1293–1296.

Lo Bue, R., Rappisi, F., Firetto Carlino, M., et al.; 2024: Crustal structure of Etna Volcano (Italy) from P-wave anisotropic tomography. Geophys. Res. Lett., 51, e2024GL108733.

Magrini, F., Lauro, S., Kästle, E. and Boschi, L.; 2022: Surface-wave tomography using SeisLib: a Python package for multiscale seismic imaging. Geophys. J. Int., 231, 1011–1030.

Riel, N., Kaus, B. J. P., Green, E. C. R., and Berlie, N.; 2022: MAGEMin, an efficient Gibbs energy minimizer: Application to igneous systems. Geoch. Geophys. Geosys., 23, e2022GC010427.

Seats, K. J., Lawrence, J. F., and Prieto, G. A.; 2012: Improved ambient noise correlation functions using Welch's method. Geophys. J. Int., 188, 513–523.

Tromp, J., Luo, Y., Hanasoge, S. and Peter, D.; 2010: Noise cross-correlation sensitivity kernels. Geophys. J. Int., 183, 791–819.

Yang, Y., and Ritzwoller, M. H.; 2008: Characteristics of ambient seismic noise as a source for surface wave tomography. Geoch. Geophys. Geosys., 9, 2, Q02008, doi:10.1029/2007GC001814

Corresponding author: simone.floridia@unito.it

2005–2024 Time–Space Features of VT Seismicity at Stromboli: New Insights into the Volcano Plumbing System and Link to Effusive Eruptions

S. Gambino [1], A. Scaltrito[1]

[1] *Istituto Nazionale di Geofisica e Vulcanologia, Osservatorio Etneo, Catania, Italy.*

In the 2005–2024 period, we recognized about 160 Volcano-Tectonic seismic events with a magnitude ML ≥ 0.3, within a radius of 10 km around the summit of Stromboli. We relocated a dataset of 98 events from the 2005–2024 period, using the double difference location method (Waldhauser, F.; Ellsworth, W.L. A, 2000). We report an improved relocation of VT events here. Relocated earthquakes are mainly distributed on the island and in an area located SSW of Stromboli (Fig. 1).

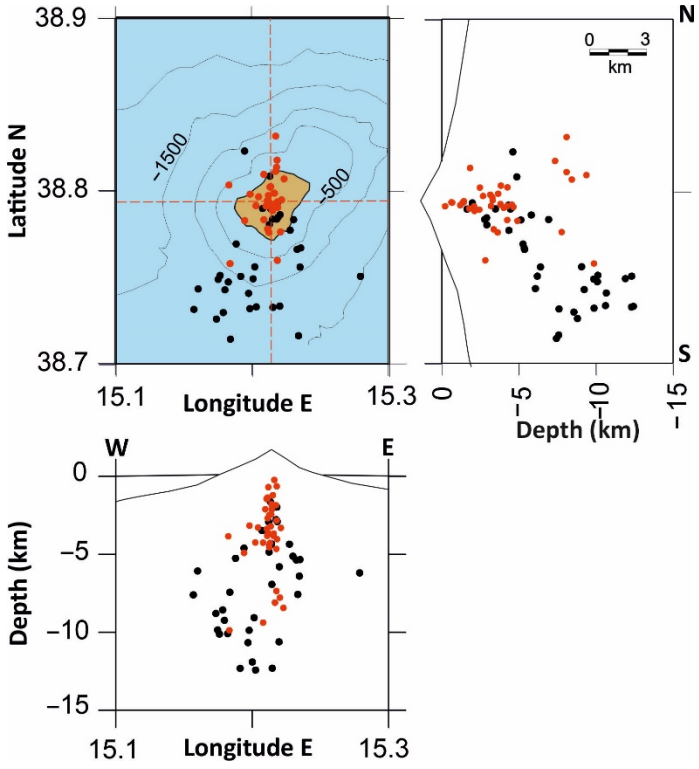

Fig. 1 – Map and vertical cross-sections of the seismicity relocated using HypoDD. Black dots indicate 2005–2016 events, and red dots indicate the 2017–July 2024 ones.

These VT events are related to the activation of seismogenic structures by a stress increase related to magma ascent. The shallowest seismicity (4–5 km) is positioned under the Stromboli summit, with a high occurrence in 2006–2007 and in 2019–2024, suggesting a major recharge of the HP magma reservoir. Its occurrence reflects changes in the stress field caused by LP magma ascent and mixing processes with HP.

The deepest VT seismicity affects a depth of 7–12 km located in the submerged edifice SSW of the summit and is attributable to the dynamics of the LP magma reservoir (Fig. 2), which was more active in 2006–2014 and much less so in the successive years.

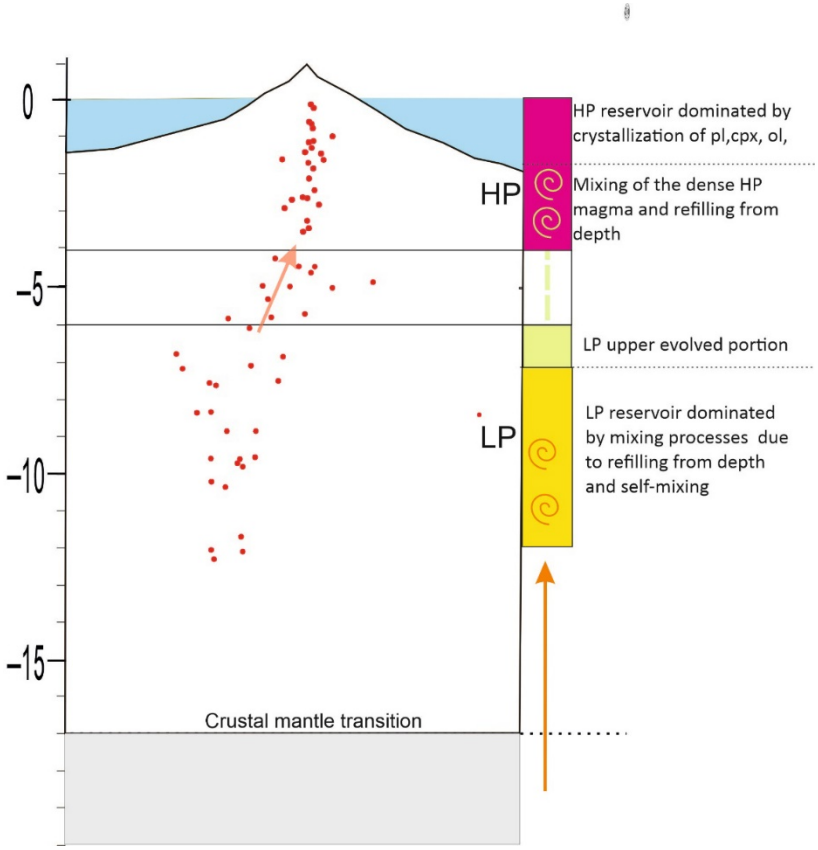

Fig. 2 – N-S schematic representation of the relocated VT seismicity distribution related to the vertically extended magmatic system feeding persistent activity at Stromboli volcano (redrawn from (Landi et al., 2006).

The increase in the occurrence rate of VT shallow seismicity seems to precede the most significant Stromboli activities, such as the 2007 and 2024 lava effusions followed by paroxysms. For these episodes, VT seismicity would appear to indicate a recharging in the first 4–5 km during the months preceding them, thereby representing a medium–short-term warning signal.

References

Landi, P., Francalanci, L., Pompilio, M., Rosi, M., Corsaro, R.A., Petrone, C.M., Nardini, I., Miraglia, L (2006). *The December 2002–July 2003 effusive event at Stromboli volcano, Italy: Insights into the shallow plumbing system by petrochemical studies*. J. Volcanol. Geotherm. Res. 155, 263–284.

Waldhauser, F., Ellsworth, W.L. (2000). *A double-difference earthquake location algorithm: Method and application to the northern Hayward fault.* Bull. Seism. Soc. Am. 90, 1353–1368.

Corresponding author: antonio.scaltrito@ingv.it

Deeply sounding a stratovolcano: the Mt Etna example

G. Giacomuzzi[1], P. De Gori[2] and C. Chiarabba[2]

[1]Istituto Nazionale di Geofisica e Vulcanologia (INGV), Sezione di Bologna
[2]Istituto Nazionale di Geofisica e Vulcanologia (INGV), Sezione Osservatorio Nazionale Terremoti

Mount Etna, a prominent stratovolcano located at the convergent plate margin between the African and Eurasian Plates, is Europe's most active and extensively studied volcano, with a documented eruptive and intrusive history spanning millennia.
Understanding the stable, long-term structure of Mount Etna's plumbing system is of paramount importance. This static architecture, resolved through years of detailed tomographic imaging, represents the framework that constrains the movement of magma and fluids from the mantle to the surface. In magmatic environments, transient velocity anomalies are to be expected, for example those related to fluid migration, magmatic intrusions, stress changes, and variations in the state of fracturing. However, a model that averages the velocity structure over the time interval has the advantage of defining velocity structures (both those related to tectonics and to the magmatic feeding system) that exhibit more stable characteristics over time.
Identifying magma storage regions, whether transient or long-lived, from the deep mantle source poses considerable difficulty. The deep crust is still poorly imaged, while most tomographic studies illuminate the uppermost 15 km, revealing the presence of a broadly rooted, high-velocity body beneath the Valle del Bove region. Many questions remain open, such as how the intrusive body is rooted at depth and whether and how magma ascends and/or stagnates within it, along its margins, or through both pathways. Tomographic studies have consistently found no stationary, widespread low Vp or high Vp/Vs anomalies, which would be evidence for large, distinct, melt-filled magma chambers. Instead, the data reveal a multi-faceted system of reservoirs and fluid-rich volumes distinguished by varying seismic signatures.
In this work, in addition to presenting a new velocity model obtained from data of the last 20 years using a non-linear Bayesian method, we provide a review of the main constraints that seismic tomography has offered to characterize the magmatic feeding system and the deep structure, related to the underthrusting of the Ionian/Iblean crust beneath the volcanic edifice. We also aim to facilitate the use of tomographic images, and thus their interpretation, even for non-specialists, by clarifying their potential and limitations.

Corresponding author: genny.giacomuzzi@ingv.it

Inside a mud volcano: first multiparametric signals recorded during the 2025 paroxysmal event at Macalube di Aragona (Sicily, Italy)

F. Grassa[1], A. Caracausi[1], P. Cusano[2], P. Madonia[3], S. Petrosino[2], A. Sciarra[4], A. Costanza[5], G. Fertitta[5], F. Macaluso[5], C. Di Maggio[6], E. Li Castri[6], D. Gucciardo[7], M.R. Falanga[2,8], S. Pinzi[4]

[1] INGV-Palermo, Palermo, Italy
[2]INGV-OV, Naples, Italy
[3]INGV-OE, Catania, Italy
[4]INGV-Roma 1, Rome, Italy
[5]INGV-OE, Gibilmanna, Italy
[6]UNIPA, Palermo, Italy
[7]Legambiente Sicilia, Aragona, Italy
[8]UNISA, Fisciano, Italy

Mud volcanoes (MVs) are geological structures typically located within accretionary wedges and fold-and-thrust belts where rapid sedimentation and compressional tectonic regimes facilitate fluid and mud expulsion. The expelled gases are generally methane dominated, waters are saline or brackish and the solid materials are mud breccias. Their characteristic quiescent degassing is sometimes interrupted by high-energy events better known as paroxysmal phases or "overturnings". These events are characterized by violent expulsions of hydrocarbon gas accompanied by the eruption of massive volume (tens of thousands of cubic meters) of mud breccias, thus representing a significant geohazard risk.
The Maccalube di Aragona (Figure 1) is one of the most active terrestrial mud volcano areas of Italy. Protected as a nature reserve, it has experienced approximately ten paroxysmal events over the last 25 years. During one of these events, occurred in September 2014, two children were tragically killed, buried by the expelled mud. This led to a legal trial concluded in 2025, during which judicial authorities confiscated a large portion of the area was by the rendering it inaccessible for scientific activities. Since the 2014 event, two more paroxysms have occurred: the first one in May 2020 and the most recent one on August 29, 2025 (Fig.1).
With the aim of developing a surveillance protocol of MVs activity, the INGV Pianeta Dinamico project, supported the PROMUD sub-project, carried out in the years 2023-2025. In the framework of the PROMUD activities, we have installed a real time and near real time multiparametric monitoring network (seismic, geochemical, meteorological and soil parameters), thanks to which we had the opportunity to record, for the first time ever, signals associated to a MV paroxysmal event. Location of the monitoring sites are reported in figure 1; it is worth noting that, due to the confiscation, ended in January 2025, seismic and meteorological-soil stations were located outside the restricted area, while the geochemical ones were installed just after its release.

Methods

Water temperature, Electrical Conductivity (EC) and pressure were measured in the water column of the Polla 1 (P1 site in figure 1), every 10 minutes using a CTD-DIVER submersible probe installed

in February 2025, at a fixed depth of 4.20 meters a few tens of centimetres above the bottom surface. Since the mud pool water level remains constant due to the presence of a natural overflow channel, the water column pressure has been converted in terms of average density (ρ_{av}). Soil and meteorological parameters have been recorded since February 2024, with an acquisition period of 30 minutes, using a Onset (now LICOR) data logger equipped with a UMTS modem for data transmission, equipped with wired and wireless smart sensors measuring: i) Air temperature and Rh; ii) Wind speed; iii) Atmospheric pressure; iv) Rainfall amount; v) Soil temperature, water content and electric conductivity.

Two seismic stations, equipped with 5S three-component sensors, were installed on 24 June 2024 and are still recording local seismicity in continuous mode. Station MCA08 is located near the main vent area, while MCA01 is located approximately 800 m away. Both the stations acquire data with a sampling rate of 200 samples-per-seconds.

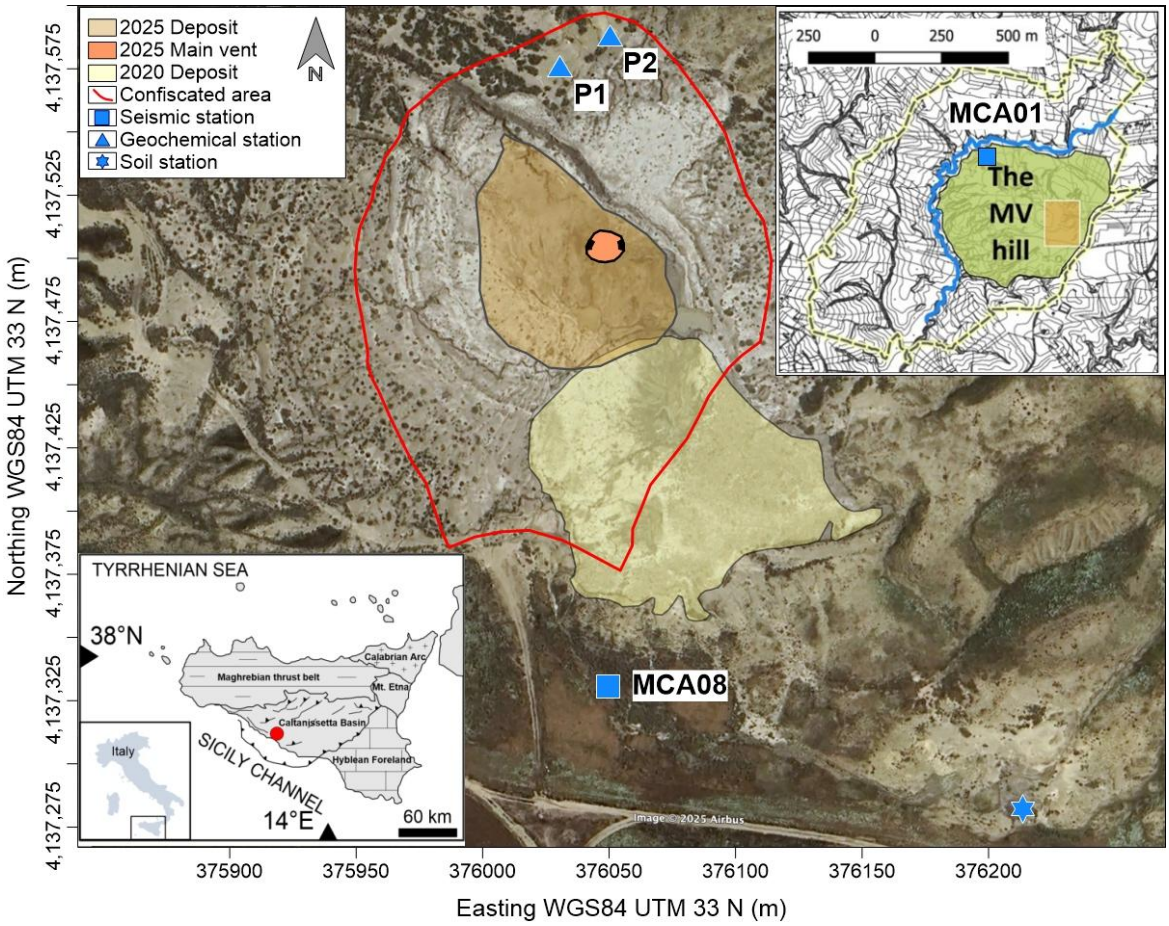

Fig. 1 – Map of the Maccalube di Aragona area, located in the general geodynamic context of Sicily (lower left inset), showing the location of the monitoring network, the perimeter of the confiscated area and the mud neo-deposits created by the 2020 and 2025 paroxysms. In the upper right inset the whole hill created in recent geological times by the MV activity, is shown. The black-dashed, yellow-highlighted line is the perimeter of the nature reserve, the orange polygon the presently main active area detailed in the main figure.

Preliminary results

The seismic recordings of paroxysm

In figure. 2, we show the signals recorded by the two seismic stations starting at 20:30 UTC on 29 August. The transient event with the onset at 23:16 UTC is likely associated with the overturning.

Since the seismic instrumentation is homogeneous, a clear amplitude attenuation effect is observed with increasing distance from the main 2025 vent location.

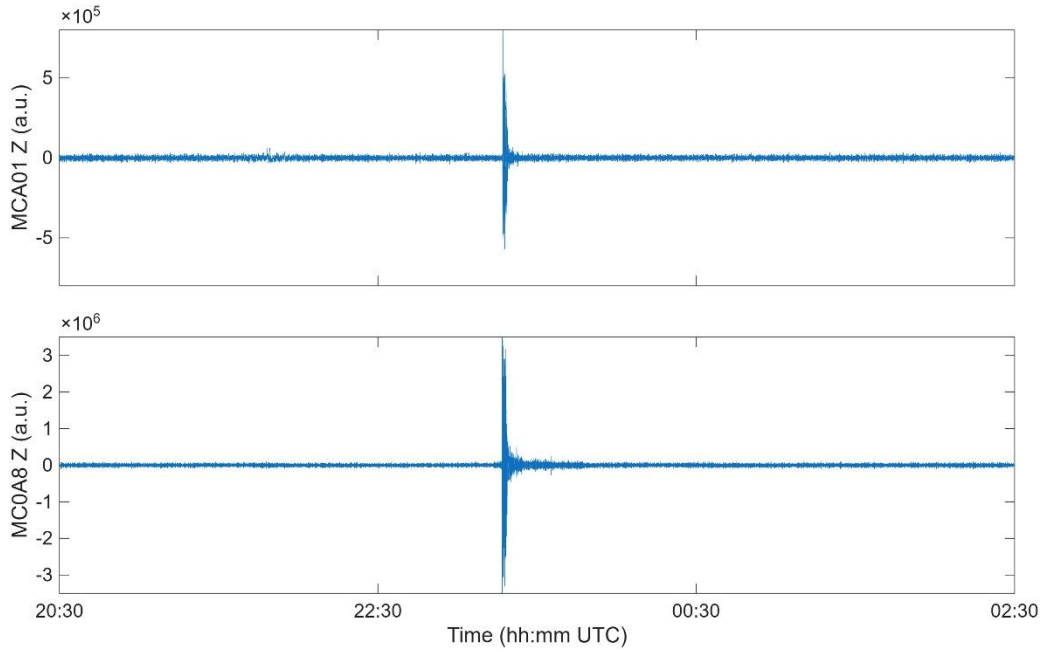

Fig. 2 – The seismic signals recorded by the vertical components (Z) of MCA01 and MCA08 seismic stations starting at 20:30 UTC on 29 August 2025. The vertical axes are in counts.

Physical parameters recorded in the water column and in the soil

The temporal trends of Temperature (T), Electrical Conductivity (EC) and water density (ρ_{av}) in the water column of Polla 1 from March 04, to October 29, 2025 are shown in figure 3.

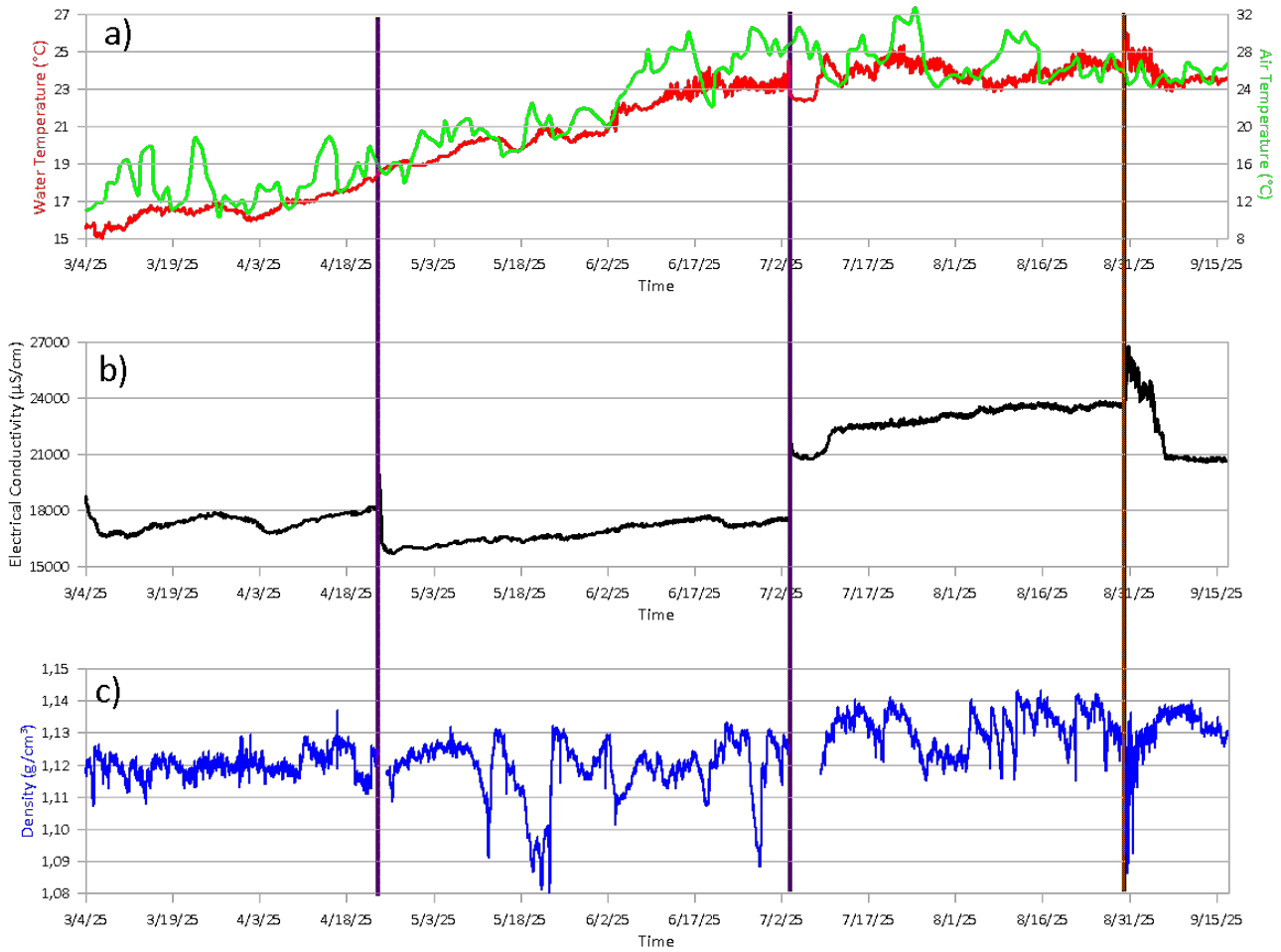

Fig. 3 – Temporal variation of T (a), EC (b) and ρ_{av} (c) in the water column at Polla 1. Purple lines: recovering of the probe. Orange line: paroxysmal event

Water temperature ranges from 15.0°C to 26.0°C, reflecting a seasonal trend and sometimes also diurnal variations driven by air temperature. The highest temperature values were observed a few hours after the paroxysmal event (indicated by the orange line in figure 3a). This could provide evidence of a potential thermal input as a transient change in the deep fluid flow regime triggered by the overturning.

Electrical Conductivity values are in the range between 16.200 to 26.800 µS/cm (Fig. 3b), corresponding to a salinity between 13 and 15 g/L. The most significant changes in EC values occurred under two specific circumstances:

- during the recovering of the probe for data download (purples lines);
- concurrently with the occurrence of the paroxysmal event (orange line).

The former should indicate a water column disturbance while the latter could suggest that the violent eruption might led to an input of more saline waters.

The average density (ρ_{av}) of the water column, ranging between 1.080 and 1.142 g/cm^3 (Fig. 3c), is always higher than the density of pure water. This is mainly due to the presence of suspended sandy-clay sediment particles with a density of about 1.8-2.0 g/cm^3. A further increase of density is due to the salts dissolved in the waters. In fact, the density of a solution with a salinity of about 14 g/L, is approximately 1.008 g/cm^3 at 25°C. Conversely, gas bubbles rising along the water column tends to decrease the density of the water column being methane density (≈6.5x10^-4 g/cm^3 at SATP) far lower than water.

Density shows high-frequency fluctuations over time with major negatives recorded in May, at the beginning of July and in August. The rapid drops are thought to be the result of increases in the degassing rate (higher output of gas volume) rather than decreases in the ratio between suspended solid materials and water, because extensive settling times required for fine-grained, clay-size particles are incompatible with the rapid decreasing observed in density.
The paroxysmal event was accompanied by several rapid, consecutive decreases in density. These fluctuations are likely attributable to high-frequency cycles of increased and decreased gas output in a very narrow time interval. This evidence is confirmed by visual observations from the personnel of the natural reserve of Maccalube di Aragona who reported substantial visible variations in the gas bubbling some days before the overturning.
The soil monitoring station started to record variations in the acquired parameters, with particular reference to electric conductivity, since some days before the paroxysm; these variations started to increment their amplitudes a few hours before the event.

Conclusions

The time series recorded in the water column at Polla 1 revealed interesting dynamics likely triggered by the paroxysmal event that occurred in late August, 2025. This eruption episode may have temporarily modified the fluid regime flow. The increase in the degassing rate could be associated with a relevant input of high-temperature and more saline water. However, the present dataset is not adequate to definitively explain the mechanisms driving these variations. Therefore, longer time series and a more comprehensive dataset, including supplementary geochemical measurements (vertical profiles, additional probes installed at different depths), is required to fully constrain and to model the physical processes responsible for the dynamics recorded in the water column at Polla 1.

Acknowledgments

This work is supported by project PROMUD “definition of a multidisciplinary monitoring PROtocol for MUD volcanoes”. funded by the Italian Ministry of University and Research INGV Pianeta Dinamico Project.

Corresponding author: fausto.grassa@ingv.it

Two-stage Deep Learning framework for Mud Volcano Mapping: Multiple Instance Learning Screening and Patch-Level Object Detection

M. Guastella[1,2], R. Martorana[2], A. Pisciotta[3], S. Speciale[3], A. D'Alessandro[3]

[1] *Dipartimento di Ingegneria Civile, Edile ed Ambientale, Università di Roma Sapienza, Italy*
[2] *Dipartimento di Scienze della Terra e del Mare, Università degli Studi di Palermo, Italy*
[3] *Istituto Nazionale di Geofisica e Vulcanologia (INGV), Italy*

1. Introduction

Mud volcanoes develop where overpressured fluids in shallow sedimentary successions find a pathway to the surface, carrying water, fine-grained sediment and gas (Kopf et al., 2002; Mazzini et al., 2017). Their emissions, generally rich in methane, links mud volcanism to active hydrocarbon systems and to broader processes of natural gas release from the upper crust (Etiope et al., 2002; Mazzini and Etiope, 2017). Mud volcanoes often occur in oil and gas regions, and their surface distribution often reflects faults, structural highs and overpressured intervals. For this reason, they can provide information regarding basin structure and fluid migration. Furthermore, they may pose local risks to infrastructure when embedded in urban context, so reliable detection is important for both exploration and hazard assessment. Satellite and aerial imagery can be employed to monitor surface changes, such as freshly extruded mud, crack patterns and pathways formed by mud outflow. However, mapping these features over wide areas is still largely manual and therefore slow and difficult to reproduce. This study tests a two-stage pipeline based on deep learning to identify mud volcanism expressions. The first stage performs scene screening through binary classification ("mud volcano presence" and "no mud volcano"), comparing patch-based Multiple Instance Learning (MIL) (Ilse et al., 2018) models that aggregate predictions from overlapping patches with a standard image-level classifier operating on the full scene. The second stage is activated only for scenes labelled as positive and applies a YOLOv5 (Jocker et al., 2020; Redmon et al., 2016), object detector to localize the area, moving toward spatial positioning of the target. The aim is to test how reliably neural networks can learn mud volcano morphology from optical imagery and to assess the potential for scalable, semi-automatic recognition workflow.

2. Dataset and Preprocessing

The dataset was manually sampled from Google Earth and includes 941 images (496 positive, 445 negative). Scenes were collected from several geographic areas to reflect variability in appearance (season, illumination) and were constrained by minimum quality (sharpness, contrast, limited atmospheric effects). Images were exported at 1920 × 1080 pixels and cropped

to 1920 × 1010 pixels to enable uniform tiling. For patch-based models, each scene was decomposed into 10 overlapping 512 × 512 patches (2 × 5 grid) as illustrated in Fig. 1. Overlap was used to reduce sensitivity to patch boundaries and to limit splitting of diagnostic features across edges. For the image-level model, the full scene was resized to 512 × 512 pixels. The negative class was deliberately selected as visually challenging (hard negatives), including erosional landforms, quarries, and agricultural/anthropic patterns that can mimic mud-volcano-like geometry. Data augmentation included rotations (90°, 180°, 270°) and horizontal/vertical flips. Dataset samples are displayed in Fig. 2.

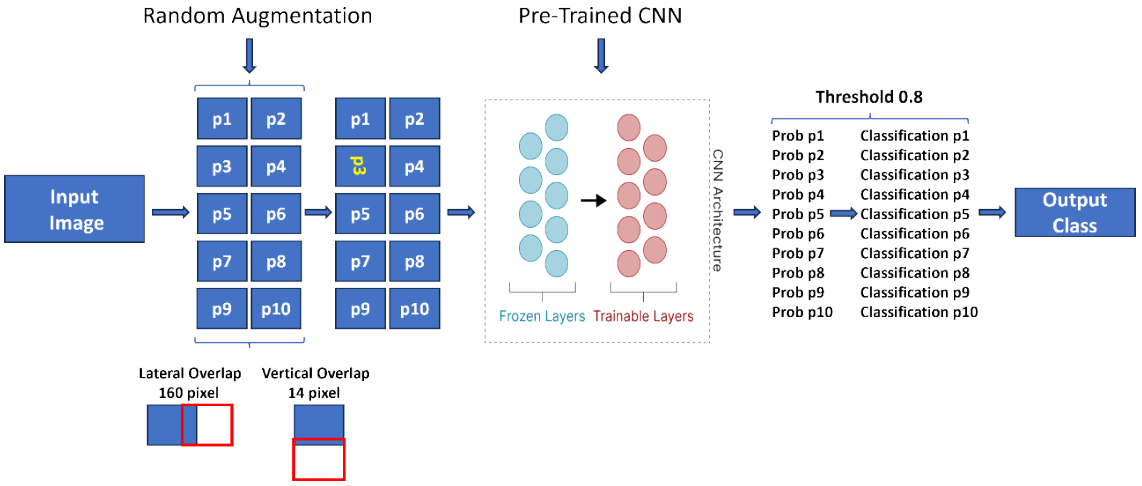

Fig. 1 – Workflow of the patch-based classification stage. Each input scene is split into 10 overlapping patches (p1 – p10), which are processed independently by a CNN backbone with pretrained (frozen) layers and fine-tuned (trainable) layers. Patch-level outputs are then aggregated at scene level to produce a single prediction and the final output class.

Fig. 2 – Representative samples from the dataset. The top row shows scenes containing mud volcanoes, with typical morphology and textures (cones, extrusion areas, radial patterns and flow features). The bottom row shows no mud volcano examples, deliberately selected as hard negatives including erosional landforms, quarries and agricultural/anthropic geometries to make the class separation more challenging and realistic.

3. Methods and Models

For the initial recognition stage, we implemented and compared four deep-learning models for classification, which we called as M1, M2, AM1 and M4. All four are binary classifiers, but they differ in how they process the input image and the backbone architecture employed.

- M1: ResNet-18 with max-pooling MIL

Each patch is processed by a ResNet-18 backbone pretrained on ImageNet (He et al., 2016) and adapted to output a single score for mud volcano presence. Patch scores are then aggregated with max-pooling to obtain the prediction for the whole scene. As a consequence, a scene is classified as positive if at least one patch provides a strong positive response, which corresponds to the standard MIL assumption for sparse targets.

- M2: MobileNetV3-Small with max-pooling MIL

M2 follows the same max-pooling MIL formulation as M1, but replaces ResNet-18 with MobileNetV3 (Howard et al., 2019), a lighter backbone designed to reduce computational cost. The purpose is to assess whether a compact network can retain adequate sensitivity to mud volcano morphology while improving efficiency and suitability for deployment even in scenarios with limited resources.

- AM1: ResNet-18 with attention-based MIL

AM1 also operates on patch sets, using ResNet-18 to extract patch-level features. Instead of max-pooling, patch contributions are combined through a learned attention mechanism (Ilse et al., 2018), which assigns a weight to each patch and produces a weighted scene-level representation before classification. This formulation can improve stability when the target signature is distributed across multiple patches and provides a direct way to inspect which patches contribute most to the final decision.

- M4: ResNet-18 global image-level classifier

M4 provides a baseline image-level approach. The entire scene was resized to 512 × 512 and fed as a single input by a ResNet-18 network (He et al., 2016) that outputs one prediction per image. Unlike the MIL models, M4 has no explicit patch decomposition and therefore tests whether a standard global CNN can achieve comparable performance losing details.

Object-detection was implemented in the second stage of the pipeline, using Yolov5 model (Jocher et al., 2020; Redmon et al., 2016), to localize mud volcano areas within scenes. YOLO family model can be described as a three-part architecture. The backbone is a CNN that extracts visual features from the image and produces feature maps at different scales. The neck then combines and refines the feature maps so that both coarse context and fine details are retained. Finally, the head uses the refined features to output the model predictions as the location of bounding boxes and the associated class scores. To avoid loss of detail from resizing full scenes, YOLOv5 was applied at the same patch level adopted for image classification. Bounding boxes were first annotated on the full-resolution images, using LabelMe, and patch-level labels were then derived automatically by projecting and clipping the original boxes within the same overlapping patching scheme used for the classification models. During inference, predictions on individual patches can be mapped back to the original image coordinates and duplicate boxes arising from patch overlap are removed using non-maximum suppression. Intersection over Union (IoU) was used to evaluate the performance of the detector (Cheng and Han, 2016). The dataset split for both classification and object detection was set to 80:20 and the total

number of epochs was equal to 100.

4. Results

Across the five-fold cross-validation, all four classification models showed similar behavior, with mean validation accuracies consistently above 80%. The highest score is obtained by the attention-based AM1 at 88%, followed by the M1 model at 85%. Performance is slightly lower for M2 (84%) and for the global image-level model M4 (83%), but the overall differences between architectures remain modest. A modest performance gain is observed for patch-based approaches, especially when attention is used to combine information from multiple tiles. This is consistent with the structure of the problem, because mud volcano sites are often local and may occupy only a fraction of the scene. Patch-based training preserves the local features and reduces the loss of detail that can occur when the full image is resized into a single input, while attention further improves aggregation by increasing the weight of the most informative patches. The error patterns are broadly consistent across architectures and are informative in terms of what limits performance. False negatives are concentrated in images where the mud volcano expression is weak or partially degraded, for example when the vent area is small relative to the scene, when cones and flow margins are subdued by erosion, when vegetation masks the surface texture or when image artefacts reduce contrast and sharpness. In these cases, the diagnostic morphology is present but not sufficiently clear at the available spatial resolution to trigger a confident positive decision. False positives are dominated by landforms and human features that reproduce similar geometry or tonal patterns. Typical examples include quarries and agricultural layouts, where the combination of shape and texture can resemble mud cones or flow lobes. In Fig. 3 is illustrated the classification result for a challenging negative class instance in the test set.

Building on this classification output, a YOLOv5 model was then tested to localize the main mud-extrusion areas. In the proposed pipeline, detection is applied only after a positive classification decision, so the detector operates in a constrained setting where mud volcanism is expected, and the aim is spatial localization rather than scene rejection. To avoid losing detail through resizing, YOLO was run on overlapping patches, and the resulting boxes were mapped back to the original image coordinates and merged to remove duplicates. Object Detection results are promising but still preliminary due to the limited number of annotated images and the strong inter-site variability. On the labelled set, the detector provides reliable coarse localization (mean average precision about 0.55 at 0.5 IoU), but performance drops under stricter overlap requirements (mean average precision of 0.28 from 0.5 to 0.95 IoU). This drop is expected because mud-extrusion margins are often diffuse and irregular and may be obscured by erosion, vegetation and variable imaging conditions, making tight bounding boxes difficult. Overall, to improve robustness more annotations are required and broader training coverage across different geological and environmental settings.

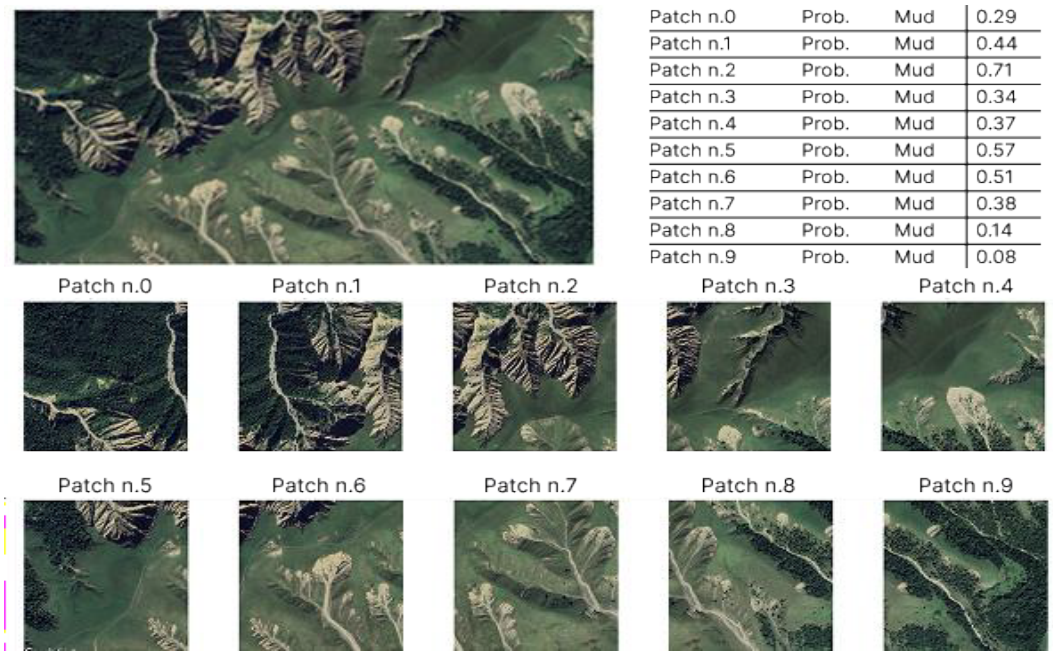

Fig. 3 – Challenging negative example from the test set. The full scene (top) was correctly classified as "no mud volcano", but some patches in the 2 × 5 tile grid (bottom) reached probabilities up to 0.71. The landscape is dominated by erosional forms that can mimic dry mud-volcano cones and flow-like structures.

5. Discussion

This work shows that mud volcano patterns can be recognized from optical aerial and satellite imagery with good reliability using standard CNNs and established deep learning paradigms for remote sensing (Ma et al., 2019; Zhu et al., 2017). All four classifiers reach mean accuracies above 80%, with the attention-based MIL (AM1) performing best and only modest differences across architectures. Patch-based MIL slightly outperforms the global image-level approach, which is consistent with mud volcano features often occupying only a limited portion of the scene. Attention further improves aggregation by emphasizing the most informative patches. Errors highlight the main limitations: false negatives mostly occur when the expression is weak or partially masked, while false positives are driven by geomorphic and anthropic structures such as quarries or agricultural patterns, consistent with known challenges in optical remote sensing detection (Cheng and Han, 2016). Image-level cross-validation may place scenes from the same site in both training and validation, inflating generalization. Future work should use leave-one-site-out testing and expand the dataset.

References

Cheng, G., and Han, J.; 2016: A survey on object detection in optical remote sensing images. ISPRS Journal of Photogrammetry and Remote Sensing, 117, 11–28. https://doi.org/10.1016/j.isprsjprs.2016.03.014

Etiope, G., Caracausi, A., Favara, R., and Italiano, F.; 2002: Methane emission from the mud volcanoes of Sicily (Italy). Geophys. Res. Lett., 29(8), 1215. https://doi.org/

10.1029/2001GL014340

He, K., Zhang, X., Ren, S., and Sun, J.; 2016: Deep residual learning for image recognition. In Proceedings of the IEEE Conference on Computer Vision and Pattern Recognition (CVPR) (pp. 770–778). https://doi.org/10.1109/CVPR.2016.90

Howard, A., Sandler, M., Chu, G., Chen, L.-C., Chen, B., Tan, M., Wang, W., Zhu, Y., Pang, R., Vasudevan, V., Le, Q. V., and Adam, H.; 2019: Searching for MobileNetV3. In Proceedings of the IEEE/CVF International Conference on Computer Vision (ICCV) (pp. 1314–1324). https://doi.org/10.1109/ICCV.2019.00140

Ilse, M., Tomczak, J. M., and Welling, M.; 2018: Attention-based deep multiple instance learning. In J. Dy & A. Krause (Eds.). Proceedings of the 35th International Conference on Machine Learning (ICML) (Proceedings of Machine Learning Research, Vol. 80, pp. 2127–2136). PMLR.

Jocher, G., Changyu, L., Hogan, A., Yu, L., et al.; 2020: ultralytics/yolov5: Initial Release (Version v1.0) [Computer software]. Zenodo. https://doi.org/10.5281/zenodo.3908560

Kopf, A. J.; 2002: Significance of mud volcanism. Rev. Geophys., 40(2), 1005. https://doi.org/10.1029/2000RG000093

Ma, L., Liu, Y., Zhang, X., Ye, Y., Yin, G., and Johnson, B. A.; 2019: Deep learning in remote sensing applications: A meta-analysis and review. ISPRS Journal of Photogrammetry and Remote Sensing, 152, 166–177. https://doi.org/10.1016/j.isprsjprs.2019.04.015

Mazzini, A., and Etiope, G.; 2017: Mud volcanism: An updated review. Earth-Sci. Rev., 168, 81–112. https://doi.org/10.1016/j.earscirev.2017.03.001

Redmon, J., Divvala, S., Girshick, R., and Farhadi, A.; 2016: You Only Look Once: Unified, Real-Time Object Detection. In Proceedings of the IEEE Conference on Computer Vision and Pattern Recognition (CVPR) (pp. 779–788). https://doi.org/10.1109/CVPR.2016.91

Zhu, X. X., Tuia, D., Mou, L., Xia, G.-S., Zhang, L., Xu, F., and Fraundorfer, F.; 2017: Deep learning in remote sensing: A comprehensive review and list of resources. IEEE Geoscience and Remote Sensing Magazine, 5(4), 8–36. https://doi.org/10.1109/MGRS.2017.2762307

Corresponding author: massimiliano.guastella@uniroma1.it

Porosity calculation of Marsili rocks through imaging analysis and samples measurements

G. Maurizio[1], C. Braitenberg[1] , T. Trua[2], M. Marani[3], F. Bernardini[4,5], A. De Min[1]

[1] Department of Mathematics, Informatics and Geosciences, University of Trieste, Italy.
[2] Department of Chemistry, Life Sciences and Environmental Sustainability, University of Parma, Italy.
[3] Institute of Marine Sciences, ISMAR – CNR, Italy.
[4] Department of Humanities, Ca' Foscari University of Venice, Italy.
[5] Multidisciplinary Laboratory, The Abdus Salam International Centre for Theoretical Physics, Italy.

In this study, we present the findings of an analytical investigation conducted on samples obtained from the Marsili Seamount. The objective of the investigation was to characterize the petrophysical characteristics of the rocks, particularly the porosity. The Marsili Seamount is the largest submarine volcano in the Mediterranean Sea. The summit cone of Marsili is located at a depth of 490 meters below sea level, with the volcano rising approximately 3,000 meters above the seafloor. The formation extends for a distance of 60 kilometers along a NNE-SSW orientation, with an average width of 16 kilometers (Trua et al., 2002).

Porosity measurements were performed using two different methods:

1. Mass and density measurements using hydrostatic balance.

2. Microtomography (MCT) scanning of rock samples and imaging segmentation.

The eight samples that were analyzed were obtained from a dredging campaign. The samples collected are representative of different areas of the volcano and sea depths, from 600 meters below sea level (top of the volcano) to 3,000 meters below sea level.

The hydrostatic balance was employed to collect analytics measurements of mass and density of the samples. To mitigate potential errors resulting from instrumentation, five distinct weights were carried out on dry samples using two distinct balances. Subsequently, the samples were immersed in water for a period of 72 hours, after which the measurements were repeated to calculate the mass and density of the saturated sample. The porosity was then calculated from the obtained data. Concurrently, a segmentation analysis was conducted on the ultra-resolute images of the samples collected from the MCT scan. The cone-beam MCT station was constructed by ICTP and Elettra Sincrotrone in Trieste. The system has been meticulously engineered for the analysis of large objects, such as rock samples, with a resolution of 40-50 micrometers. The apparatus consists of two primary components: a tube for X-ray production, which is generated by a microfocus X-ray source (150 kV maximum voltage, 500 µA maximum current, 5 µm minimum focal spot size); and a

detector, which is a flat panel sensor coupled to a fiber optic plate under the GOS scintillator. The device under consideration is noteworthy for its high efficiency in converting radiation, and it is equipped with a sample positioning system that incorporates two linear translation axes and a rotation stage.

MCT scan provides a series of slices of the sample, enabling three-dimensional analysis. The segmentation process was employed to distinguish pixels associated with the rock from those associated with voids, indicative of the porosity. From these results it is possible to determine the calculated porosity for each sample, knowing the size of the single pixel in the image.

Subsequently, a comparison was made between the measured and calculated porosities. The two measurements generally align with each other and estimate a porosity for Marsili rocks that, in some cases, reaches 10-12%. In rocks with higher porosity, the measurements on the samples resulted in a porosity estimation greater than the calculated one, while for less porous rocks, the results exhibited substantial consistency, with a slightly higher estimate for the calculated porosity values compared to the measured ones. These two alternative approaches to porosity estimation are significant in facilitating more precise modeling of fluid movements within the volcanic area.

References

Trua T., G. Serri, M. Marani, A. Renzulli, F. Gamberi; 2002: Volcanological and petrological evolution of Marsili Seamount (southern Tyrrhenian Sea). Journal of Volcanology and Geothermal Research. 114, 3–4. 441-464. https://doi.org/10.1016/S0377-0273(01)00300-6.

Corresponding author: gerardo.maurizio@units.it

Magma chamber failure and dyke injection threshold for magma-driven unrest at Campi Flegrei caldera

Jacopo Natale[1], Stefano Votaòe[2]

[1] *Dipartimento di Scienze della Terra e Geoambientali, Università di Bari Aldo Moro*

[2] *Dipartimento di Scienze della Terra, dell'Ambiente e delle Risorse, Università di Napoli Federico II*

How much magma must be added to a shallow chamber to trigger rupture, dyke injection, and potentially an eruption? Developing models that robustly answer this question is essential for reliable eruption forecasting during volcanic unrest. Because a long-lived shallow reservoir requires periodic recharge from deeper sources, detecting the signals associated with pressurization and volume change is of critical importance. Integrating high-resolution seismic tomography (Giacomuzzi et al., 2024), geological data (Natale et al., 2026), and petrologic constraints (Arienzo et al., 2025), and continuum- and fracture-mechanics modelling (Gudmundsson, 2011), we calculate the excess pressure required to rupture the magma chamber and initiate dyke propagation at Campi Flegrei caldera, southern Italy. We reconstruct the geometry and physical properties of the dyke that fed the ~3.9 ka Nisida eruption, a ~0.16 km³ fissure-fed phreatomagmatic event located on the caldera rim (Fig. 1).

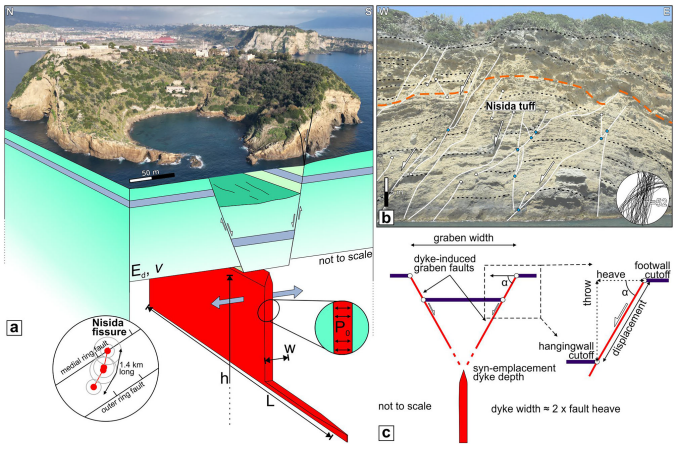

Fig. 1 – UAV photograph of the Nisida tuff cone and simplified illustration of the feeder dyke (Natale & Vitale, 2025).

Our results show that the feeder dyke ascended from a ~5 km-deep reservoir (Natale and Vitale, 2025), consistent with petrologic estimates identifying a 4–6 km depth range as the principal zone of eruptible magma storage (Fig. 2a) during the last 5 kyr (Amstutz et al., 2025), and consistent with magma emplacement and degassing source depth in the last few years (Caliro et al., 2025). We estimate the active chamber volume at 85–150 km³, considering a fully molten and a

poroelastic mush, respectively, with a rupture threshold at ~9 MPa of excess pressure, corresponding to ~170 MPa of magmatic overpressure at depth.

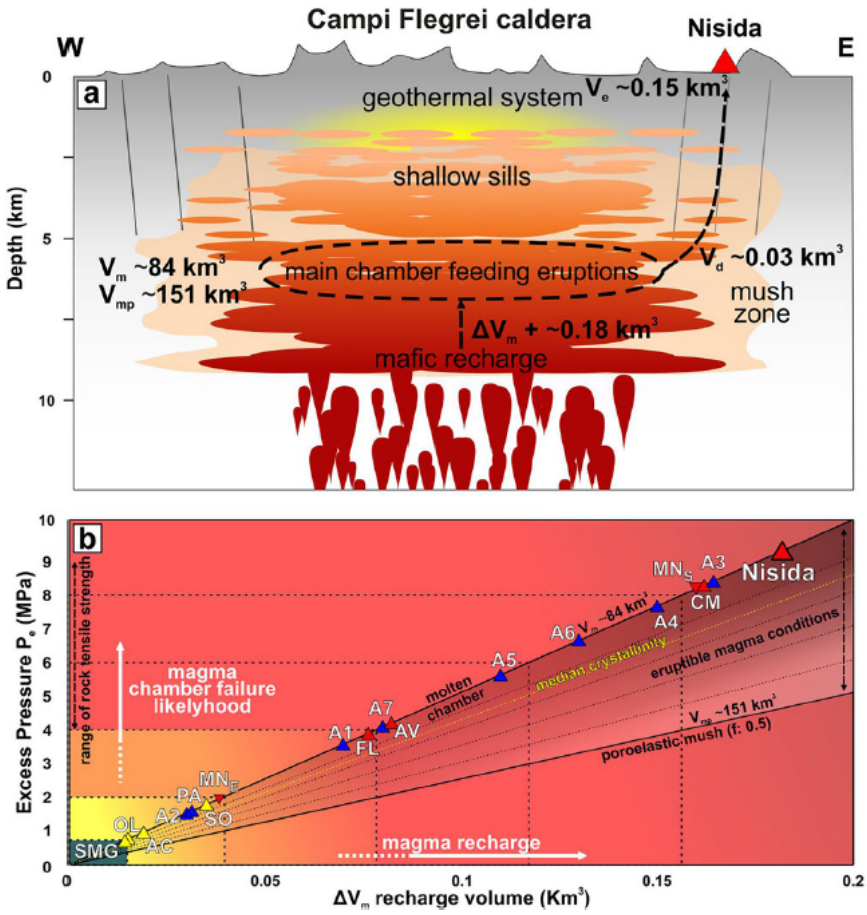

Fig. 2 – a) Simplified sketch of the Campi Flegrei magma domain; b) Diagram showing the calculated relationship between magma volume change and magmatic excess pressure required to rupture the reservoir.

A similar 4–9 MPa excess-pressure threshold characterizes moderate-sized eruptions along the caldera margin during Epoch 3b, supporting the existence of a shared magma reservoir, corroborating isotopic evidence (Fig. 2b). Finally, by evaluating the volume change needed to reach rupture, we simulate the resulting ground deformation (Fig. 3a) and show that the predicted pattern is distinct from current geodetic observations, implying that a distinct geodetic signature may precede near-rupture conditions (Fig. 3b), crucially anticipating the formation of a dyke.

This work provides a quantitative framework for recognizing the transition from magma-driven unrest to eruption at Campi Flegrei caldera and should stimulate further characterization of the physical properties of the shallow crust, pivotal to accurately estimate rupture conditions at depth. Altogether, this information can timely inform decision-makers and stakeholders involved in the management of a highly challenging crisis.

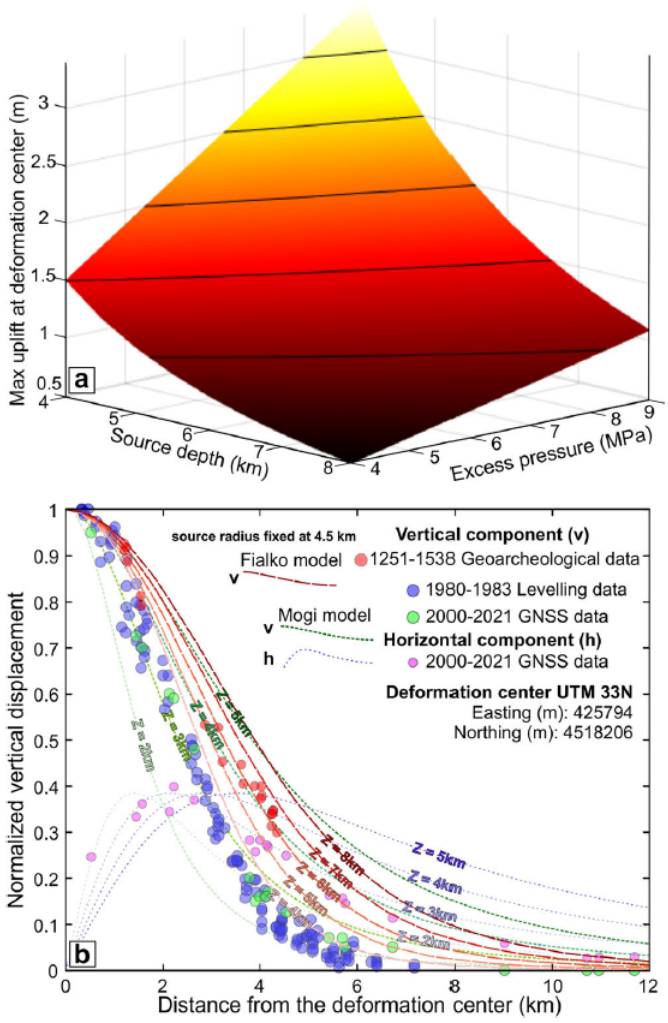

Fig. 3 – Geodetic modeling of Campi Flegrei deformation source. a) 3D plot showing the tradeoff between the source depth and magmatic excess pressure of a sill-like source in producing a spectrum of uplift values at the deformation center. b) Plot showing the comparison between normalized vertical displacement of a Mogi point source and a Fialko sill-like source displaying a bell-shaped pattern as computed for different source depths with a fixed radius of 4.5 km.

References

Giacomuzzi,G., Chiarabba, C., Bianco, F., DeGori, P. and Agostinetti, N. P.; 2024: Tracking transient changes in the plumbing system at Campi Flegrei Caldera. Earth and Planetary Science Letters, Vol. 637, 118744, https://doi.org/10.1016/j.epsl.2024.118744

Natale, J., Cascella, E. and Vitale, S.; 2026: Tracking the growth and deformation of fissure phreatomagmatic eruptions: insights from the ~3.9 ka Nisida eruption at Campi Flegrei caldera. Geological Society of America Bulletin, Vol. 138, n. 1-2, pp. 445-468. https://doi.org/10.1130/B38367.1

Arienzo, I., Mazzeo, F. C., Moretti, R., Cavallo, A. and D'Antonio, M.; 2016: Open-system magma evolution and fluid transfer at Campi Flegrei caldera (Southern Italy) during the past 5 ka as

revealed by geochemical and isotopic data: the example of the Nisida eruption. Chemical Geology, Vol. 427, pp. 109-124, https://doi.org/10.1016/j.chemgeo.2016.02.007

Gudmundsson, A.; 2011: Rock Fractures in Geological Processes. Cambridge University Press.

Natale, J., and Vitale, S.; 2025: Magma chamber failure and dyke injection threshold for magma-driven unrest at Campi Flegrei caldera. Nature Communications, Vol. 16, n 1, 7658, https://doi.org/10.1038/s41467-025-62636-7

Amstutz, F. M. et al.; 2025: Volcano-tectonic controls on magmatic evolution at Campi Flegrei, Italy: insights from thermodynamic modelling. Journal of Petrology, Vol. 66, n. 8, egaf068, https://doi.org/10.1093/petrology/egaf068

Caliro, S. et al.; 2025: Escalation of caldera unrest indicated by increasing emission of isotopically light sulfur. Nature Geoscience, Vol. 18, pp. 167-174, https://doi.org/10.1038/s41561-024-01632-w

Corresponding author: jacopo.natale@uniba.it

When gravity data lie: how thermo-poro-elastic processes mask magma

Massimo Nespoli[1], Maurizio Bonafede[1], Maria Elina Belardinelli[1]

[1] Alma Mater Studiorum, University of Bologna, Department of Physics and Astronomy " Augusto Righi", Viale Berti Pichat 8, Bologna 40127, Italy

Understanding the processes that drive ground deformation and gravity changes in volcanic areas is essential for interpreting unrest episodes and assessing volcanic hazards. While magmatic intrusions have traditionally been considered the dominant source of such signals (e.g. Walsh and Rice, 1979; Trasatti and Bonafede, 2008; Nikkhoo and Rivalta, 2022), recent work has highlighted the important role played by shallow hydrothermal systems (Nespoli et al., 2026). In this study, we investigate the gravimetric effects produced by Thermo-Poro-Elastic (TPE) inclusions. The latter represent rock volumes that undergo changes in pore pressure and temperature due to the arrival of hot, pressurized fluids released from deeper magma reservoirs (Fig. 1).

Building on recent analytical and semi-analytical solutions for TPE sources (a review of them was done by Nespoli et al., 2025), we compute the gravity variations induced by disk-shaped inclusions embedded in an elastic half-space and quantify the contributions associated with solid and fluid compressibility, thermal expansion, and deformation-related density changes.

We explore several scenarios involving both liquid- and vapor-saturated inclusions, choosing pressure–temperature variations that generate identical uplift but distinct gravity responses. Our results demonstrate that the fluid phase strongly controls the resulting gravity residuals. Liquid-filled inclusions produce significant negative gravity variations, while vapor-dominated inclusions lead to negligible changes even when the associated uplift is large. This reveals a strong potential decorrelation between deformation and gravity signals, fundamentally different from the behaviour of classical magmatic sources in which increased volume typically requires an associated mass influx.

We also show that if the fluid is near the equilibrium curve of water (Clapeyron's diagram), small pressure perturbations can trigger phase transitions that generate abrupt density changes within a thin layer at the top of the TPE inclusion. These transitions can produce measurable positive gravity residuals without notable surface uplift, offering an explanation for gravity fluctuations observed in several volcanic systems during periods of weak deformation. This mechanism is particularly relevant for hydrothermal zones.

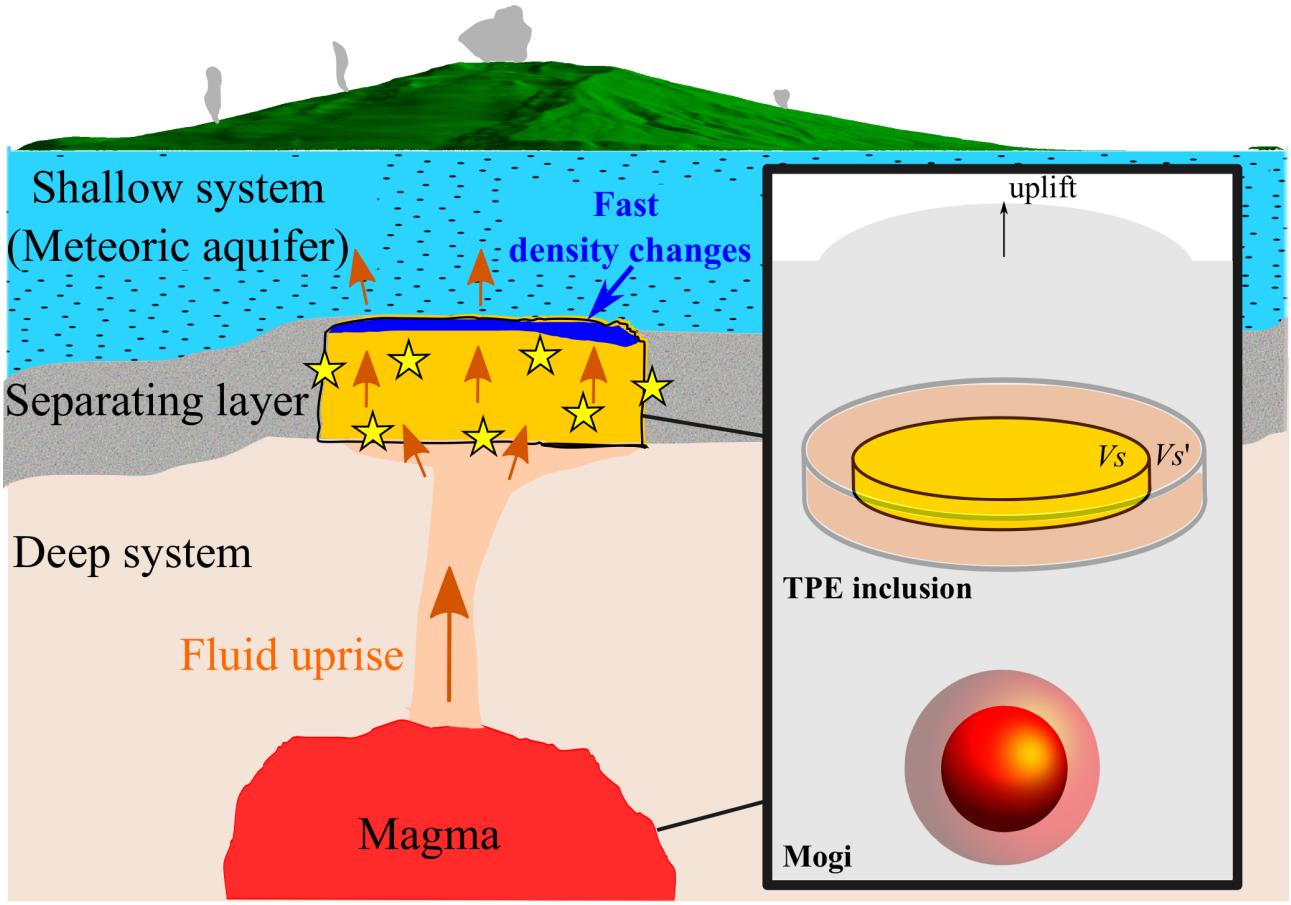

Fig. 1 – Sketch a possible scenario in which a TPE inclusion (orange) undergoing a variation of volume from Vs to Vs' is located above a deeper magma chamber (red) in a volcanic system. The exsolved fluids (arrows) released from the magma chamber rise toward a brittle layer (gray) separating the deep circulation from the shallower (meteoric aquifer in light blue) one. The fractured, permeable part of the layer can be represented by a TPE inclusion that acts as a deformation source and it is able to generate seismicity. In the inset the reference system is shown which is employed in the following computations, assuming a disk-shaped TPE inclusion and a spherical magma chamber (Mogi's).

Applying these results to the ongoing unrest at Campi Flegrei (Italy), we compare synthetic gravity variations from TPE inclusions with long-term measurements. Our analysis indicates that TPE processes alone cannot reproduce the positive gravity residuals observed during the past 1982–84 uplift episode, suggesting a substantial magmatic contribution. However, TPE effects are consistent with the gravity oscillations observed after 1985, which are not associated with significant deformation. Furthermore, when combined with a deeper magmatic source, a shallow TPE inclusion can partially or completely mask the gravity signature of magma ascent, implying that the absence of clear gravimetric signals cannot be taken as evidence against magmatic involvement. Overall, our findings demonstrate that TPE processes significantly influence gravity observations in volcanic environments.

References

Nespoli, M., Yu, H., Rinaldi, A.P., Harrington, R., Belardinelli, M.E., Martinelli, G. and Piombo, A.; 2025: Applications and future developments of the (thermos-) poro-elastic theory in geophysics. Earth-Science Reviews, Vol. 260, 104996. https://doi.org/10.1016/j.earscirev.2024.104996

Nespoli M., Bonafede M. and Belardinelli M.E.; 2026: The role of Thermo-Poro-Elastic effects in the interpretation of gravity data. Earth and Planetary Science Letters, Vol. 674, 119762, https://doi.org/10.1016/j.epsl.2025.119762

Nikkhoo, M., and Rivalta, E.; 2022: Analytical solutions for gravity changes caused by triaxial volumetric sources. Geophysical Research Letters, Vol. 49, e2021GL095442, https://doi.org/10.1029/2021GL095442

Trasatti, E., and Bonafede, M.; 2008: Gravity changes due to overpressure sources in 3d heterogeneous media: application to campi flegrei caldera. Annals of Geophysics, Vol. 51, n. 1, pp. 119-133, https://doi.org/10.4401/ag-4444

Walsh, J.B., and Rice, J.R.; 1979: Local changes in gravity resulting from deformation. Journal of Geophysical Research, Solid Earth, Vol. 84, pp. 165-170, https://doi.org/10.1029/JB084iB01p00165

Corresponding author: massimo.nespoli2@unibo.it

Sassolite precipitation at the restless Campi Flegrei volcano in Italy points to hydrothermal flashing by deep boron-rich brines

M. Piochi[1], A. Mormone[1], G. Solomita[1,2], R. Moretti[3]

[1] Istituto Nazionale di Geofisica e Vulcanologia, Osservatorio Vesuviano, Naples, Italy.
[2] Università di Napoli Federico II Dipartimento di Scienze della Terra, dell'Ambiente e delle Risorse, Naples, Italy.
[3] Università degli Studi della Campania Luigi Vanvitelli, Dipartimento di Ingegneria, Naples, Italy.

Boron, a rare, but remarkable compounds in geoscience and industry (Helvacı, 2017; Kot, 2009), is mainly found in the continental crust and seawater, linked to subduction processes, slab metasomatism, acidic magmatism, and evaporitic environments. Boron-bearing minerals typically occur in pegmatitic settings around plutons, marine evaporite deposits and volcano-sedimentary playa lake. However, volcanic activity plays a key role in borate formation, being sassolite, or crystalline boric acid (H_3BO_3), "*the most common boron mineral known to be of direct volcanic-exhalation origin or to be generated by the evaporation of hot-spring waters*" (Schaller, 1936). Sassolite was reported for example (Bernard et al., 2011; Peretyazhko et al., 2000; Schaller, 1936), at Vulcano and Lipari (Italy), Yellowstone (US), Shiveluch and Bezymyannyi (Russia), Los Humeros (Mexico). From the original magmatic source, boron is in fact transported by geothermal fluids and post-volcanic gases to hot springs, fumaroles and solfataras (Ellis et al., 2022; Peretyazhko et al., 2000; Pollard et al., 1987; Simmons & Webber, 2008; Thomas et al., 2006). B-mineralogy has then the potential to be an informative marker of steam-related processes occurring at volcanoes with important hydrothermal systems, such as in the case of calderas.

Building on this perspective, we investigated borate appearance as a novel finding for the geothermal dynamics during the ongoing unrest at the Campi Flegrei (CF, Italy; Fig. 1). CF, particularly in the Pozzuoli area, is the archetype of a "dormant", meaning it is likely to erupt in future, and "restless" volcanic caldera, meaning that it shows signs of subterranean evolution related to magmatic activity. Here, the large size of the inflating hydrothermal system masks deeper signals and leads to blurred or even contrasting interpretations about the involvement of ascending magmas and/or infiltrating brines originating unrest. In this context, the appearance of new minerals during the progression of an unrest fixes undoubted thermodynamic constraints about changes occurring in the source composition, pressure and temperature of uprising fluids.

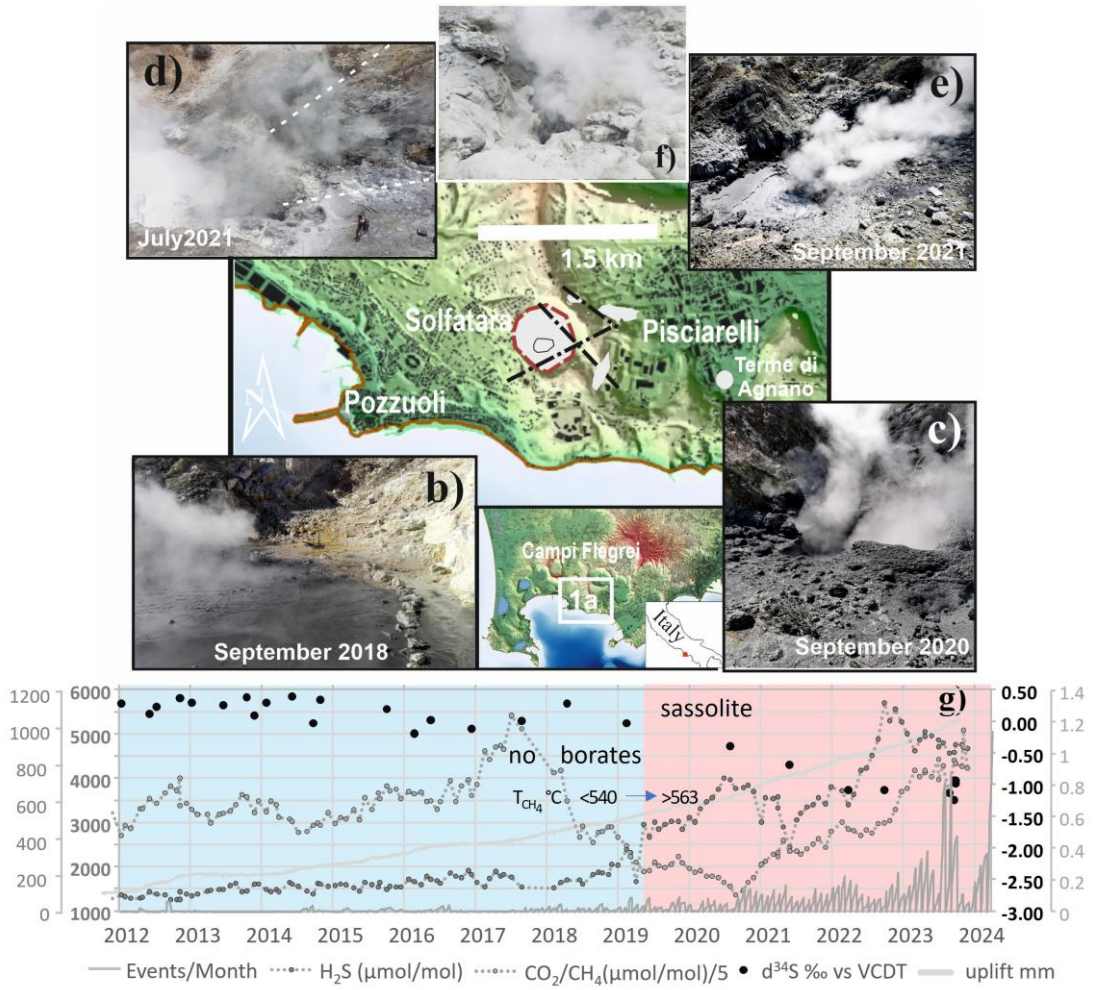

Fig. 1 – Study area and timeline of main bradyseism related variations since 2012. **(a)** CF location and view showing in gray sulfate areas of the Solfatara cone, with its crater circled by a red line, the Pisciarelli discharge site and main tectonic faults, as modified from (Piochi et al., 2019); **(b, c, d, e, f)** Pisciarelli characterized by a water-filled pool in September 2018 and the variated drying up conditions in 2020 and 2021; **(g)** The period with lack of borate phases and sassolite occurrence within the surveyed hydrothermal assemblage, compared with seismicity, ground deformation, H_2S, CO_2/CH_4 and $\delta^{34}S$ (‰) patterns at the Bocca Grande fumarole since 2012 (data from (Bevilacqua et al., 2024; Caliro et al., 2025); http:// https://terremoti.ov.ingv.it/gossip/, access on June 9, 2025). Interestingly, equilibrium temperatures of CH_4 formation at 3-4 km (Marini et al., 2025b) also mark a substantial increase at the time of the sassolite appearance.

Owing to a decadal-long periodical mineralogical survey of hydrothermal mineral assemblage at CF, we point out an unexpected widespread presence of sassolite at Pisciarelli, coinciding with dried-up hydrothermal waters (Fig. 1) and escalating bradyseism (Bevilacqua et al., 2024; Danesi et al., 2024). Through literature and new mineral, chemical and $\delta^{11}B$ data in volcanic rocks and waters, we examine the meaning of its abrupt appearance in the light of intensified seismicity (Danesi et al., 2024; di Uccio et al., 2023), increased H_2S and a drop of its $\delta^{34}S$ (Caliro et al., 2025; Marini et al., 2025a) recorded from 2021 to 2024 (Fig. 1).

The sassolite was univocally identified by major peaks at 3.06, 6.02 and 5. 89 Å in our experimental spectra and well-reproduced by the ICDD standard 96-900-7676; together with koktaite, sulfur, mascagnite, alunite and pyrite, it simulated the mineralogical assemblage of the Pisciarelli mud pool. Data collected from 2012 onwards (Fig. 2), matches in terms of mineralogical association except for sassolite, which appeared when NH_4-sulfates, previously abundant, vanished.

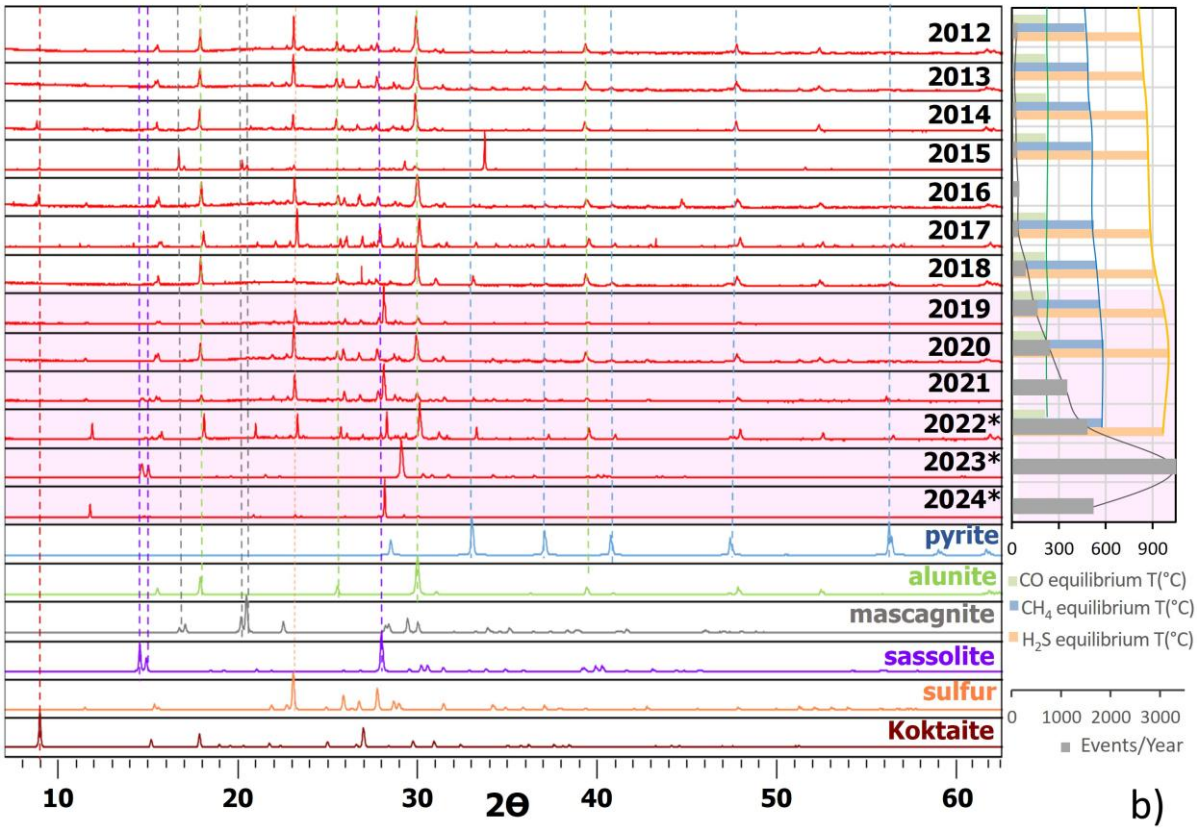

Fig. 2 – Mineral changes at the Pisciarelli mud pool. **(a)** Stacked XRD patterns of representative samples across different sampling times. The colored vertical lines indicate peaks of crystalline standards from the ICSD database, utilized for simulating experimental spectra. **(b)** Variation of equilibrium temperature (T) of CO, CH_4 and H_2S emitted at Bocca Grande fumarole (Marini et al., 2025b) and seismic monthly count. The purple box highlights the sassolite appearance period. * indicates disappearance of springs with pH<2.

Our study also considers and integrates previous information and modeling of elemental boron and its phases from CF (Caprarelli et al., 1997; Chiodini et al., 1988; De Vivo et al., 1989; Guglielminetti, 1986; Iovine et al., 2024; Moretti et al., 2018; Piochi et al., 2019, 2019; Valentino & Stanzione, 2003) and other volcanic sites (Boschetti, 2011; Kracek et al., 1938; Peretyazhko et al., 2000; Pollard et al., 1987; Simmons & Webber, 2008; Taguchi et al., 1981; Thomas et al., 2006) leading us to propose that sassolite appearance relates to the direct ascent from the deep roots (i.e., >2 km) of the geothermal system of vapors close to the critical point of water. Specifically, we show that the shallow system can no longer buffer the steam during the actual unrest, as it has instead occurred over the last 40 years (Fig. 3).

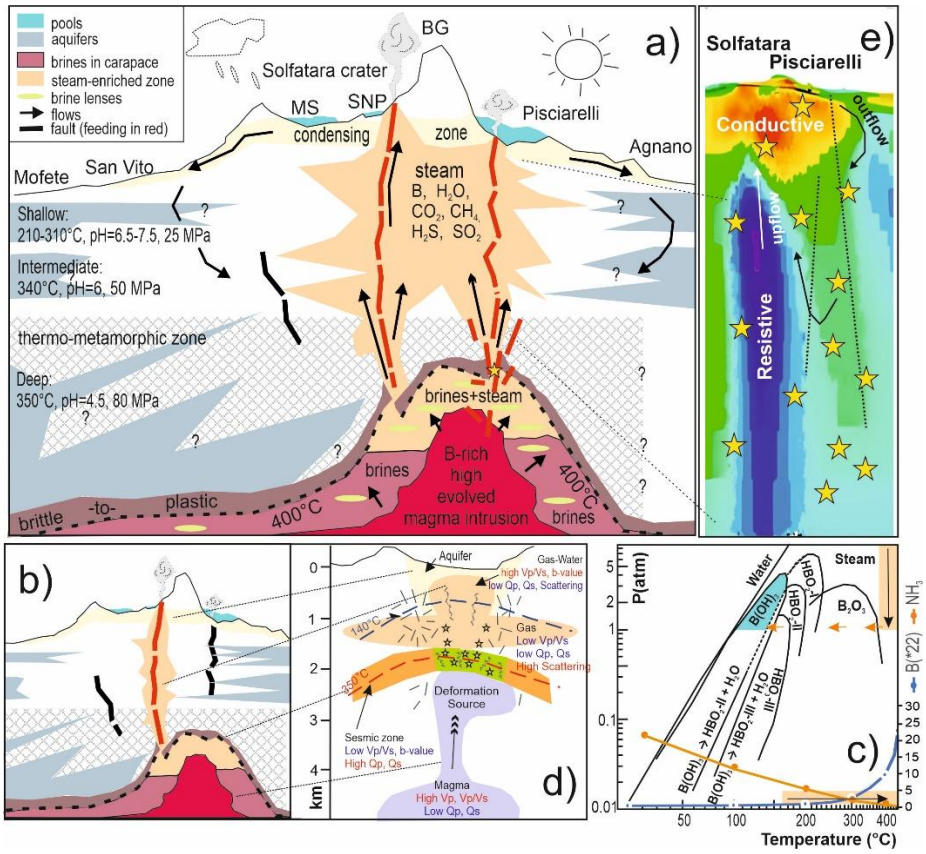

Fig. 3 – Conceptual model for CF and constraining geophysical data. **(a)** Model of boron brines flashing into steam due fracturing of the carapace (adapted from Fournier, 1999 and Helvacı, 2017). The sketch assemblies from surface downwards the sulfate area with a steam-heated condensing zone (Piochi et al., 2015, 2019) above the high temperature geothermal system and the thermo-metamorphic zone with two main shallow aquifers and the deeper ones featured by brines (AGIP, 1987; De Vivo et al., 1989) and the degassing pressurizing source with the fluids-enriched carapace and the brittle-to ductile transition as derived by (Tramelli et al., 2024). Red lines are fracturing zones. **(b)** Model before the sassolite onset; the degassing pathway from the deep source only reaches the surface at the fumaroles of the Solfatara crater. **(c)** Diagram redrawn from (Kracek et al., 1938) illustrating the field stability of boron crystalline phases, steam and water as function of pressure and temperature variation. The orange upper box with a black arrow indicates the thermo-barometric condition of the deeply-sourced B-rich fluids and the isothermal pathway up to the surface where a rapid cooling allows crossing the $B(OH)_3$ field (horizontal orange arrow) and the sassolite crystallization. The two lines at the plot bottom indicate the B and NH_3 distribution in the steam vs. water as a function of temperature according to experimental data of (Chiodini et al., 1988). The arrow at the bottom of the diagram shows how the system heating associated with the steam flashing determines the volatilization of B, whilst the ammonia remains in the liquid, in agreement with the disappearance of NH_4-sulfates at the sassolite onset. **(d)** Seismic tomography identifying aquifers, gas reservoir, caprock which differ for seismic parameters (Calò & Tramelli, 2018; Tramelli et al., 2024). **(e)** Magnetotelluric tomography showing the conductive liquid volume overlying a resistive plume ascending toward the Solfatara areas; arrows for the main fluids pathways, stars for qualitative seismicity representation, and dashed lines for main faults (Siniscalchi et al., 2019). MS: La Fangaia mud pool; SNP: New pool; BG: Bocca Grande fumarole into the Solfatara crater.

References

AGIP. (1987). *Geologia e geofisica del sistema geotermico dei Campi Flegrea.* AGIP, Internal Report, pp. 624.

Bernard, R., Taran, Y., Pennisi, M., Tello, E., & Ramirez, A. (2011). Chloride and Boron behavior in fluids of Los Humeros geothermal field (Mexico): A model based on the existence of deep acid brine. *Applied geochemistry*, *26*(12), 2064–2073.

Bevilacqua, A., Neri, A., De Martino, P., Giudicepietro, F., Macedonio, G., & Ricciolino, P. (2024). Accelerating upper crustal deformation and seismicity of Campi Flegrei caldera (Italy), during the 2000–2023 unrest. *Communications Earth & Environment*, *5*(1), 1–14.

Boschetti, T. (2011). Application of brine differentiation and Langelier–Ludwig plots to fresh-to-brine waters from sedimentary basins: Diagnostic potentials and limits. *Journal of Geochemical Exploration*, *108*(2), 126–130.

Caliro, S., Chiodini, G., Avino, R., Carandente, A., Cuoco, E., Di Vito, M., Minopoli, C., Rufino, F., Santi, A., Lages, J., & others. (2025). Escalation of caldera unrest indicated by increasing emission of isotopically light sulfur. *Nature Geoscience*, 1–8.

Calò, M., & Tramelli, A. (2018). Anatomy of the Campi Flegrei caldera using enhanced seismic tomography models. *Scientific reports*, *8*(1), 16254.

Caprarelli, G., Tsutsumi, M., & Turi, B. (1997). Chemical and isotopic signatures of the basement rocks from the Campi Flegrei geothermal field (Naples, southern Italy): Inferences about the origin and evolution of its hydrothermal fluids. *Journal of Volcanology and Geothermal Research*, *76*(1–2), Articolo 1–2. https://doi.org/10.1016/S0377-0273(96)00072-8

Chiodini, G., Comodi, P., & Giaquinto, S. (1988). Ammonia and boric acid in steam and water. Experimental data from geothermal wells in the Phlegrean Fields, Naples, Italy. *Geothermics*, *17*(5–6), 711–718.

Danesi, S., Pino, N. A., Carlino, S., & Kilburn, C. R. (2024). Evolution in unrest processes at Campi Flegrei caldera as inferred from local seismicity. *Earth and Planetary Science Letters*, *626*, 118530.

De Vivo, B., Belkin, H. E., Barbieri, M., Chelini, W., Lattanzi, P., Lima, A., & Tolomeo, L. (1989). The campi flegrei (Italy) geothermal system: A fluid inclusion study of the mofete and San Vito fields. *Journal of Volcanology and Geothermal Research*, *36*(4), Articolo 4. https://doi.org/10.1016/0377-0273(89)90076-0

di Uccio, F. S., Lomax, A., Natale, J., Muzellec, T., Festa, G., Nazeri, S., Convertito, V., Bobbio, A., Strumia, C., & Zollo, A. (2023). Delineation and fine-scale structure of active fault zones during the 2014-2023 unrest at the Campi Flegrei caldera (southern Italy) from high-precision earthquake locations. *Authorea Preprints*.

Ellis, B. S., Neukampf, J., Bachmann, O., Harris, C., Forni, F., Magna, T., Laurent, O., & Ulmer, P. (2022). Biotite as a recorder of an exsolved Li-rich volatile phase in upper-crustal silicic magma reservoirs. *Geology*, *50*(4), 481–485.

Guglielminetti, M. (1986). Mofete geothermal field. *Geothermics*, *15*(5–6), Articolo 5–6. https://doi.org/doi.org/10.1016/0375-6505(86)90091-X

Helvacı, C. (2017). Borate deposits: An overview and future forecast with regard to mineral deposits. *Journal of Boron*, *2*(2), 59–70.

Iovine, R. S., Galli, G., Rufino, F., Caliro, S., Cuoco, E., Minopoli, C., Santi, A., Avino, R., & Piochi, M. (2024). Radon and water geochemistry at the active Campi Flegrei volcano (Italy): The role of pore-water phenomena. *Geochemistry*, *84*(3), 126171.

Kot, F. S. (2009). Boron sources, speciation and its potential impact on health. *Reviews in Environmental Science and Bio/Technology*, *8*, 3–28.

Kracek, F., Morey, G., & Merwin, H. (1938). The system. Water-Boron oxide. *American Journal of Science*, *5*, 143–171.

Marini, L., Principe, C., & Lelli, M. (2025a). Closed-System Magma Degassing and Disproportionation of SO2 Revealed by Changes in the Concentration and δ34S Value of H2S (g) in the Solfatara Fluids (Campi Flegrei, Italy). *Geosciences*, *15*(5), 162.

Marini, L., Principe, C., & Lelli, M. (2025b). Time changes during the last 40 years in the Solfatara magmatic–hydrothermal system (Campi Flegrei, Italy): New conceptual model and future scenarios. *Solid Earth*, *16*(6), 551–578.

Moretti, R., Troise, C., Sarno, F., & Natale, G. D. (2018). Caldera unrest driven by CO2-induced drying of the deep hydrothermal system. *Scientific Reports*, *8*(1), Articolo 1. https://doi.org/10.1038/s41598-018-26610-2

Peretyazhko, I., Prokof ev, V. Y., Zagorskii, V., & Smirnov, S. (2000). Role of Boric Acids in the Formation of Pegmatite and Hydrothermal Minerals: Petrologic Consequences of Sassolite (H∼ 3BO∼ 3) Discovery in Fluid Inclusions. *PETROLOGY C/C OF PETROLOGIIA*, *8*(3), 214–237.

Piochi, M., Mormone, A., Strauss, H., & Balassone, G. (2019). The acid sulfate zone and the mineral alteration styles of the Roman Puteoli (Neapolitan area, Italy): Clues on fluid fracturing progression at the Campi Flegrei volcano. *Solid Earth*, *10*(6), Articolo 6. https://doi.org/10.5194/se-10-1809-2019

Pollard, P., Pichavant, M., & Charoy, B. (1987). Contrasting evolution of fluorine-and boron-rich tin systems. *Mineralium Deposita*, *22*, 315–321.

Schaller, W. T. (1936). Volcanological boron compounds. *Eos, Transactions American Geophysical Union*, *17*(1), 234–235.

Simmons, Wm. B. S., & Webber, K. L. (2008). Pegmatite genesis: State of the art. *European Journal of Mineralogy*, *20*(4), 421–438. https://doi.org/10.1127/0935-1221/2008/0020-1833

Siniscalchi, A., Tripaldi, S., Romano, G., Chiodini, G., Improta, L., Petrillo, Z., D'Auria, L., Caliro, S., & Avino, R. (2019). Reservoir Structure and Hydraulic Properties of the Campi Flegrei

Geothermal System Inferred by Audiomagnetotelluric, Geochemical, and Seismicity Study. *Journal of Geophysical Research: Solid Earth*, *124*(6), Articolo 6. https://doi.org/10.1029/2018JB016514

Taguchi, S., Parmentier, P. P., & Yamasaki, T. (1981). Sassolite sublimated in a steam well at the Yunotani geothermal field, Aso Caldera, Kyushu. *Mineralogical Journal*, *10*(7), 338–343.

Thomas, R., Webster, J. D., & Davidson, P. (2006). *Understanding pegmatite formation: The melt and fluid inclusion approach*.

Tramelli, A., Convertito, V., & Godano, C. (2024). B value enlightens different rheological behaviour in Campi Flegrei caldera. *Communications Earth & Environment*, *5*(1), 275. https://doi.org/10.1038/s43247-024-01447-y

Valentino, G. M., & Stanzione, D. (2003). Source processes of the thermal waters from the Phlegraean Fields (Naples, Italy) by means of the study of selected minor and trace elements distribution. *Chemical Geology*, *194*(4), Articolo 4. https://doi.org/10.1016/S0009-2541(02)00196-1

Corresponding author: monica.piochi@ingv.it

Detection and characterization of resonant signals in global seismology: Evidence for shallow fluid reservoirs and their interaction with the oceans

Piero Poli[1]

[1] *Dipartimento di Geoscienze, Università di Padova*

Using a new global seismological analysis technique designed to detect long-lasting coherent signals, we identify both previously known and entirely unrecognized resonant-like seismic emissions at periods longer than 10 seconds. A detailed examination of these signals allows us to locate their sources with remarkable precision. Strikingly, they cluster in offshore sedimentary basins near major river fans and beneath ice-covered regions. Although their resonant character resembles classic volcanic tremor, the source locations indicate that they are not associated with any known volcanic system.

A careful analysis of their frequency content, spatial distribution, and radiation patterns instead suggests that these signals may originate from the resonance of fluids within shallow subsurface reservoirs. This interpretation aligns with the presence of large volumes of gas, oil, and water in thick sedimentary basins, and with seafloor seepage structures that release substantial amounts of naturally generated fluids from depths of roughly 5–10 km.

By tracking the temporal evolution of these signals, we also identify a pronounced seasonal modulation that mirrors oceanic variability. This observation points to a significant coupling between the oceans and the solid Earth, potentially mediated by static or dynamic stress transfer.

The detection of these newly recognized signals opens a promising path toward probing the largely unexplored dynamics of sedimentary layers and their sensitivity to external environmental forcing. More broadly, these findings introduce a new class of geophysical observables capable of revealing how the shallow lithosphere responds to, and interacts with, oceanic processes on seasonal to long-term timescales.

Corresponding author: piero.poli@unipd.it

Seismological Evidence of Resonant Fluid-Filled Fractures at Campi Flegrei

Giacomo Rapagnani[1,2,3], Simone Cesca[3], Gilberto Saccorotti[2], Gesa Petersen[3], Torsten Dahm[3,4], Francesca Bianco[5], Francesco Grigoli[1,2]

1University of Pisa (Italy)
[2]INGV, Pisa (Italy)
[3]GFZ, Potsdam (Germany)
[4]University of Potsdam (Germany)
[5]Istituto Nazionale di Geofisica e Vulcanologia (INGV), Sezione Osservatorio Vesuviano, Napoli (Italy)

The Campi Flegrei (CF) caldera is a large and active volcanic system located beneath a densely populated area west of Naples, Southern Italy, and represents the largest active caldera in Europe. It is characterised by intense hydrothermal activity, recurrent earthquake swarms, and episodes of pronounced ground deformation (bradyseism), consisting of rapid uplift phases usually accompanied by seismicity, followed by slower aseismic subsidence. The current unrest episode, which began in 2005 and is driven by a degassing magma source and subsequent magmatic–hydrothermal interactions, has resulted in a cumulative uplift of approximately 1.5 m. Seismicity has increased exponentially over the past decade, culminating in 2024–2025 with more than 1500 earthquakes per month and the largest recorded events to date, with magnitudes up to Md 4.4–4.6.

In this study, we analyse the seismic catalogue of the INGV–Osservatorio Vesuviano from 2014 to 2025 to investigate earthquake source processes and their relationship with caldera dynamics. For a selected subset of more than 100 earthquakes with Md > 2.5, we perform time-domain, full-waveform Moment Tensor (MT) inversion with a probabilistic framework, using data from publicly available seismic stations. We performed waveform similarity analysis, allowing us to identify 6 earthquake clusters, each characterised by closely spaced hypocenters and similar focal mechanisms. Most solutions indicate normal faulting. Offshore earthquakes show locations and fault plane orientations consistent with the inferred geometry of the caldera rim, whereas earthquakes in the highly active Solfatara area predominantly strike WSW–ENE. These results reveal the geometry and kinematics of the active fault structures within the CF caldera and their relationship with major volcano-tectonic lineaments.

In addition to shallow volcano-tectonic earthquakes associated with brittle failure, we identify for the first time 14 very long-period (VLP) seismic signals. VLPs display high waveform similarity and stable spectral characteristics over multiple years. Our analysis indicates the presence of a resonant, inclined, fracture system at approximately 3.6 km depth, located between the inferred inflation source and the Solfatara maar, an active degassing centre exhibiting increasing CO_2 flux. The VLP signals are triggered by volcano-tectonic earthquakes occurring at different locations and indicate resonance of a gas-filled fracture system that has been active at least since 2018. This structure likely represents a mechanical and hydraulic connection between the inflating

source region, characterised by shallow brittle deformation, and the surface fumarolic activity, potentially providing new insights on the coupled magmatic–hydrothermal processes during the ongoing unrest at Campi Flegrei.
This study highlights the importance of applying advanced source characterisation techniques to identify and monitor fluid-filled fracture systems in volcanic environments, with the ultimate aim of better understanding the role they play in volcanic unrest.

Corresponding author: giacomo.rapagnani@phd.unipi.it

Insights into Fluid–Rock Interaction from Kinematic Analysis in the Southern Apennines

P. Roselli, L. Valoroso, F. Di Luccio

Istituto Nazionale di Geofisica e Vulcanologia, Roma (Italy)

Within the framework of the FURTHER project (https://progetti.ingv.it/en/further), we investigate the role of fluids during the preparatory phase of earthquakes in the Southern Apennines (SA, Italy). The main objective is to elucidate the cause–effect relationship between fluids and seismicity, as well as the evolution of the active tectonic dynamics of the SA (Di Luccio et al., 2022). From a seismological perspective, we analyze recorded microseismicity with particular focus on the Mefite d'Ansanto, Sannio–Matese, and Pollino areas (Fig. 1), aiming to improve our understanding of the mechanisms controlling seismic source activation within a complex seismotectonic framework influenced by non-volcanic fluid circulation.

The study is based on high-resolution earthquake locations and on a systematic analysis of the spatial relationships between seismicity and the regional fault network. For each analyzed event, we compute moment magnitudes, perform full seismic moment tensor inversions, and estimate source kinematic parameters. These source parameters are used to identify faulting styles and rupture kinematics, providing robust constraints on active deformation processes. Stress tensor inversion is subsequently applied to the derived focal mechanisms to reconstruct the local stress field and to assess its consistency with observed fault orientations and rupture patterns.

In parallel, crustal properties and fluid-related effects are investigated through the analysis of Vp/Vs variations, derived from local earthquake data and used as a proxy for fluid presence and migration within the crust. The integration of Vp/Vs anomalies with source kinematics, stress orientation, and fault geometry allows us to evaluate whether seismic ruptures preferentially occur in regions characterized by elevated fluid content or enhanced pore pressure. This integrated seismological framework provides new insights into the coupled interactions among microseismicity, stress regime, crustal structure, and fluid diffusion in a non-volcanic yet fluid-rich tectonic environment of the SA.

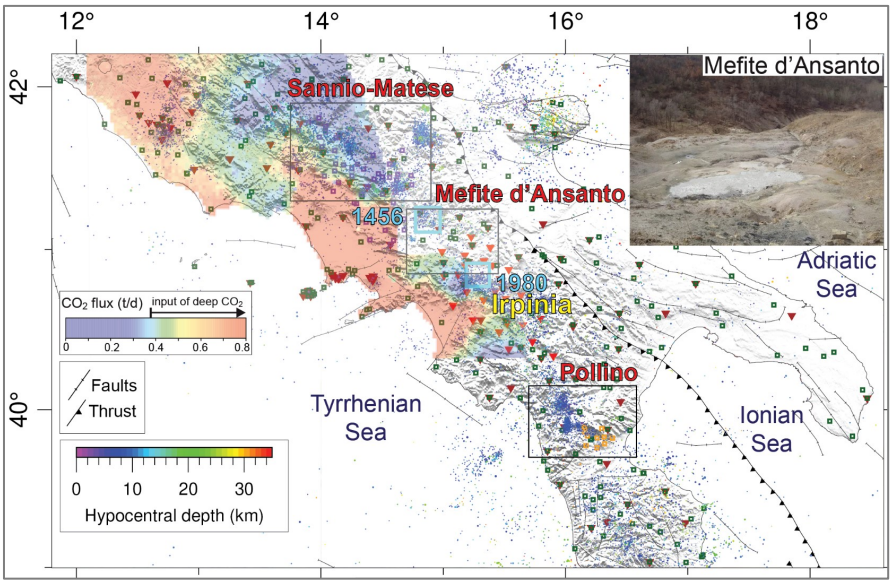

Fig. 1 – Map and CO_2 flux of the SA. Seismicity (ML>2) is color-coded with depth (https://terremoti.ingv.it). The FURTHER target areas are shown in map view as well as in the three bottom panels. The largest earthquakes (M7.1, 1456 and M6.9, 1980) of SA are shown as cyan squares. The CO_2 flux is from Chiodini et al. (2004). The inset in the upper right corner shows the huge degassing area located inside the river Ansanto, the Mefite d' Ansanto Valley. Thrust and faults are from Palano, 2015. Coloured squares in the maps indicate the GNSS stations (see legend for details).

References

Chiodini G., Cardellini C., Amato A., Caliro S., Frondini F. Ventur, G., E. Boschi; 2004: Carbon dioxide Earth degassing and seismogenesis in central and southern Italy. Geophysical Research Letters, 31, L07615. https://doi.org/10.1029/2004GL019480

Di Luccio F., Palano M., Chiodini G, et al.; 2022: Geodynamics, geophysical and geochemical observations, and the role of CO_2 degassing in the Apennines. Earth-Science Reviews, 234, 104236, 2022, ISSN 0012-8252. https://doi.org/10.1016/j.earscirev.2022.104236

Palano M.; 2015: On the present-day crustal stress, strain-rate fields and mantle anisotropy pattern of Italy. Geophysical Journal International, 200(2), 969-985. https://doi.org/10.1093/gji/ggu451

Corresponding author: pamela.roselli@ingv.it

Fluid dynamics during the paroxysmal activity of Mount Etna

F. Sortino[1] , L. Calderone[1], S. Giammanco[2] & C. Ferlito[3]

[1]Istituto Nazionale di Geofisica e Vulcanologia (INGV), Sezione Palermo
[2]Istituto Nazionale di Geofisica e Vulcanologia (INGV), Sezione Osservatorio Etneo
[3]Università di Catania, Catania

The study focused on the results of geochemical monitoring from a fixed station located on the North-East Rift of Mt. Etna (2500 m a.s.l.). This site was specifically selected due to the presence of stable steam fumaroles with distinct chemical and isotopic signatures. The dominant non-condensable gas species is carbon dioxide (CO_2), followed by methane (CH_4); the isotopic ratios of carbon of CO_2 and of He indicate a magmatic source, while CH_4 carbon isotopic ratios point to its thermogenic origin.

Between 2019 and mid-July 2021, negative peaks in CO_2 concentration served as consistent precursory signals of summit eruptions. In almost every instance, a sharp decrease in CO_2 concentrations was followed 24–48 hours later by increased volcanic activity-either Strombolian or paroxysmal-at the summit craters.

Our interpretation proposes a complex fluid-dynamic event in which gas-rich magma migrates rapidly from a deep reservoir 1–6 km b.s.l.) to a shallow one (1–2 km a.s.l.). This sudden, high-velocity movement of magma and its associated gas phase would induce a marked pressure drop within the surrounding volcanic conduits. Similar to the Venturi effect, the rapid variation in gas flow within the volcano's central conduits drags gases away from the peripheral fumaroles, thereby reversing the normal outward flow gradient. This process consequently leads to the significant CO_2 decreases measured at the surface.

The transition from steady degassing to violent lava fountains is theorized to be the result of the magmatic column's composition. Strombolian activity typically begins the eruptive cycle, gradually "consuming" or ejecting the thick, already degassed and cooler magma that is normally residing in the top-most part of the magma column. Once this magma cap becomes sufficiently thin, it can no longer suppress the pressure of the underlying fresh and gas-rich magma. In this case, the ascending gas-rich magma disrupts the equilibrium, leading to rapid expansion of gas bubbles and thence triggering of a lava fountain.

Corresponding author: francesco.sortino@ingv.it

Time Series of Radon in the Etna Area: Integrated Analysis with Meteorological, Seismic, and Volcanic Data (2022-2025)

G. Stissi[1], S. Giammanco [2] , A. Ursino [2], V. Maiolino [2] , A. Cannata[1]

[1] *Dipartimento di Biologia, Geologia, e ambientali, Università degli Studi di Catania, Italy*

[2] *Istituto Nazionale di Geofisica e Vulcanologia, Sezione Osservatorio Etneo, Catania, Italy*

This study is part of multidisciplinary research aimed at improving our understanding of the geophysical and geochemical processes that govern active volcanic systems, such as Mt. Etna. The main objective is to examine the potential of radon gas (^{222}Rn) in soil emissions as a geochemical tracer and early indicator of dynamic variations within the plumbing system.

We analyzed radon time series collected at a fixed monitoring site (ERN7, in the geochemical network of INGV-Osservatorio Etneo) near the village of Santa Venerina on the eastern flank of the volcano between November 7, 2022, and July 12, 2025. The radon data were supplemented with environmental, volcanological, and seismic data, and we sought to identify patterns and correlations that could contribute to the understanding of the geo-structural mechanisms of radon release at the surface. The aim was to potentially use this natural gas to recognise possible precursors of seismic and volcanic activity on Mount Etna. The adopted approach combines time series analysis with an integrated geophysical and volcanological interpretation.

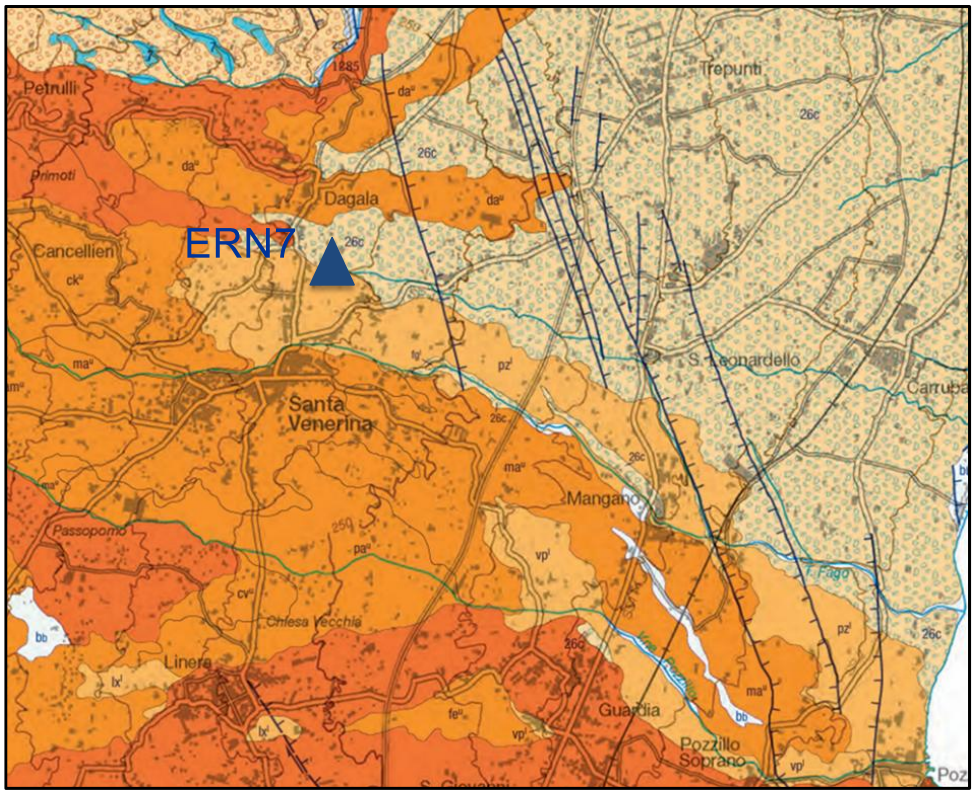

Fig. 1 – Location of the radon monitoring station used for the present study (Blue triangle). The base map is an excerpt from the Geological Map of Etna (Branca et al., 2011).

This study is based on the integration among three main datasets: the activity of ^{222}Rn in the soil (Bq/m^3) recorded hourly by the ERN7 probe; meteorological data (relative humidity, rainfall, air temperature, acquired by the Linera station of the ÆGIS meteorological network); and seismological-volcanological data (eruptive activity from INGV-OE bulletins and seismic tremor - RMS in the 0.5-2.5 Hz band from the EPLC station located near the summit craters). Mt. Etna seismicity is monitored by the the Istituto Nazionale di Geofisica e Vulcanologia - Sezione Osservatorio Etneo (INGV-OE) permanent seismic network.

We used a dual approach to process the hourly radon data, in order to filter out all possible environmental influences on the radon signal. The first was based on a purely mathematical analysis, whereas the second was based on a cross-correlation between radon values and the available meteorological parameters. In all cases we used the software Matlab to perform our analyses. The first step in both approaches was to interpolate the radon signal, in order to fill all time gaps greater than one hour.

According to the first approach, we then applied a Continuous Wavelet Transform (CWT) to the interpolated signal, in order to highlight persistent periodicities (the main ones being 12 hours, 5, 7, 14 days, 6 and 8 months) and seasonal fluctuations (Fig. 2), using the Matlab implementation based on analytic Morse wavelets (Lilly & Olhede, 2009; Mathworks, R2O24b).

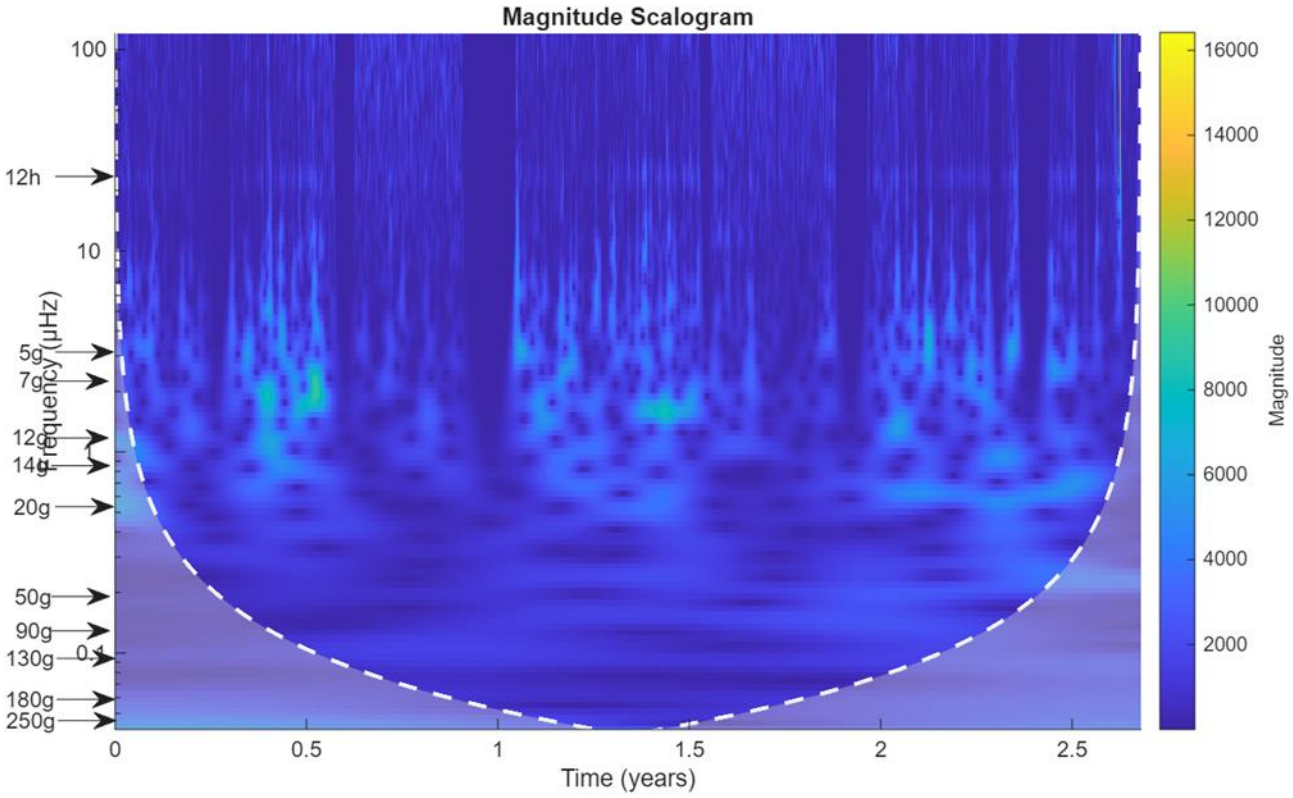

Fig. 2 – CWT plot for to the whole radon data series. Arrows on the left side indicate the most intense cyclic frequencies for the studied period (indicated as hours or days).

Subsequently, the signal was filtered from periodic and environmental components using the "Signal Multiresolution Analyzer" algorithm, optimized with 8 wavelet filters and 14 levels of decomposition, each one corresponding to a progressive range of decomposed frequencies. Reconstructing the filtered signal made it possible to isolate variations due to non-seasonal or non-periodic origin.

In order to define the anomalous radon values in the filtered signal, a robust statistics based on the Normal Probability Plot (implemented using the normplot function in MATLAB) was applied (Hahn and Shapiro, 1967).

The results of this analysis indicated six distinct populations of data (named A to F) and two thresholds of anomalies, one for very low values (< -8553.6) and the other for very high values (> 6265.1). In particular, the very high values of population F correspond to the maximum values observed in the peak described. Population D shows only slightly anomalous values and is therefore classified as weakly anomalous as a precautionary measure.

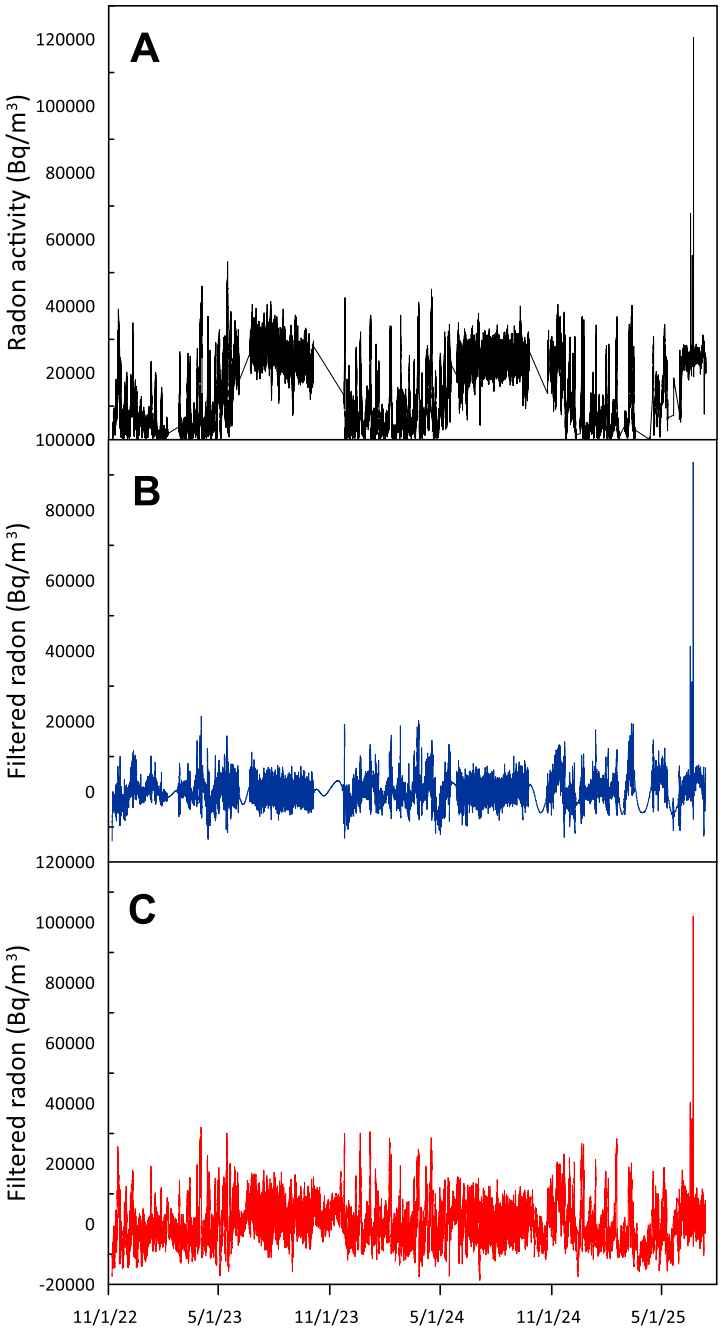

Fig. 3 – A) Time series of raw radon data; B) time series of filtered radon values after signal processing analysis; C) time series of filtered radon values after applying regression analysis using meteorological data.

According to the second approach, we used the available meteorological data (air temperature, air humidity, rainfall), to apply a Multiple Linear Regression Analysis. The synthetic radon signal obtained was subtracted from the original signal and the residuals were confronted with the filtered radon signal from the time series analysis. The two filtered signals show a good temporal agreement (figures 3B and 3C), thus confirming the effectiveness of mathematical filtering in removing environmental influences.

In addition, a correlation analysis was also conducted between radon and variations over time in the amplitude of the seismic signal at a station on Mount Etna, which largely reflects variations in the amplitude of volcanic tremors.

The resulting dataset contains 19,310 values, recorded at hourly resolution. The 0.5–2.5 Hz band provides the best results for analyzing tremor variations.

Acknowledgments

We would like to thank the Istituto Nazionale di Geofisica e Vulcanologia, Sezione Osservatorio Etneo, Catania, (Italy) for providing the radon, seismic, and volcanological data used for the integrated analysis.

References

Barberi, G., Di Grazia, G., Ferrari, F., Firetto Carlino, M., Giampiccolo, E., Maiolino, V., Mostaccio, A., Musumeci, C., Scaltrito, A., Sciotto, M., Tusa, G., Tuvè, T., and Ursino, A. . Mt. Etna Revised Seismic Catalog from 2020 (EtnaRSC2020) (Version 1) [Data set]. Istituto Nazionale di Geofisica e Vulcanologia (INGV) 2020. [https://doi.org/10.13127/ETNASC/ETNARSC2020]

Hahn, G. J. and S. S. Shapiro. *Statistical Models in Engineering*. New York: Wiley, 1967.

Lilly, J. M., & Olhede, S. C. (2009). *Higher-Order Properties of Analytic Wavelets.* IEEE Transactions on Signal Processing, 57(1), 146–160.

MathWorks. (2024). *cwt*. In *MATLAB Wavelet Toolbox Documentation* (R2024b). The MathWorks, Inc.

MathWorks. (2025). *normplot — Normal probability plot*. In *MATLAB Documentation*. The MathWorks, Inc. Retrieved December 5, 2025, from https://www.mathworks.com/help/stats/normplot.html

Corresponding author: giuseppina.stissi98@gmail.com

Seismicity and Vp and Vp/Vs models around the Mefite d'Ansanto deep-CO2 degassing site (Southern Apennines, Italy)How to organize a successful conference

Valoroso L.[1], Bagh S.[1], De Gori P.[1], Improta L.[1], Piccinini D.[1], Cianetti S.[1], Roselli P.[1], and Di Luccio F.[1]

[1] *Istituto Nazionale di Geofisica e Vulcanologia (Italy)*

Mantle-derived fluids play a primary role in the generation of large upper crustal earthquakes in extensional domains. Here, we focus on the Mefite d'Ansanto degassing site, the largest low-temperature non-volcanic deep-CO2 emission site in the world (about 2000 tons per day, Chiodini et al., 2010), located at the northern tip of the Mw6.9 1980 Irpinia faults in the Southern Apennines (Italy). The area, characterized by high heat flow and pervasive CO2 rich fluids circulation, experienced strong historical earthquakes (M6+) but it is characterised by low background seismic rate, with respect to the nearby Sannio and Irpinia regions.

To investigate this key-sector of the Southern Apennines, within the multidisciplinary FURTHER project (https://progetti.ingv.it/en/further), a collaborative initiative exploring the role of fluids in seismogenesis within the Southern Apennines, we collected high-quality microseismicity data during a two-year dense temporary passive survey (May 2021 to May 2023). The seismic network integrates the 10 temporary stations with 39 permanent stations of the INGV and ISNet network.

Starting from about 360 accurately manually-picked earthquakes, we applied the EqCorrScan template-matching algorithm to detect low-magnitude seismicity. We computed a best fit 1D Vp velocity model of the area through a non-linear technique, and 1D earthquake locations using the probabilistic non linear location method NonLinLoc. The final catalog is composed of 1573 earthquakes (-0.7 < ML < 3.0).

We also computed new 3D Vp and Vp/Vs seismic tomography models of the area following a graded local earthquake tomography (LET) inversion scheme (from a regional 10x10x5km to a local 3x3x2 km grid spacing).

Most of the seismicity has small magnitude (ML<1), confirming the low seismic rate of this area compared to the adjacent regions, and occurs in small clusters (sometimes along small faults) characterized by either short-lived or sustained seismic activity.

The combined interpretation of Vp and Vp/Vs velocity model, seismicity distribution and full moment tensor solutions (i.e., double-couple vs non-double-couple component) helped us to investigate the relationship between seismicity, crustal structure and fluid pressure in this crucial sector of the Southern Apennines seismic belt.

References

Chiodini, G., Granieri, D., Avino, R., Caliro, S., Costa, A., Minopoli, C., Vilardo G., 2010. Non-volcanic CO2 Earth degassing: Case of Mefite d'Ansanto (southern Apennines), Italy, Geophys. Res. Lett., 37, L11303, doi:10.1029/2010GL042858

Corresponding author: luisa.valoroso@ingv.it

New insights on hydraulic behaviour of normal faults and thrusts of Irpinia area (Southern Italy), based on well exploration pressure profiles

Eleonora Vitagliano[1], Luigi Improta[1], Luca Pizzino[1], Nicola D'Agostino[1]

[1] *Istituto Nazionale di Geofisica e Vulcanologia (Roma, Italia)*

We present the results of a recently published study that applied methodologies traditionally employed in the oil industry to analyse pressure profiles derived from exploration wells (Fig. 1). This research explores the connections between subsurface fluid flow and both normal and reverse faults in the Irpinia area (Southern Apennines, Italy), a region that has experienced significant seismic activity over the past century.

Fluid–fault interactions can be studied at various scales, ranging from laboratory settings to field observations. Our research focuses on a regional scale, integrating well data, tectono-stratigraphic frameworks, and geochemical information to evaluate the hydraulic behaviour of faults and their capacity to either facilitate or hinder fluid flow. Recent geophysical investigations, particularly seismic tomography, suggest that overpressured fluids are primarily contained within highly permeable carbonates of the Apulian Platform that are sealed by a low-permeability tectonic mélange. In this case, regional low-dipping overthrusts separating the deep Apulian units from the root-less Apennine nappes would act as a barrier for fluid flow.

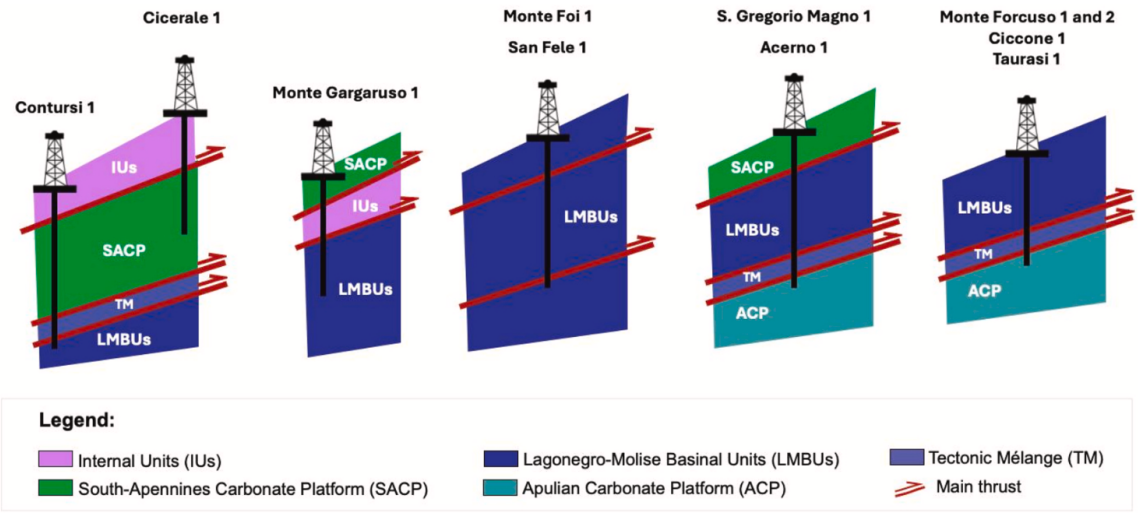

Fig. 1 – Analyzed exploration wells in the Irpinia region and a simplified tectono-stratigraphy at the well site.

In our study, we have re-assessed the hydraulic characteristics of normal faults in the vicinity of the Irpinia Fault, source of the 1980 Ms 6.9 Irpinia earthquake, and analyzed the vertical pressure gradients to discriminate the behaviours of regional thrusts and their associated tectonostratigraphic units. Notably, we investigate the impact of the 1980 earthquake on fluid dynamics. The San Gregorio Magno-1 well, which intersects the seismogenic fault, reveals a continuous pressure profile that ranges from hydrostatic to slightly overpressured conditions down to a depth of 5.9 kilometres (Fig. 2). This finding indicates a relatively uniform fluid distribution within a highly fractured rock volume, contradicting earlier seismological models that suggested the existence of significantly overpressured fluids within the Apulian carbonates. Additionally, in regions characterized by intense CO_2 degassing, such as Mefite d'Ansanto located 10 km to the north of the Irpinia Fault, the Monte Forcuso-1 and Monte Forcuso-2 wells exhibit continuous hydrostatic pressure gradients. We interpret this phenomenon as a consequence of active normal faulting, which has compromised the sealing effectiveness of the overlying clay-rich tectonic mélange, thereby facilitating increased fluid movement within the fractured Apulian carbonates. Our findings suggest that high-angle thrust faults in the upper rootless nappes can also serve as conduits for vertical fluid migration. These tectonic boundaries allow groundwater to flow downward from the upper Apennine Platform carbonates into the lower Lagonegrese basin formation, enabling a gravitationally-driven circulation flow in the upper 0-4 kilometres of the crust consisting of strongly fractured rocks.

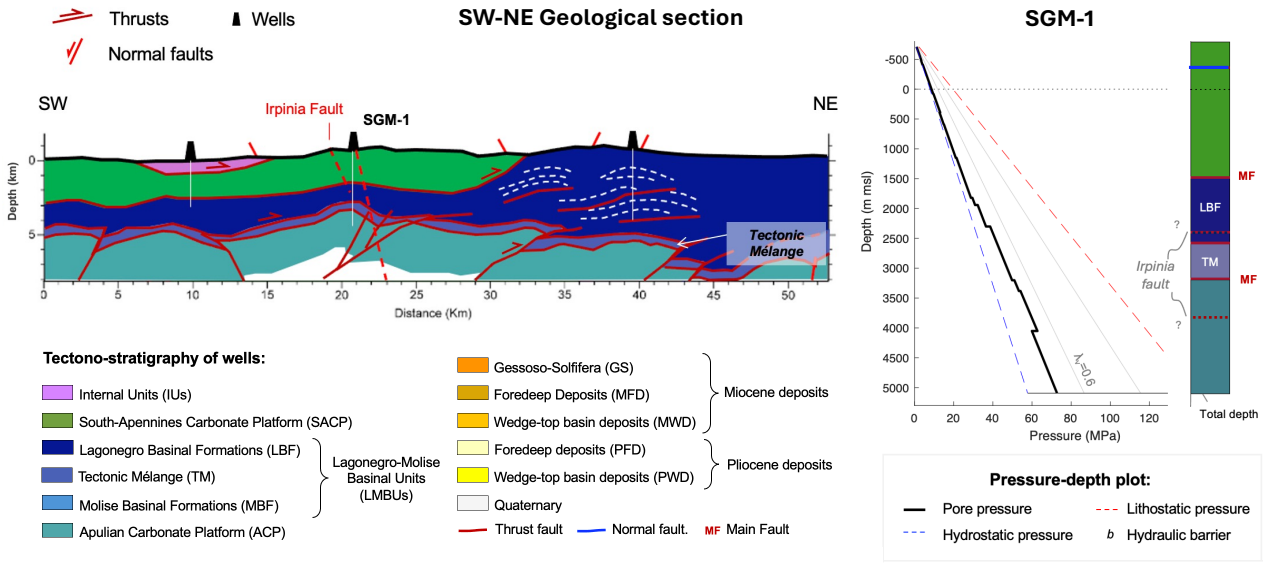

Fig. 2 – Cross section modified from Feriozzi et al. (2024) and pressure profile at San Gregorio Magno-1 well (SGM-1).

References

Feriozzi F., Improta L., Maesano F.E., De Gori P. and Basili R.; 2024: The 3D crustal structure in the epicentral region of the 1980, Mw 6.9, Southern Apennines earthquake (southern Italy). New

constraints from the integration of seismic exploration data, deep wells, and local earthquake tomography. Tectonics, Vol. 43, e2023TC008056, https://doi.org/10.1029/2023TC008056.

De Landro G., Amoroso O., Russo G., D'Agostino N., Esposito R., Emolo A. and Zollo A.; 2022: Decade-long monitoring of seismic velocity changes at the Irpinia fault system (southern Italy) reveals pore pressure pulsations. Scientific Report, Vol. 12, 16039, https://doi.org/10.1038/s41598-022-05365-x.

Vitagliano E., Improta L., Pizzino L. and D'Agostino N.; 2025: Study of well data reveals fluid pressure distribution and origin in the upper crust of the Irpinia region (Southern Apennines, Italy). Tectonophysics, Vol. 908, 230761, https://doi.org/10.1016/j.tecto.2025.230761

Vitagliano E., Mariucci M.T., Tarabusi G.; 2025: Database of Italian Pressures (DIPs). Istituto Nazionale di Geofisica e Vulcanologia (INGV), https://doi.org/10.13127/dips1

Corresponding author: eleonora.vitagliano@ingv.it